UNITED STATES DEPARTMENT OF THE INTERIOR, Stewart L. Udall, *Secretary*

FISH AND WILDLIFE SERVICE, Clarence F. Pautzke, *Commissioner*

BUREAU OF COMMERCIAL FISHERIES, Donald L. McKernan, *Director*

ATLAS OF THE OCEANOGRAPHIC CLIMATE OF THE HAWAIIAN ISLANDS REGION

BY GUNTER R. SECKEL

FISHERY BULLETIN 193

From Fishery Bulletin of the Fish and Wildlife Service

VOLUME 61

PUBLISHED BY U.S. FISH AND WILDLIFE SERVICE • WASHINGTON • 1962

PRINTED AT U.S. GOVERNMENT PRINTING OFFICE, WASHINGTON

For sale by the Superintendent of Documents, U.S. Government Printing Office, Washington 25, D.C. - Price 40 cents

Library of Congress catalog card for the series, Fishery Bulletin of the Fish and Wildlife Series:

U.S. *Fish and Wildlife Service.*
Fishery bulletin. v. 1–
Washington, U.S. Govt. Print. Off., 1881–19

v. in illus., maps (part fold.) 23–28 cm.

Some vols. issued in the congressional series as Senate or House documents.
Bulletins composing v. 47– also numbered 1–
Title varies: v. 1–49, Bulletin.
Vols. 1–49 issued by Bureau of Fisheries (called Fish Commission, v. 1–23)

1. Fisheries—U.S. 2. Fish-culture—U.S. I. Title.

SH11.A25 639.206173 9–35239 rev 2*

Library of Congress [r55e½]

CONTENTS

		Page
Part I.	Distribution of surface variables	373
1.	Depth of the mixed surface layer	373
	A. Definition and practical means of determination	373
	B. Distribution in the Hawaiian islands region	375
2.	Surface temperature	377
3.	Surface salinity	380
4.	Geopotential topography	383
Part II.	Physical processes and their relation to the distribution of surface variables	383
1.	Heat (salt) budget	384
2.	Events at the sea surface	385
	A. Net heat exchange across the sea surface	385
	B. Evaporation minus precipitation	392
3.	Advection	394
	A. Characteristic advection diagram	394
	B. Intrinsic temperature and the heat advection chart	398
	C. Characteristic heating curve	400
Part III.	Oceanographic climate of the Hawaiian Islands region	404
	Literature cited	408
	Appendix A	409
	Source of data	409
	Treatment of data	410
	Appendix B	411
Charts:		
I.	Distribution of the depth of mixed layer	411–416
II.	Distribution of the surface temperature	417–422
III.	Distribution of the surface salinity	423
IV.	The surface dynamic topography	424
V.	Characteristic advection diagrams	425
VI.	Heat advection charts	426–427

ABSTRACT

In the area bounded by 10° N., 30° N., 150° W., and 180°, the distribution of surface variables is investigated in terms of associated physical processes. (1) Using all available data, seasonal changes in the distribution of the mixed surface layer, surface temperature, surface salinity, and the dynamic topography are described. (2) With the aid of a simplified heat (salt) budget, the physical processes (net heat exchange across the sea surface, evaporation minus precipitation, advection) and their relation to the distribution of surface variables are analyzed. (3) The results are interpreted in terms of a climatic circulation model in the vicinity of Hawaii.

The distribution of surface variables reveals three types of climatic boundaries: (1) a depth-of-mixed-layer boundary separating areas in which the time of maximum and minimum depths differs; (2) temperature boundary separating an area where the seasonal range of temperature is relatively constant from one in which it increases northward; (3) salinity boundary separating different types of water.

Investigation of processes reveals three cold advection periods, June-July, October-November, December-January; the first is dominant in the northwest portion of the area and the second in the southeast portion. In the course of analysis, characteristic advection diagrams, intrinsic temperatures, heat advection charts, and characteristic heating curves are defined.

In terms of the North Pacific circulation, the salinity boundary is interpreted as separating North Pacific Central water from the transition water of the California Current Extension. The June-July and October-November advection periods reflect dilations and contractions of the North Pacific Central and North Pacific Equatorial circulation systems believed to be associated with the seasonal variation of trade wind intensity. The differing times of maximum and minimum depths of the mixed layer and dominant advection periods reflect the differing climates of the North Pacific Central and North Pacific Equatorial systems.

ATLAS OF THE OCEANOGRAPHIC CLIMATE OF THE HAWAIIAN ISLANDS REGION

By GUNTER R. SECKEL, *Oceanographer*, BUREAU OF COMMERCIAL FISHERIES

A study of the oceanographic climate of the Hawaiian Islands region is a part of the Hawaii skipjack investigations conducted by the staff of the Biological Laboratory,[1] Bureau of Commercial Fisheries (Honolulu). This seasonal fishery has been described by Yamashita (1958). The catch rate generally begins to rise rapidly in April from 200,000 pounds or less a month during the winter to 2 million pounds or more in August. Thereafter it drops off rapidly in September and October, again reaching the minimum catch rate per month during the latter part of the year. The fishery also shows relatively large annual fluctuations ranging from a low of about 6 million pounds, as in 1957, to about 14 million pounds, as in 1954. Because both the seasonal nature of the fishery and its annual fluctuations were believed to be associated with changes in the physical environment, oceanographic studies were included as part of the skipjack investigations.

Oceanographic information for the waters bathing the Hawaiian Islands was summarized by Schott (1935) and Sverdrup et al. (1942), and bathythermograph observations from 1941 to 1949 were analyzed by Leipper and Anderson (1950). Since 1949, six oceanographic surveys were made in the vicinity of the high islands of the Hawaiian archipelago (McGary, 1955; Seckel, 1955). The information from these sources can be summarized as follows: The Hawaiian Islands are located in the trade wind zone of the Pacific Ocean, where seasonal changes of surface variables are relatively small. The seasonal temperature range, for example, is approximately 4° to 5° F. (2° to 3° C.). The mean summer high is about 78° F. (25.6° C.) and varies locally from 75° (23.9° C.) to 80° F. (26.7° C.). The mean winter low is about 74° F. (23.3° C.) with local variations from 73° (22.8° C.) to 76° F. (24.4° C.).

The mean salinity is about 35 °/₀₀, ranging from 34.4 to 35.3 °/₀₀. Definite seasonal salinity variations, because of insufficient data, were believed to be obscured by large annual variations.

Available surface inorganic phosphate data show that the concentration to be found in the vicinity of the Hawaiian Islands approaches the limit of precision in present experimental techniques (0.3μg-at./L.). This, together with the scarcity of observations, made it impossible to detect seasonal changes.

Zooplankton catches in the area have been discussed by King and Hida (1954, 1957) and Waldron, Nakamura, and Shippen (MS). Mean catches indicate annual variations of 15 to 25 cc. per thousand cubic meters of water strained in 200-meter oblique hauls, with a suggestion of a similar range in seasonal catch variations (King and Hida, 1957, figs. 7 and 8).

Current charts generally show a weak set toward the west throughout the year. Geostrophic currents indicate a complex flow pattern in the vicinity of the high islands, without providing any information about seasonal changes. In short, these environmental parameters are well within the limits within which skipjack are known to occur, so that their changes appear to be insufficient to explain the seasonal nature of the skipjack fishery and its annual variations.

All data, however, have not been exhausted. There are many isolated observations from cruises either originating or terminating in the Hawaiian Islands. In addition, many thousands of bathythermograph observations have been obtained by the Bureau of Commercial Fisheries Biological Laboratory (Honolulu), and other organizations since the end of World War II. These data, if treated by means of a different approach, could yield information which is not now apparent.

One can postulate, for example, that the surface variables such as temperature or salinity, are not randomly distributed in space, but that they are

[1] Formerly Pacific Oceanic Fishery Investigations (POFI). Renamed December 1, 1959.

NOTE.—Approved for publication February 27, 1961. Fishery Bulletin 193.

associated with certain physical processes. Or, if the space and time distribution of surface variables is known, then one should be able to obtain some information about the physical processes. To be more specific, one can formulate a heat budget and say that the rate of change of heat content in the surface water (approximately proportional to the surface temperature) must depend on the rate at which heat enters or leaves across the sea surface, the diffusion (a change of concentration due to mixing), and advection (a change of concentration due to currents introducing water with different properties). Similarly, one should be able to formulate salt budgets in which evaporation and precipitation at the surface must be considered and, possibly, momentum budgets in which the surface wind stress must be considered.

Such an approach has been described in the chapter on the Theory of Distribution of Variables in the Sea, by Sverdrup et al. (1942). In practice, of course, the formulae presented there must be simplified before application. However, the equations state that whenever physical processes are to be related to the distribution of variables, such as temperature, salinity, momentum, oxygen, and phosphate, the following data must be available about the variable in question: (1) the local-time rate of change and (2) the three-dimensional space distribution. This requirement, as it concerns the heat budget of the surface water in the Hawaiian Islands region, can be satisfied by using all the available data mentioned.

In weather analysis, the seasonal changes in temperature at any location are explained in terms of solar energy received and in terms of the motions of high- and low-pressure systems. In central North America, for example, the cold, dry, winter weather is associated with the southward motion of the polar high pressure system. In summer, as this system's boundaries move northward, the cold, dry air is replaced by the maritime-tropical air moving inland through the Gulf of Mexico producing warm and highly humid weather. This type of weather analysis is called climatology and, therefore, by analogy, the investigation to be described here can be called "climatic oceanography."

In order to study the oceanographic climate of the Hawaiian Islands, the results of previous surveys (McGary, 1955; Seckel, 1955) made it evident that an area larger than the immediate vicinity of the main Hawaiian Islands must be chosen. Natural boundaries for this area, to be referred to as the Hawaiian region, are the vicinity of the northern edge of the equatorial countercurrent, or 10° N., and the vicinity of the salinity maximum, or 30° N. In the west, the 180th meridian was chosen, and in the east, lack of data limited the area to 150° W.

For this region, then, the climatic study will be divided into two parts. First, the distribution of surface parameters, such as the depth of mixed layer, temperature, salinity, and geopotential topography, will be described essentially without interpretation. Second, the processes with which these parameters are associated will be investigated. Because adequate salinity and current data are lacking, the present paper will primarily be concerned with the processes of heat exchange across the sea surface and heat advection as they are related to the distribution and rate of change of temperature throughout the region.

In the course of the analysis, "characteristic advection diagrams," "characteristic heating curves," and "intrinsic temperatures" will be defined. It will then be shown how these can be used to interpret continuous surface temperature data, such as are obtained at the Koko Head monitoring station on Oahu.

The final portion of the analysis will consist of an integrated account of the oceanographic climate of the Hawaiian Islands region. Here features of interest described in part I will, as far as is possible, be explained by the processes described in part II. Readers who are primarily interested in the results of the study can proceed directly to part III, and turn to parts I and II for details of the analysis.

The sources of data will be indicated in the Appendix, with an account of the manner in which they were treated.

Finally, the aims of the study have been achieved. Despite the fact that the data used do not readily lend themselves to an analysis of processes because they were collected for other purposes, over a period of years, at unrelated times and places, and in an area where their seasonal and annual variations are of the same order of magnitude, a gross picture of the oceanographic climate in the vicinity of Hawaii has been developed.

Although reasons for the occurrence of skipjack in Hawaiian waters are not known, the seasonal and annual variations in their abundance, as reflected by catch statistics, are associated with climatic features such as the seasonal movement of different types of water through the island area. These climatic changes can be monitored with the aid of surface temperatures and salinities as obtained at Koko Head, Oahu.

I would like to express my appreciation to the members of the faculty of the Department of Oceanography, University of Washington, for making their facilities available during a portion of the work and for providing encouragement and valuable suggestions. I would also like to thank Drs. C. A. Barnes, N. P. Fofonoff, and M. Rattray for reading the manuscript and for their valuable suggestions—T. S. Austin, J. C. Marr, and K. D. Waldron for reviewing the manuscript, Mrs. M. K. Robinson for supplying the bathythermograms from the Scripps Institution of Oceanography deck, and T. Nakata for drawing the figures and charts.

PART I. DISTRIBUTION OF SURFACE VARIABLES

1. DEPTH OF THE MIXED SURFACE LAYER

A. Definition and Practical Means of Determination

In this paper an attempt will be made to relate the space and time distribution of a surface variable, such as temperature, to physical processes such as heat exchange and advection. Although these processes will be discussed in part II, one of the parameters entering into budget considerations is the depth to which the processes at the sea surface are effective. For example, the change of temperature due to a certain amount of net heat exchange across the sea surface depends on the volume of water through which this heat has been distributed. Thus, the depth of this effective layer must be defined and its distribution must be determined.

Since the processes at the sea surface involve energy changes, it is appropriate to consider the stability generally encountered in the upper 300 meters of the Hawaii region. The stability $E=\frac{1}{\rho}\frac{\delta\rho}{dz}$ has been discussed by Sverdrup et al. (1942) and is a function of the vertical density gradient. It is also proportional to the force required to displace a parcel of water vertically by a unit length.

Figure 1 illustrates the vertical winter and summer density (σ_t) distribution at 10° N., 20° N., and 30° N., approximately along a meridian

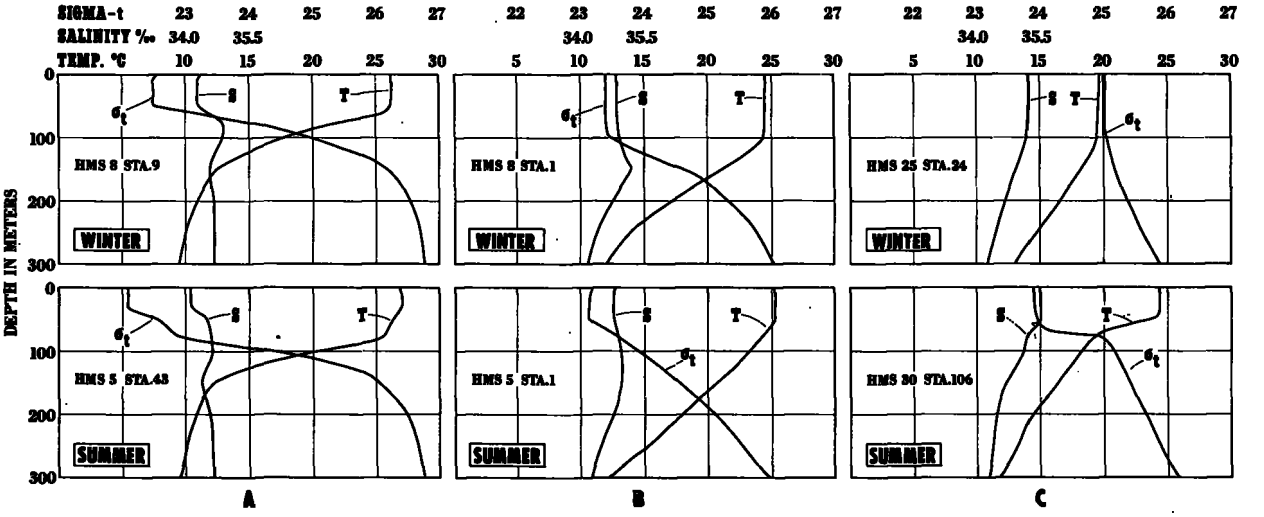

FIGURE 1.—Temperature, salinity, and density (σ_t) depth curves. Panel A, winter and summer near 10° N., 158° W.; panel B, winter and summer near 21° N., 158° W.; panel C, winter and summer 30° N., 160° W. (158° W.).

through the Hawaiian Islands. Three density layers can be readily distinguished. The first is the mixed surface layer with neutral stability $\left(\frac{\delta\rho}{dz}=0\right)$. The second, the pycnocline, is a layer within which there is a rapid increase in density with depth. The third, in which the density increases very slowly with depth, is below the pycnocline.

Approximate stabilities, $E'=10^{-3}\frac{d\sigma_t}{dz}$ (Sverdrup et al. 1942: 417), in the three layers are as follows: in the mixed surface layer $E'=0$: in the pycnocline $10^{-5}\frac{d\sigma_t}{dz}$ ranges from 3400 m.$^{-1}$ to 5000 m.$^{-1}$, 1400 m.$^{-1}$ to 2300 m.$^{-1}$, and 350 m.$^{-1}$ to 2500 m.$^{-1}$ at 10° N., 20° N., and 30° N., respectively. These compare with stabilities of 120 m.$^{-1}$ at 10° N. to 170 m.$^{-1}$ at 30° N. in the deeper layer below the pycnocline. Thus, stability changes from layer to layer are large. In addition, whereas the change from the second to the third layer is gradual, the change from neutral stability in the mixed surface layer to high stability in the pycnocline is abrupt. The bottom of the mixed surface layer can therefore be regarded as a surface of dynamic significance. Above this surface, parcels of water can move up and down with a minimum expenditure of work. In the pycnocline, a comparatively large amount of work must be done to displace water vertically. For this reason, the depth of the effective layer through which energy changes due to processes at the sea surface are distributed is assumed to be the mixed surface layer.

In order to measure the depth of the mixed surface layer and determine its distribution, it is useful to remember that the density of the surface sea water is a function of both the temperature and the salinity. These were also drawn in figure 1 to such a scale as to demonstrate their relative effect on the density. It is apparent that the vertical density structure is primarily a function of the temperature and that the salinity in the latitudes under consideration is of less importance. It is also apparent that the top of the pycnocline corresponds approximately with the top of the thermocline and that the surface layer in which $E=0$ corresponds approximately with the layer in which the vertical temperature gradient is also zero $\left(\frac{\partial\theta}{\partial z}=0\right)$. The depth of the mixed surface layer can therefore be determined from temperature-depth curves in the Hawaiian region.

In practice it is not always as simple to determine the depth of the mixed layer from the vertical temperature distribution as indicated in the examples of figure 1. It will therefore be useful to briefly review features of the vertical temperature distribution which are discussed in detail in the Application of Oceanography to Subsurface Warfare (National Defense Research Committee, 1946). The most important of these is the thermocline, in which the maximum temperature change occurs. It is between the surface layer of constant temperature and a deeper layer in which the vertical rate of change of temperature is small. In the Hawaiian region, this thermocline, which we call the main or permanent thermocline, is always present. Below the mixed layer, the average temperature gradient, $\frac{\partial\theta}{\partial z}$, is approximately 15° C., 6° C., and 5° C. per 100 m. at 10° N., at 20° N., and 30° N., respectively. Superimposed on the permanent thermocline may be a seasonal thermocline. This is illustrated by the vertical temperature distribution at about 30° N. in winter and summer (fig. 1C). In addition to the permanent and seasonal thermocline, there may be a diurnal thermocline, defined as a small rise in surface temperature of the order of 1° C., which may extend to a depth of 10 m. Finally, the stable layer may extend to the sea surface; i.e., the constant temperature surface layer may be absent.

The last two rarely occur in the area under investigation and the practical problem remains one of determining the depth of the mixed surface layer with consistency from temperature-depth curves. In low latitudes the depth of this layer is generally well defined by what Munk and Anderson (1948) called the "knee." However, more than one knee may occur, as at 10° N. in August, illustrated in figure 1A. In examining temperature-, salinity-depth curves in the Hawaiian region, one finds that the first knee, after excluding the diurnal thermocline, also defines the layer of constant salinity, whereas deeper knees are in more saline water.

Difficulty also arises when the depth of the knee is not well defined and may actually lie within a layer of changing salinity with depth, the halocline. In other words, the temperature decreases gradually below a layer of constant

temperature or below the sea surface. It is useful, then, to define a vertical temperature gradient which separates the mixed surface layer from the thermocline. A gradient of 3.6° C. per 100 m. (1° F. per 50 ft.), which apparently is of significance in connection with underwater sound properties,[2] has been used by the Scripps Institution of Oceanography. By examining temperature- and salinity-depth curves it was found that this gradient was too large and that the apparent depth of the surface layer in many cases was well within the halocline. Lumby (1956) took as the criterion for the homogeneous layer the depth of the isothermal layer as judged by the absence of temperature gradients in excess of 1° C. per 100 m. Upon examination, it was found that the apparent depth of the mixed layer, using Lumby's criterion, was in good agreement with the depth of mixed layer as determined from temperature and salinity depth curves.

To summarize, it was shown that the change from neutral stability in the mixed surface layer to high stability in the pycnocline was abrupt and that the surface separating the two layers was one of dynamic significance. For this reason, the effective depth through which energy changes due to processes at the sea surface were distributed was assumed to be the mixed surface layer.

Further examination of figure 1 showed that the vertical density distribution is primarily a function of the vertical temperature distribution. The depth of the mixed layer could therefore be determined from temperature depth curves by using the first knee below the surface (excluding the diurnal thermocline) and Lumby's criterion that the isothermal layer be judged by the absence of temperature gradients in excess of 1° C. per 100 m.

B. DISTRIBUTION IN THE HAWAIIAN ISLANDS REGION

The definition of the mixed surface layer and an understanding of the vertical density and temperature relationships enable us to use bathythermograph observations in the Hawaiian region to determine the areal distribution of the depth of mixed layer. Thus, the pertinent data were taken from several thousand bathythermograms and assembled into monthly charts showing the distribution of the depth of the mixed layer (appendix B, chart I). The original data, their treatment, and manner of construction of the charts is described in appendix A.

Here, it should be mentioned that these charts have been based on data which were collected for diverse purposes at unrelated times. Information to be gained from them, therefore, is limited and attention will be focused on gross features in the distribution of the depth of mixed layer rather than details of individual contours. Even though many undulations in contours are believed to be due to shortcomings in the data, they have not been smoothed unless warranted by some evidence. One can say, however, although undulations in depth of the mixed layer contours may not reflect an actual situation, they do point to the fact that the ocean is not smooth and changes do not occur at regular time intervals. In that respect, then, they reflect reality.

A prominent feature in the January and February charts (chart I) is a trough in which the depth of the mixed layer is greater than in surrounding areas extending east to west between 15° and 20° N. Its depth is generally greater than 250 feet (76 m.), exceeding 400 feet (122 m.) west of 165° W. Another trough, centered about 165° W., extends from 30° N. southward and then eastward between the high islands and 25° N., where its depth is greater than 350 feet (107 m.). To the north of this feature is a shallow area, with a mixed layer depth of less than 200 feet (61 m.). The two troughs are separated by a ridge of less than 250 feet (76 m.) and a minimum depth of less than 150 feet (46 m.) in the northwest portion of the area.

South of the main east-west trough, between 10° and 15° N. and east of 175° W. (January), the depth of mixed layer is as shallow as 150 feet (46 m.) or less. In February, the shallow area is reduced in size by the deepening of the mixed layer west of 167° W. and along the southern boundary of the region. Also of interest here is the formation of a shallow "dome" at 15° N. and 163° W.

Charts for the months of March, April, and May, indicate a period of change. In March, although the January–February features are still evident, a change in the depth distribution of the mixed layer is beginning to take place. The small dome of February, at 15° N. and 163° W., has

[2] Personal communication, Mrs. Margaret Robinson, Scripps Institution of Oceanography.

619237 O—62——2

spread sufficiently to interrupt the main east-west trough between 158° and 163° W. In general, the depth of the mixed layer is decreasing throughout most of the survey area, except along the southern boundary, east of 162° W., where it is increasing. During April and May, the depth of the mixed layer continues to decrease throughout the survey area, except in the southern portion where it is increasing.

In June, a new distribution pattern of the depth of the mixed layer has been established. A trough is now located between 10° N. and 13° N., west of 156° W., where the depth reaches approximately 300 feet (91 m.). East of 156° W. the trough, now 200 to 250 feet (61–76 m.) deep, turns northeastward. Over much of the area north of 20° N., the mixed layer is less than 100 feet (30 m.) deep.

The distribution of the depth of mixed layer during July and August does not differ materially from that during June. It shows little of interest north of 20° N., where the depth has increased but is still less than 150 feet (46 m.). The trough in the southern portion of the survey region remained between 10° and 15° N., except that it now curves northeastward between 160° and 165° W. with depths in excess of 300 feet (91 m.).

In the southeast portion of the region the depth has been steadily decreasing from about 200 feet (61 m.) in June to less than 100 feet (30 m.) in August.

The September depth of mixed layer chart shows that the trough has started, as it were, a northward movement and is now centered about 15° N., west of 160° W. with depths between 250 (76 m.) and 300 feet (91 m.).

In October, the trough has essentially resumed its winter (January and February) position. The depth north of 20° N. is increasing and the beginnings of the typical January and February structure are visible. This trend continues during November and December, and throughout this period the depth of mixed layer is shallow in the southern portion of the region.

The primary feature, then, of the distribution of the depth of the mixed layer in the Hawaiian region is a trough and seasonal differences in its location. Maximum development of this feature occurs in January, when the depth of the trough may exceed 400 feet (122 m.) and extends from east to west between 15° and 20° N. The June distribution typifies the other extreme, when it is found in its southernmost position. At this time the depth is also at a minimum in the northern portion of the region. It is interesting to note that the converse to the gradual northward motion of the mixed layer trough is not true during the March-April-May transition period. During that time the irregular depth distribution suggests disintegration of a pattern rather than a southward movement.

These features can also be illustrated by showing meridional profiles of the depth of mixed layer. The January and June profiles representing the mean depth of the mixed layer between 153° and 161° W. are given in figure 2A and those for 168° to 176° W. in figure 2B. The January profiles are similar. They show ridges in the vicinity of 12°, 20°, and 26° N. and troughs at 17°–18° N. and 23° N. The western profile is generally deeper than the eastern profile, except for the trough at 23° N. Both figures convey the impression of standing waves in the southern portion of the region, with nodes between 14° to 15° N. in the eastern portion and 12° to 13° N. in the western portion.

Although January and June exhibit extremes in the winter and summer distribution patterns, the depth of mixed layer during those months is not necessarily at the extreme in all portions of the survey region. To illustrate this, the maxi-

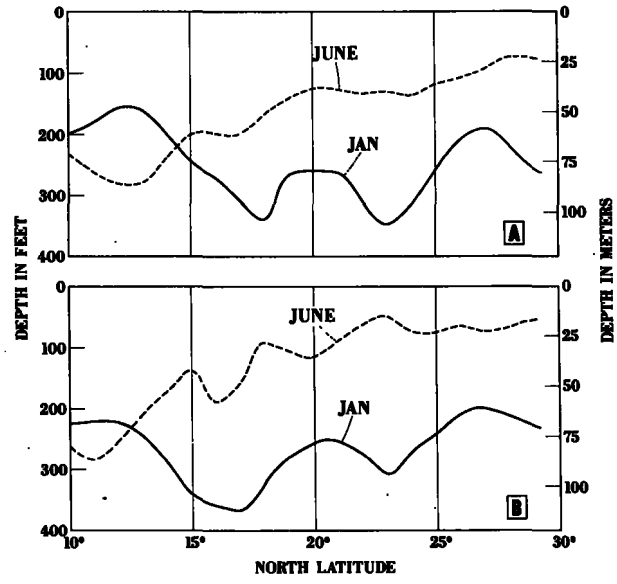

FIGURE 2.— Meridional profile of the depth of mixed layer in January and June, 10° to 30° N. Panel A, 153°–161° W.; panel B, 168°–176° W.

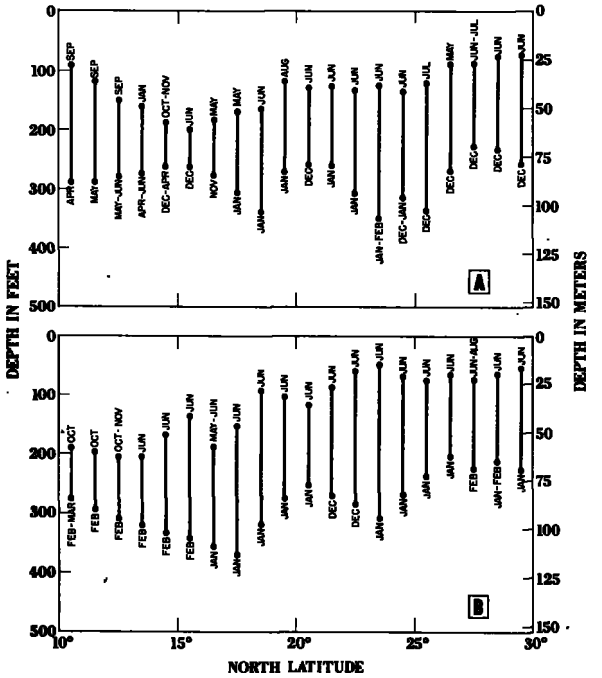

FIGURE 3.—Minimum and maximum mean depth of mixed layer 10° to 30° N. Panel A, 153°–161° W.; panel B, 168°–176° W.

mum and minimum depth of mixed layer has been indicated in figures 3A and B, together with the month of occurrence. These figures also indicate the annual depth range both in the eastern and western portion of the survey region between 10° and 30° N.

In figure 3A, for the eastern section, one notes that south of 14° N. the extremes in depth of the mixed layer occur in spring and autumn, whereas north of 15° N. they occur at the beginning of winter and summer. This suggests that the area south of about 14° N. belongs to a region with a different oceanographic climate, where extremes in the depth of the mixed layer follow those to the north of 14° N. by approximately three months.

Figure 3A also shows that the maximum difference in the average depth of the mixed layer between summer and winter is 220 feet (67 m.) and occurs at 23° N. The minimum difference occurs, as might be expected, at the nodal point, 15° N., where it is about 60 feet (18 m.). At 10° N. the seasonal range is again 200 feet (61 m.).

In the western section, figure 3B, the boundary between the two climatic regions lies at approximately 13° N. during the minimum depth of the mixed layer period. South of this latitude the minimum occurs in October (one month later than in the eastern section) and north of this latitude in June. During the maximum depth of the mixed layer period, the boundary is less distinct. At 10° N. the maximum occurs during February–March, between 11° and 15° N. in February, and north of 15° N. it occurs in January. This suggests that the boundary which separates the two climatic regions at 13° N. during the minimum depth of the mixed layer period, has shifted southward during the maximum depth of the mixed layer period. That is, in winter the western portion of the region between 10° and 30° N. lies within the same oceanographic climate.

Figure 3B also shows that the maximum difference in the average depth of the mixed layer between summer and winter is about 260 feet (79 m.) at 23° N., as in the eastern section. The minimum difference is about 90 feet (27 m.) at 10° N. Although a node is indicated between 12° and 13° N. in figure 2B, the minimum difference in the summer and winter depth of mixed layer did not occur at this latitude because of the apparent seasonal motion of the climatic boundary.

The mean seasonal variation in the depth of the mixed layer at 12°, 18°, 20°, and 22° N. in the meridinal storip between 153° and 161° W., is illustrated in figure 4. Comparison of the data for 12° N. with those to the north indicates the phase difference in extremes. It also shows that in the vicinity of the high islands of the Hawaiian archipelago the seasonal range in the depth of the mixed layer is less than that to either the north or south. Finally, figure 4 shows the seasonal variation in the depth of the mixed layer for the vicinity of 27° N. and 175° W. Here the depth decreases at a time (Dec. and Jan.) when it approaches the maximum throughout the northern portion of the region.

2. SURFACE TEMPERATURE

In oceanography as well as in weather analysis, temperature has long been recognized as an important climatic character. Surface temperature charts of the oceans, such as the U.S. Navy Hydrographic Office, Monthly Surface Temperature Charts of the North Pacific Ocean, (Misc. No. 10577), are readily available. A standard reference in oceanography is the temperature charts of Schott (1935). A new set of monthly temperature charts (appendix B, chart II) have been pre-

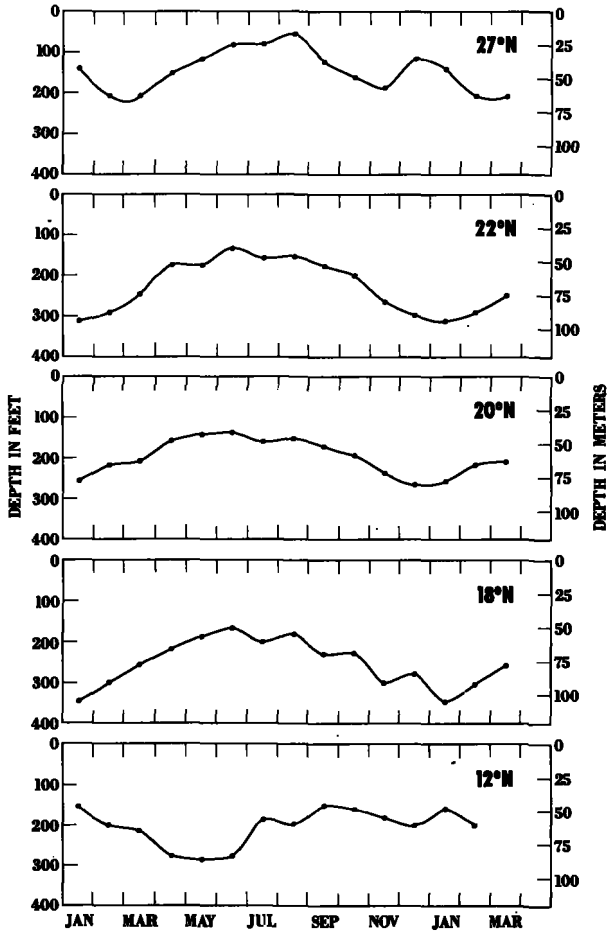

FIGURE 4.—Seasonal variation of the depth of the mixed layer at 12°, 18°, 20°, and 22° N., 153°–161° W., and at 27° N., 175° W.

pared for the Hawaii region, using the same bathythermograms mentioned in the previous section. Treatment of these data, and the manner of construction of the charts is discussed in appendix A.

The introductory comments of the previous section dealing with the distribution of the depth of the mixed surface layer also apply here. Attention will therefore again be focused on gross features in the distribution of the surface temperature rather than the details of individual contours. For example, if the irregular isotherm pattern to the southeast of the island chain in winter (chart II) were to be smoothed, the average temperature and its distribution would correspond well with the charts of Schott (1935) and those of the U.S. Hydrographic Office. It is believed, however, that these irregularities, persisting for several months, reflect large-scale mixing processes or eddies which may be real in nature.

Scanning the temperature charts one notes a parallel isotherm structure north of the island chain between November and April, with a latitudinal temperature gradient in the order of 1° to 1.5° F. (0.6° to 0.8° C.) per degree of latitude. In May, the beginnings of a change in the temperature structure become apparent, followed by the breakdown of the parallel isotherm pattern in June. The irregular temperature structure persists in the northern section of the region throughout July, August, and September, until, in October, isotherms become parallel again.

To the south of the island chain, the temperature structure is irregular during the winter and spring months. The temperature pattern from December through March, between 160° and 165° W., is suggestive of large-scale mixing processes or eddies.

The July, August, and September distributions show tongue-shaped areas of low temperature protruding westward in the southern portion of the region. Then, during October and November, it appears as if these tongues, between 155° and 165° W., were given a counterclockwise, 90° rotation, followed by disintegration into the irregular winter pattern.

The charts also show that minimum and maximum temperatures generally occur in March and September. In some areas, the minimum may occur in February and the maximum in either August or October. For these exceptions, however, the temperatures differ little from those in March and September. The March and September mean temperature profiles in figures 5A and B for the meridional strips between 153° to 161° W. and 168° to 176° W. therefore represent those for minimum and maximum temperature conditions.

During March, the temperature in the eastern section of the survey region (fig. 5A) decreases from about 78° F. (25.6° C.) at 10° N. to 75° F. (23.9° C.) at 17° N., at a rate of a little more than 0.4° F. (0.2° C.) per degree of latitude. After a slight increase of temperature just to the south of the Hawaiian Islands (also see chart II, March), the temperature decreases again northward to about 67° F. (19.4° C.) at 29° N., at an average rate of 1° F. (0.6° C.) per degree of latitude.

In the western section (fig. 5B), the March

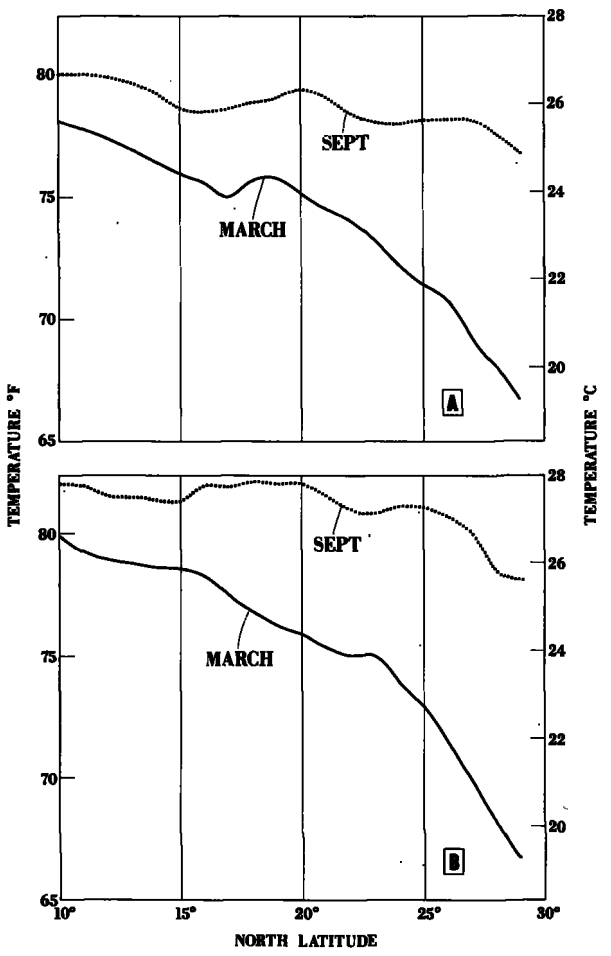

FIGURE 5.—Meridional profile of the surface temperature in March and September, 10° to 30° N.: panel A, 153°–161° W.; panel B, 168°–176° W.

surface temperature decreases in three distinct steps from 80° F. (26.7° C.) at 10° N. to 67°F. (19.4° C.) at 29° N.: First, between 10° and 16° N. at an average rate of 0.2° F. (0.1° C.) per degree of latitude; then between 16° and 23° N. at 0.5° F. (0.3° C.) per degree of latitude; and, finally, between 23° and 29° N. at 1.5° F. (0.8° C.) per degree of latitude.

During September, the temperature in the eastern section decreases from 80° F. (26.7° C.) at 10° N. to about 77° F. (25° C.) at 29° N. Equivalent temperatures in the western section are 82° F. (27.8° C.) and 78° F. (25.6° C.). Thus, there is an average decrease of 0.1° F. (0.06° C.) per degree of latitude in the eastern portion of the survey region and slightly more in the western section.

Although the changes in slope of the meridional temperature profiles cannot be explained at this time, they are believed to be of climatic significance. The temperature dips in September at about 15° N. in the eastern profile and about 13° N. in the western profile approximately correspond with the position of the depth of the mixed layer trough.

Finally, figures 5A and B show that the annual temperature range between 10° and 15° N. is approximately 2.5° F. (1.4° C.) both in the eastern and western section of the region. This increases to about 10.5° F. (5.8° C.) and 11.5° F. (6.4° C.) at 29° N. in the eastern and western sections, respectively, which is in good agreement with the charts of Schott (1935).

The mean zonal temperature profiles for 10° to 15° N., 15° to 20° N., 20° to 25° N. and 25° to 30° N, for March and September are shown in figure 6. For these months the temperature is approximately 3° F. (1.7° C.) higher in the western than in the eastern part of the region, except during September for the 15° to 20° N. and the 20° to 25° N. profiles, where the increases are 4° F. (2.2° C.) and 5° F. (2.8° C.), respectively.

Figure 6 also shows that the westward increase of temperature is not always gradual as it is between 25° and 30° N. during September, and between 20° and 25° N. during March. Between 15° and 20° N. it is stepwise both during March and September. Here, proceeding westward to about 157° W., the temperature decreases slightly and, then, during March, rises rapidly and remains fairly constant west of 160° W. During September, the temperature tends to continue the westward increase in a stepwise manner.

Between 10° and 15° N. the temperature again shows an initial westward decrease and, then, during March, an increase west of 160° W. During September, there is an increase west of 157° W., followed first by a leveling off and then another westward rise.

Between 20° and 25° N. the September westward temperature rise occurs mostly between 157° and 166° W. Thus, this temperature slope and those found in the eastern portion of the two profiles 10° to 15° N. and 15° to 20° N. may be of climatic significance, possibly delineating boundaries between climatic regions.

Finally, figure 7 has been included to show the seasonal temperature variation between 153°

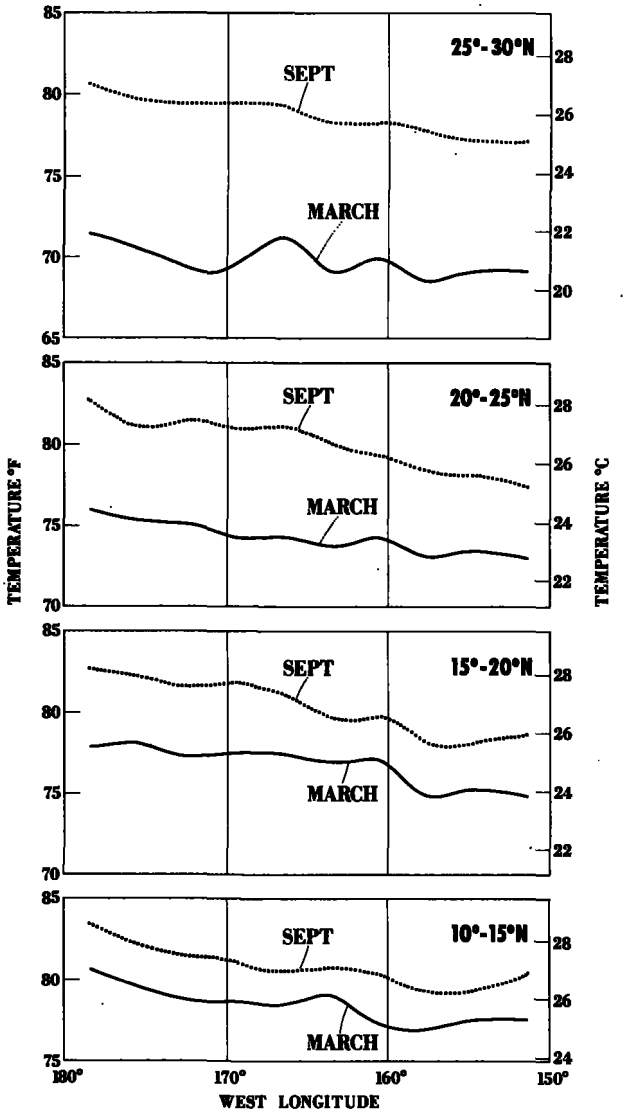

FIGURE 6.—Zonal profile of the surface temperature in March and September, 10°–15° N., 15°–20° N., 20°–25° N., 25°–30° N. and 150° W. to 180°.

and 161° W. at 12°, 17°, 20°, 22° and 26° N. It illustrates features which were demonstrated in previous figures. The seasonal temperature range increases only slightly northward from 3° F. (1.7° C.) at 12° N. to 5° F. (2.8° C.) at 22° N., and then almost doubles to 9.5° F. (5.3° C.) at 26° N. This is also reflected in the break of the meridional temperature gradient at 22° N. from November to May.

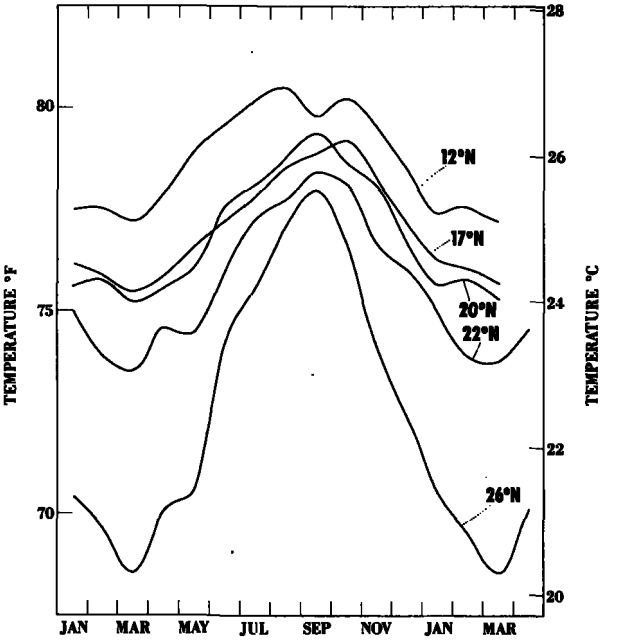

FIGURE 7.—Seasonal variation of the surface temperature at 12°, 17°, 20°, 22° and 26° N. between 153° and 161° W.

3. SURFACE SALINITY

The climatic indicator equivalent in importance to the temperature is the salinity. Unfortunately, in comparison with the temperature information, salinity data are scarce and it is therefore not possible to construct meaningful monthly charts. Despite this shortcoming, salinities obtained from oceanographic expeditions and from surface samples collected by Bureau of Commercial Fisheries vessels are sufficient to indicate features of climatic significance.

An attempt was made initially to locate the 35°/oo (salinity) isopleth throughout the year in the vicinity of the Hawaiian archipelago. This revealed that the isopleth started a generally northward movement in April, reaching an extreme position in July, as indicated in figure 8. It then begins a southward movement, reaching its extreme winter position (17° to 19° N.), during the November to February period. In the Hawaiian Islands the maximum salinity is therefore to be expected during November to February and the minimum during July.

There were also enough samples to show (fig. 9) the mean seasonal variation of salinity in the meridional strip between 155° and 160° W., at

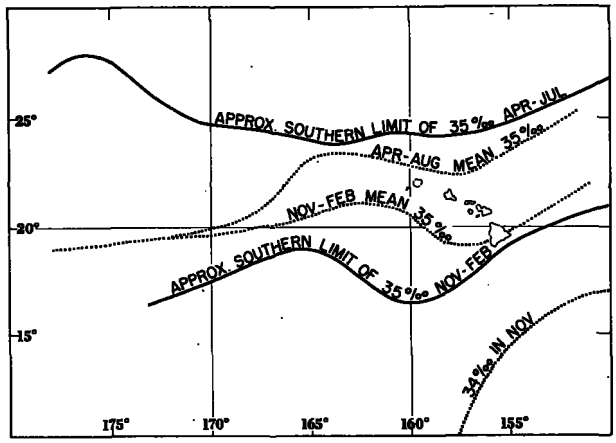

FIGURE 8.—Southern limit of the 35 °/₀₀ salinity isopleth April to July and November to February, and mean location of the 35 °/₀₀ salinity isopleth April to August and November to February.

13° N., 16° N., 21° N., 26° N., and the approximate salinity variation in the vicinity of Midway Island (28° N., 177° W.). Both at 16° N. and at 26° N. the minimum occurs during March and April, whereas at 21° N., within the island area, it occurs in July. The maximum salinity at 16° N. occurs during November and at 26° N. during November and December, whereas at 21° N. it occurs sometime during December, January, or February. The movement of the 35°/₀₀ isopleth, therefore, coincides with the minimum and maximum salinity period at 21° N., but is out of phase with those to the north and south of the islands.

At 13° N. the salinity reaches a maximum in September and then in October begins to decrease rapidly, reaching a minimum in November. In the Midway Island region, beside the double maximum and minimum, the rapid decrease in salinity from a maximum between May and June to a minimum in July should be noted.

Finally, figure 9 shows that the seasonal salinity range is .50°/₀₀, .35°/₀₀, .25°/₀₀ and .45°/₀₀ at 13°, 16°, 21° and 26° N., respectively. At 21° N. it is therefore approximately 50 percent of that either at 13° N. or 26° N.

The salinity distribution between 155° and 160° W. can be illustrated further by meridional profiles. The lack of observations made it necessary to group the data for a number of months during the minimum and maximum salinity period at 21° N. Figure 10 shows the mean salinity profiles for April through August and for November through February.

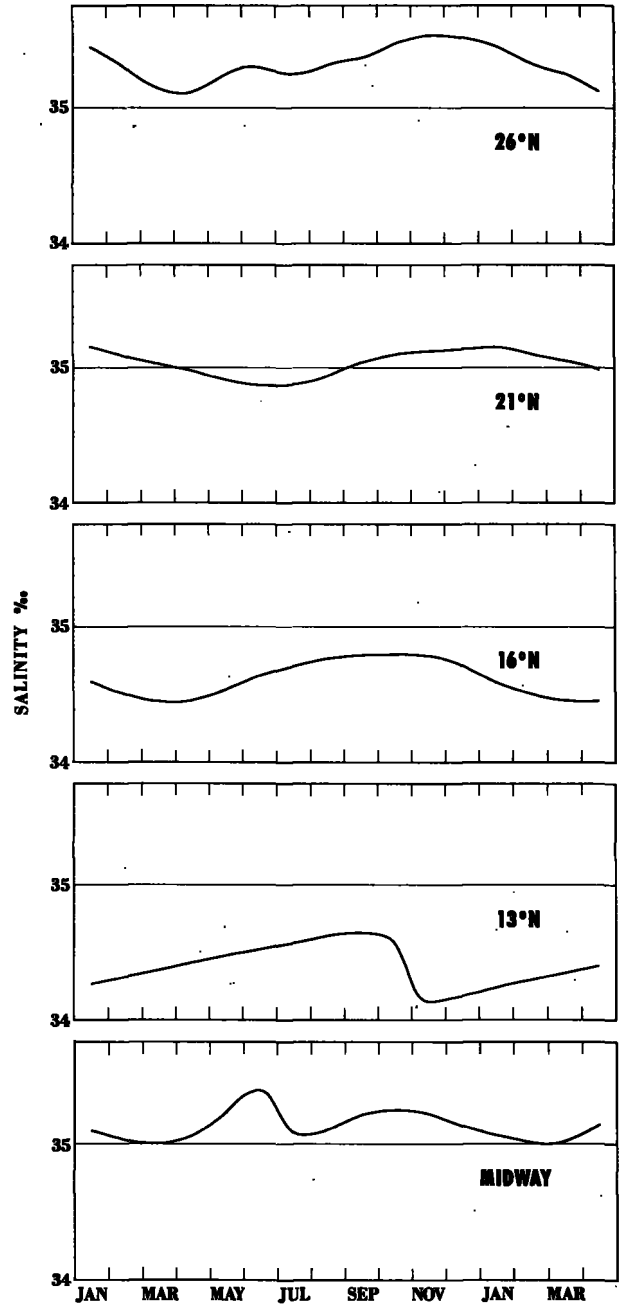

FIGURE 9.—Seasonal variation of the surface salinity at 13°, 16°, 21°, 26° N., between 155° to 160° W., and in the vicinity of Midway Island.

The low salinity profile (fig. 10A), representative of the June distribution, shows that the salinity increases northward from 34.65°/₀₀ at 10° N. to 34.75°/₀₀ at 20° N., or only by an average of .01°/₀₀ per degree of latitude. The salinity then

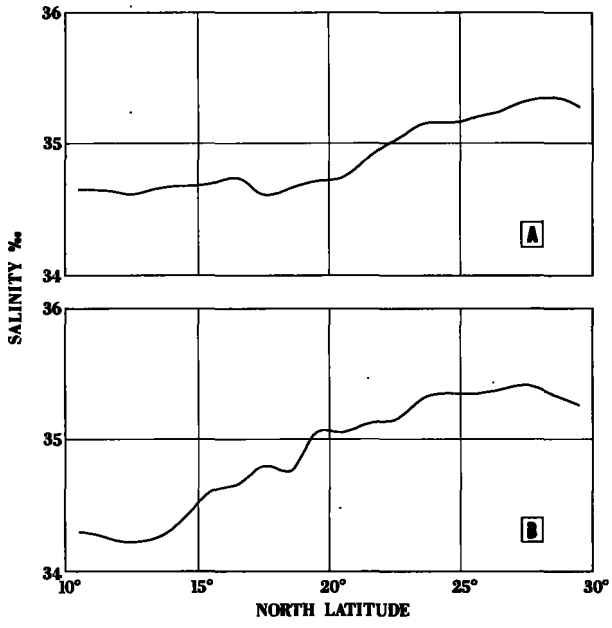

FIGURE 10.—Mean meridional salinity profile 10° to 30° N. between 155° and 160° W. Panel A, April to August; panel B, November to February.

rises at an average rate of .13°/oo per degree of latitude to 35.15°/oo at 23° N. It then increases to the maximum of 35.35°/oo at about 28° N., at a rate of .04°/oo per degree of latitude. Of importance here is the high salinity gradient within and slightly to the north of the Hawaiian Islands. This is indicative of a transition zone or boundary between different types of water. Data from individual months indicate that this boundary also moves seasonally with the previously described 35°/oo isopleth, with which it is closely associated.

During the winter months or high salinity period in Hawaii (fig. 10B), the salinity decreases from 34.3°/oo at 10° N. to a minimum of 34.2 °/oo at 12° N. and then increases rapidly to 35.05°/oo at 19° N., at an average rate of .12°/oo per degree of latitude. North of 19° N. the salinity continues to increase to its maximum of 35.4°/oo at about 27° N., at an average rate of .04°/oo per degree of latitude. Of interest here is the southward shift of the high salinity gradient to south of 19° N. and the salinity decrease at 12° N. from 34.65 °/oo during the April to August period to 34.2°/oo during the November to February period.

Finally, two salinity charts were constructed (appendix B, chart III). Data were again grouped as above into the April to August and November to February periods. The charts will therefore reflect distributions for high and low salinity periods within the main islands area, but not for high and low periods for the remainder of the region.

Presenting data for groups of months reduces the differences in the distribution between months of extreme conditions. For example, figure 8 shows that the extreme positions of the 35°/oo isopleth, corresponding to the months of July and January, are located farther apart than the equivalent isopleth on chart III. This is particularly so in the western portion of the region, where the mean April to August position of the 35°/oo isopleth does not indicate its brief northward movement during July and August.

Despite this shortcoming, the charts provide information about the salinity distribution in the vicinity of Hawaii. During the April to August period the high salinity gradient between 20° and 25° N. is well defined in the eastern half of the region. Another high salinity gradient is indicated in the southeast corner of the region. Of particular interest is the appearance of two cells in which the salinity is higher than 35.4°/oo. A portion of one is located in the northeast corner and the other in the northern half of the region west of 172° W.

The salinity distribution for the November to February period when compared to the April to August distribution, suggests that the salinity gradient in the southeast corner of the region has moved northwestward and the gradient formerly in the Hawaiian Islands area has shifted southward. These then combined to form the more or less continuous salinity gradient illustrated in figure 10B.

In the northern portion there is now only one cell of high salinity (>35.4°/oo), which extends westward from about 157° W. This may mean that either the two high salinity cells of the April to August period have combined to form one, or that both have shifted eastward or westward, so that only one cell is apparent. Data collected by the Bureau of Commercial Fisheries during January to March, 1954 (McGary and Stroup, 1956: 55), suggest that the former is the case.

Reviewing the various fragments of information, one notes that to the north and south of the Hawaiian Islands low and high salinities occur approximately at the same time as low and high

temperatures. In the vicinity of the islands, however, low and high salinities occur about three months later and at a time of minimum and maximum depth of the mixed layer. One also notes that the low salinities in the southeast portion of the region occur in the fall, approximately where the depth of the mixed layer distribution suggests a different oceanographic climate.

Finally, Midway Island is located in the vicinity of the salinity maximum, so that the sharp decline of about 0.35 °/₀₀ during July may be due to either a southward or a northward displacement of the high salinity cell. On the basis of chart III and figure 8 however, keeping in mind the scarcity of observations, the following postulate is favored: during the spring, the high salinity boundary moves northward east of 165°W. and northwestward west of this meridian, reaching Midway Island in July.

4. THE GEOPOTENTIAL TOPOGRAPHY

A fourth feature of importance in climatology is the geopotential topography, which is analogous to the pressure distribution in meteorology in that it provides a measure of the geostrophic currents. Again, data are inadequate to construct monthly charts. There have been no oceanographic expeditions to survey, as a primary objective, the region under investigation here. Dynamic height data have therefore been obtained chiefly from the Bureau of Commercial Fisheries Biological Laboratory (Honolulu) cruises in transit to other regions and from isolated expeditions passing through the area. Since potential gradients, rather than absolute values of dynamic height, are of importance in estimating geostrophic currents, combining isolated observations at different times of the year and from different years may result in charts materially different from the true flow pattern. Nevertheless, on the basis of availability and compatibility, data for the months of June through October and those for the months of December through April were combined into a summer and winter chart (appendix B, chart IV) to enable the reader to estimate the gross distribution of geopotentials.

The summer chart indicates that the subtropical convergence is approximately at 24° N., rather than at 31° N. as indicated by Schott (1935). It also shows that, as compared to the flow in the southeast portion of the region and that just south of the convergence between 158° and 170° W., there is a broad band of weak westerly flow to the southwest of the islands. Comparing the summer chart with the April to August salinity chart (chart III), one notes that the featureless geopotential distribution to the southwest of the islands corresponds with an equally featureless salinity distribution, both bounded by higher gradients to the northwest and southeast. It should be remembered that the combined data of the salinity chart are 2 months out-of-phase with those of the geopotential chart.

During the winter months, the subtropical convergence, as indicated in chart IV, (December to April) again lies to the south of the latitude indicated by Schott. In general, the area north of 20° N. appears to be one of very little net flow. In the southern portion of the region there is a large counterclockwise vortex centered at approximately 14° N. between 160° and 170° W. This feature was first apparent in data from *Hugh M. Smith* cruise 2, February 1950 (Cromwell, 1951, fig. 3) and occupies approximately the same area as the dome in the depth of the mixed layer during February (chart I).

Thus, although the geopotential topography as presented here should be regarded with caution, compatibility of special features, both with the salinity and the depth of mixed layer distributions, lends credibility to these charts.

PART II. PHYSICAL PROCESSES AND THEIR RELATION TO THE DISTRIBUTION OF SURFACE VARIABLES

In the first section of this atlas, patterns of distribution and regular periodic changes in the fields of temperature, salinity, depth of mixed surface layer, and geopotential were described. These features are associated to a varying degree of complexity with physical processes.

The importance of one or another process is usually not intuitively apparent. For example, the temperature of the water obviously depends on the heat exchange across the sea surface and the depth through which this is distributed, the manner in which heat is transported by currents,

619237 O—62——3

and other processes. It is not obvious, however, which one or combination of these factors determines the temperature of the water at any time or place. In order to gain an understanding of the physical processes, then, or to assess their relative importance, the problem must be formalized in accordance with principles discussed by Sverdrup et al. (1942). Here some of these principles will be applied to the distribution of the surface temperature, a variable of importance in any climatic study.

1. HEAT (SALT) BUDGET

On the basis of conservation of heat one can say that, at any locality in the ocean, the net heat exchange across the sea surface must be balanced by the change in heat content of the water column, heat diffused through the sides of the column, and the heat carried in or out of the column by means of currents. Such an expression can become complicated. However, since this is a climatic study, interest lies in the gross seasonal changes and, therefore, some simplifying assumptions can be made for the Hawaiian region (10°–30° N., 150° W.–180°).

In this area the mixed surface layer is generally well defined and since it has neutral stability one can say that heat exchange across the sea surface is uniformly distributed throughout this layer. Further, because of high stability in the thermocline just below the mixed layer, and small horizontal temperature gradients, vertical and lateral diffusion are assumed negligibly small compared to advection and heat exchange across the sea surface.

With these assumptions, a simple heat budget can be formulated in which the rate of change of heat content of a column of water of unit cross sectional area is balanced by the net heat exchange across the sea surface and the heat transported in and out by currents. This can be expressed in vector notation by

$$\frac{\partial(\rho c_p \theta z)}{\partial t} = H - \nabla\cdot(\rho c_p \theta z \overline{V}) \qquad (1)$$

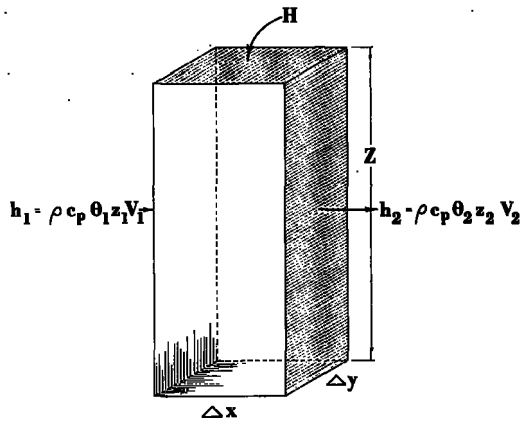

Here ρ is the density of the water and c_p its specific heat; θ is the temperature, z, the depth of the column of water (depth of mixed surface layer), and $\overline{V}$, the horizontal velocity. H is the net heat exchange across the sea surface and ∇, the two-dimensional operator

$$\bar{i}\frac{\partial}{\partial x} + \bar{j}\frac{\partial}{\partial y}$$

Similarly, the volume budget of the column of water is expressed by

$$\frac{\partial z}{\partial t} = -\nabla\cdot(z\overline{V}) \qquad (2)$$

Equations (1) and (2) can be expanded as follows, considering ρ and c_p constant:

$$z\frac{\partial\theta}{\partial t} + \theta\frac{\partial z}{\partial t} = \frac{1}{\rho c_p}H - \theta z\nabla\cdot\overline{V} - \theta\overline{V}\cdot\nabla z - z\overline{V}\cdot\nabla\theta \qquad (3)$$

$$\frac{\partial z}{\partial t} = -z\nabla\cdot\overline{V} - \overline{V}\cdot\nabla z \qquad (4)$$

After multiplying equation (4) by θ it can be subtracted from (3), leaving

$$z\frac{\partial\theta}{\partial t} = \frac{1}{\rho c_p}H - z\overline{V}\cdot\nabla\theta \qquad (5)$$

and then dividing by z, the temperature budget for a unit mass of surface water becomes:

$$\frac{\partial\theta}{\partial t} = \frac{1}{\rho c_p}\frac{H}{z} - \overline{V}\cdot\nabla\theta \qquad (6)$$

This equation is similar to equation V,5 in Sverdrup et al. (1942), except that the diffusion terms have been replaced by the heat exchange as a result of the simplifying assumptions.

Equation 6 can be divided into two portions: the term representing the temperature observations, and the terms representing the physical processes which determine the temperatures. Thus $\frac{\partial \theta}{\partial t}$, the local time change of temperature, represents the observed effect of those processes which appear on the right side of the equation.

The first one of these is associated with the net heat exchange across the sea surface, H. This is modified by the depth through which it is distributed, the density, and specific heat of the water, to appear as it affects the temperature of the water, in terms of temperature per unit mass per unit time, $\frac{1}{\rho c_p}\frac{H}{z}$.

The second term on the right side of equation 6 which affects the water temperature is the process of heat advection. It is an abstract term containing both the horizontal temperature distribution and the velocity and should not be mistaken for the heat transport. In expanded form the heat advection can be written $|V||\nabla\theta|\cos\phi$, i.e., the magnitude of the velocity (the speed) times the magnitude of the temperature gradient times the cosine of the angle between the direction ot the current and the direction of the gradient. Thus, if ϕ is 90°, then the current flows parallel to the isotherms and the heat advection is zero, although the heat transport is not. Other cases where heat advection is zero occur when there are no currents or when there is no temperature gradient. The heat advection, therefore, is simply a process affecting the temperature of the water, here expressed in temperature per unit mass per unit time, resulting from a component of the current perpendicular to the isotherm. Even though the velocity enters into the expression, heat advection, if determined from budget considerations, can never give any information about the component of velocity parallel to the isotherm.

To summarize, the heat budget equation represents the manner in which the association between observed temperatures and physical processes has been formalized. It provides a qualitative appreciation of the processes involved and determines what parameters must be measured and the manner in which they should be measured. For example, it is necessary to obtain time series of observations together with horizontal distributions in order to be able to interpret temperature observations in terms of processes. Furthermore, if an understanding of the seasonal variation of processes is desired, then a plot of the local time change rather than the absolute temperature should be made.

The preceding discussion applies equally well to other parameters. For example, the salt budget equation is

$$\frac{\partial s}{\partial t}=\frac{s}{z}(E-P)-\overline{V}\cdot\nabla s \qquad (7)$$

where s is the salinity, and $E-P$ the evaporation minus precipitation. Here the processes are the water exchange across the sea surface and salt advection.

In the following sections the heat budget considerations will be applied to the Hawaiian region. First, the processes which transpire at the sea surface and affect the surface temperature will be described. These will then be combined with the data of part I to gain some understanding of the advection processes.

2. EVENTS AT THE SEA SURFACE

Events at the sea surface which affect the physical and dynamic properties of the surface water include the net heat exchange across the sea surface, evaporation minus precipitation, and the wind stress. In this part of the atlas, attention will be focused on those processes which affect the distribution of the surface temperature. Therefore, the net heat exchange across the sea surface will be of primary concern. The evaporation minus precipitation will be briefly discussed, omitting wind information which is commonly available in climatic compilations, such as the U.S. Navy Marine Climatic Atlas of the World, vol. II (1956), and others.

A. The Net Heat Exchange Across the Sea Surface

It has long been recognized that the ocean is a vast heat reservoir which has an important role

in determining the climates of the world. Much work has been done to investigate the manyfold problems associated with the energy exchange at the air-sea boundary. A complete review of this research will not be attempted, but such general results as are of interest to this investigation may be found in Sverdrup et al. (1942) and Jacobs (1951).

Briefly, the processes of concern here are the radiant energy from sun and sky absorbed by the water (Q_s), the radiant energy lost due to back radiation (Q_b), heat energy lost by the processes of evaporation (Q_e), and conduction of sensible heat to or from the water (Q_c). The net heat exchange across a unit area of sea surface per unit of time, H, or the heat available to change the temperature of the water can be expressed by the formula:

$$Q_s - Q_b - Q_e - Q_c = H$$

These terms will now be discussed separately.

After entering the atmosphere, solar radiation is modified by scattering and absorption so that Q_o represents the energy reaching the earth's surface with a clear sky. Not all of this energy is absorbed by the water because of reflection, and further reduction may have occurred because of cloud cover. To compute the energy absorbed by the water (Q_s) the following expression has been given by Jacobs (1951):

$$Q_s = (1-r)(1-0.071\ C)Q_o$$

Here r is the percentage reflection and C is the cloudiness on a scale from 0 to 10. Q_s is generally expressed in cal. cm.$^{-2}$ day^{-1}.

Observations for the direct and diffuse solar radiation reaching the earth's surface, Q_o, are not available in the Hawaiian region, so that these values were obtained from the Smithsonian Meteorological Tables, table 135 (List, 1951), using a transmission coefficient $a=0.9$, and have been plotted in figure 11. At 10° N. the seasonal range of Q_o is 140 cal. cm.$^{-2}$ day^{-1}; from 640 cal. cm.$^{-2}$ day^{-1} in December to 780 cal. cm.$^{-2}$ day^{-1} in summer. At 30° N. the seasonal range is 460 cal. cm.$^{-2}$ day^{-1}; from 400 cal. cm.$^{-2}$ day^{-1} in December to 860 cal. cm.$^{-2}$ day^{-1} in June. It should also be noted that from April to September the difference between Q_o at 10° N. and at 30° N. is less than 100 cal. cm.$^{-2}$ day^{-1}, whereas in December this difference is 240 cal. cm.$^{-2}$ day^{-1}.

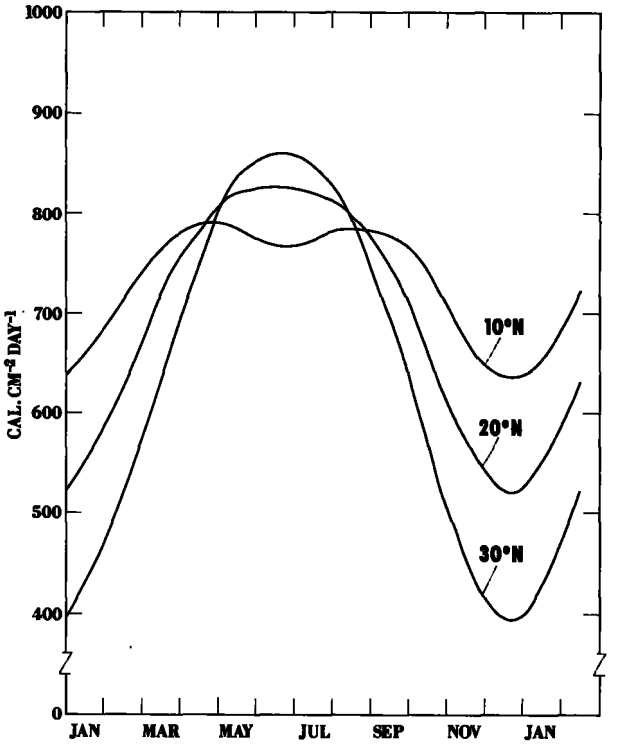

FIGURE 11.—Seasonal variation of the direct and diffuse solar radiation reaching the earth's surface at 10°, 20°, and 30° N.

On the basis of these data, even though the direct and diffuse radiation will be modified by factors, such as back radiation and evaporation, one would anticipate the following effects on the surface water temperature: (1) the seasonal temperature range increases northward, and (2) the water temperature difference between 10° N. and 30° N. would be greatest during the minimum temperature period of the year.

In order to use Jacobs' formula, the cloud cover, which ranges from four- to six-tenths of sky covered in the Hawaii region, was obtained from the U.S. Weather Bureau Atlas of climatic charts of the ocean (McDonald, 1938). The amount of radiation reflected back to the sky was quoted by Jacobs (1951) to range from 3.3 percent at the equator to 8 percent at the poles. With these data and Q_o from the Smithsonian tables, the amount of radiation absorbed in the water, Q_s, was computed.

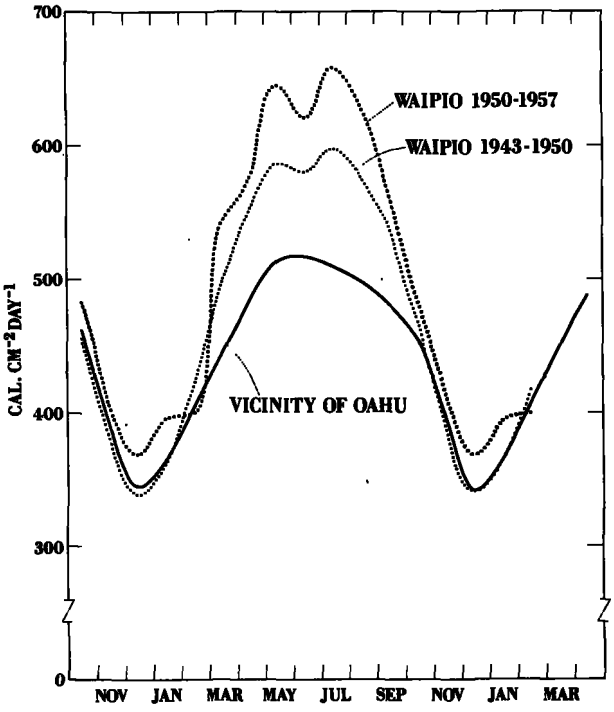

FIGURE 12.—Amount of computed radiation absorbed by the water (Q_s) in the vicinity of Oahu, and measured radiation reaching the surface at Waipio, Oahu, mean 1943–50, and mean 1950–57.

Figure 12 shows the results of this computation for the vicinity of the island of Oahu. The heat absorbed by the water ranges from 340 cal. cm.$^{-2}$ day^{-1} in December to 510 cal. cm.$^{-2}$ day^{-1} in June. Comparable values for a clear sky at 20° N. (fig. 11) are 520 cal. cm.$^{-2}$ day^{-1} and 830 cal. cm.$^{-2}$ day^{-1}, respectively. In the vicinity of the Hawaiian Islands, cloud cover, therefore, reduces the insolation by about 35 to 40 percent.

Although no direct measurements of Q_s for the marine vicinity of Oahu are available, the radiation reaching the surface has been measured at Waipio (near Pearl Harbor), Oahu, by the Sugar Planters Association and the Pineapple Research Institute of Hawaii. The mean data for the years 1943 to 1950 and 1950 to 1957 have been plotted in figure 12.[3]. The mean observed solar radiation from November through February for the 1943–50 period is approximately the same as that computed for the vicinity of Oahu. During the remainder of the year, the computed values are up to 80 cal. cm.$^{-2}$ day^{-1} (about 15 percent) too low. The mean observed values for the 1950–57 period are about 30 cal. cm.$^{-2}$ day^{-1} higher in winter and up to 140 cal. cm.$^{-2}$ day^{-1} (about 25 percent) higher in summer than the computed values. In other words, the computed insolation values are of the right order of magnitude, in good agreement with observed values during the winter, but 15 to 25 percent too low during the summer.

The seasonal discrepancy between the computed and observed insolation can be explained in several ways. During the winter months medium and high clouds are an important part of the cloud cover, whereas during the remainder of the year trade wind cumuli predominate. First, then, the discrepancy may be due to seasonal variations in the difference between the cloudiness over Waipio, located on the leeward side of the island, and that over the ocean, since orography would affect low tradewind cloudiness more than medium and high cloudiness. In addition the cloud correction formula may be sufficiently accurate for the medium and high cloudiness during the winter, but not for the trade wind cumuli in summer. Since cloud cover is observed obliquely from a ship, there is a tendency to overestimate cover of the latter type. Furthermore, the formula used above does not take into consideration the reflection from trade wind cumuli.

The next term to be considered in the net heat exchange across the sea surface is the back radiation. This is a function of the absolute surface temperature of the sea, radiating almost like a black body, the relative humidity, and the type and amount of the cloud cover. According to Sverdrup et al. (1942:112) back radiation can then be expressed by

$$Q_b = Q_{bo}\ (1 - 0.083C).$$

This applies to average conditions only, since the reduction of the effective back radiation, Q_{bo}, due to clouds depends upon the altitude and the density of the clouds. C is the cloudiness on the scale from 0 to 10.

The necessary data to compute the back radiation were obtained from the Atlas of Climatic Charts of the Ocean (McDonald, 1938) and from Sverdrup et al. (1942: fig. 25). Back radiation in the Hawaiian region ranged from 115 to 150 cal. cm.$^{-2}$ day^{-1}, and in the vicinity of Oahu from 130 to 150 cal. cm.$^{-2}$ day^{-1}, with the lower values occurring during spring and summer.

[3] Data were supplied by Dr. Paul C. Ekern, Pineapple Research Institute, Honolulu, Hawaii.

Again, no observations of back radiation are available and, as before, the principal error would be due to an incorrect cloud factor for the trade wind area.

Next in the net heat exchange across the sea surface is the evaporation. Its importance to the net heat exchange can be gauged from the fact that about 585 calories are used to evaporate 1 gram of sea water. No observations for Q_e are available, so that computed values must be used. These are based on formulae described both by Sverdrup and others (1942) and Jacobs (1951). They suggested simplified formulae for use with average climatic data to obtain the evaporation as a function of the sea and air vapor pressure difference and the wind speed. Albrecht (1951) computed the evaporation for the Indo-Pacific using the formula from Sverdrup (1936) and the meteorological data of the revised, 1944, German edition of McDonald (1938). In checking his results by means of the total Indo-Pacific water budget, he estimated the calculated evaporation to be 10 percent too low. Since most meteorological observations at sea are made from merchant ships, Albrecht assumed height-of-bridge (8 m.) for psychrometric observations and masthead (20 m.) for wind observations. By assuming both observations to be made at bridge height (8 m.), the computed evaporation would be 10 percent higher.

For computations of the net heat exchange in this paper, revised evaporation charts, received from Dr. Albrecht in a personal communication, were used. Figure 13 shows the seasonal variation in the heat used for evaporation at 20° N. and

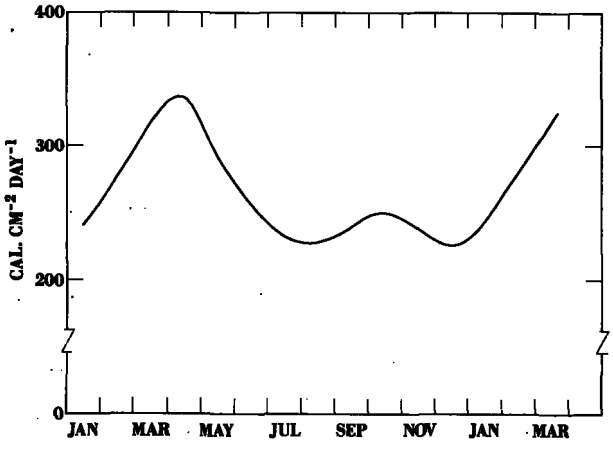

FIGURE 13.—Seasonal variation in the heat used for evaporation at 20° N. and 160° W.

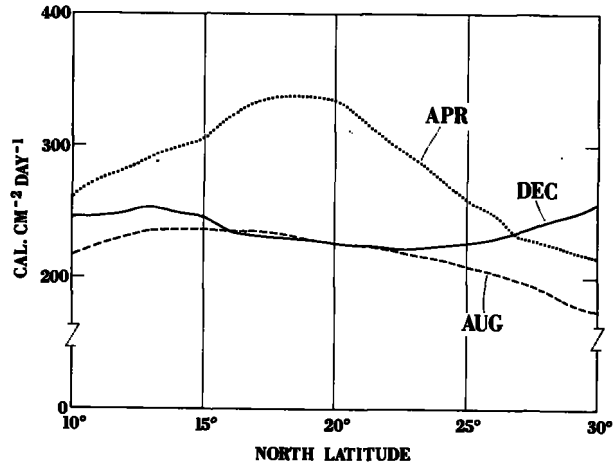

FIGURE 14.—Meridional profiles of the heat used for evaporation, 160° W. during April, August, and December.

160° W. It peaks at about 330 cal. cm.$^{-2}$ day^{-1} in April, with the low evaporation period extending from July to January at 220 to 250 cal. cm.$^{-2}$ day^{-1}.

Meridional profiles of the heat used for evaporation at 160° W. are shown in figure 14. In April, during the maximum evaporation period at 20° N., it is 260 cal. cm.$^{-2}$ day^{-1} at 10° N., 340 cal. cm.$^{-2}$ day^{-1} at 18° N., and 210 cal. cm.$^{-2}$ day^{-1} at 30° N. In August, during the minimum evaporation period at 20° N., it is 220 cal. cm.$^{-2}$ day^{-1} at 10° N., 240 cal. cm.$^{-2}$ day^{-1} at 17° N., and 170 cal. cm.$^{-2}$ day^{-1} at 30° N. In December, the evaporation is 240 cal. cm.$^{-2}$ day^{-1} at 10° N., 220 cal. cm.$^{-2}$ day^{-1} at 22° N., and 260 cal. cm.$^{-2}$ day^{-1} at 30° N.

It should be noted that whereas maximum and minimum periods of evaporation at 20° N. occur in April and August, at 30° N. they occur in winter and summer (December and June), respectively, illustrative of different climatic areas.

Riehl and others (1951) obtained an almost exact heat balance in the atmosphere northeast of Hawaii by using heat equivalents for evaporation based on Jacobs' method of computation. The values based on weather-ship observations during July to October 1945 yielded evaporations of 230 to 250 cal. cm.$^{-2}$ day^{-1} for 26° N., 149° W. and Oahu, respectively. These are in good agreement with Albrecht's results. Although Riehl's values were obtained by essentially the same method as Albrecht's, they do provide an indirect

check in that they also balanced the heat budget of the atmosphere.

The last term to be considered in the net heat exchange across the sea surface is conduction of sensible heat. It is a function of the vertical temperature gradient and turbulence above the sea surface. From Jacobs (1951), one again obtains a simple expression when average climatic data are considered:

$$Q_c = 1.45(\theta_w - \theta_a)\, W_a \text{ cal. cm.}^{-2} \text{ day}^{-1}.$$

θ_w and θ_a are the temperatures in °F. of the sea and air, respectively, and W_a is the wind speed in knots.

In the Hawaiian region, the exchange of sensible heat across the sea surface is not important and ranges from 5 to 40 cal. cm.$^{-2}$ day^{-1}, with the high values occurring during winter months in the northern portion of the region. In the vicinity of the main island group, it ranges from 4 cal. cm.$^{-2}$ day^{-1} in August to 25 cal. cm.$^{-2}$ day^{-1} in February.

To summarize, figure 15 shows the relative magnitude of the terms discussed in this section, as they affect the net heat exchange at 20° N., 100° W. It is apparent that the heat absorbed by the water, Q_s, determines the seasonal pattern of the net heat exchange, H, although this may be modified, as it is during the months centered about April, because of high evaporation rates.

The total rate of heat loss from the sea surface is at a maximum of 490 cal. cm.$^{-2}$ day^{-1} during April and at a minimum of 370 cal. cm.$^{-2}$ day^{-1} during July and August. During the former period, the relative contribution to the total daily heat loss from back radiation, evaporation and conduction is 27 percent, 69 percent, and 4 percent, respectively. During the latter period, these relative losses are 37 percent, 62 percent, and 1 percent, respectively. This illustrates again the importance of evaporation in the net heat exchange across the sea surface.

The relative importance of the terms contributing to the net heat exchange across the sea surface is also illustrated in figure 16 by meridional profiles at 160° W. for June and December. During June (fig. 16A), the rapidly rising net heat exchange north of 19° N. is seen to be due to northward declining evaporation from 260 cal. cm.$^{-2}$ day^{-1} at 19° N. to 130 cal. cm.$^{-2}$ day^{-1} 30° N.

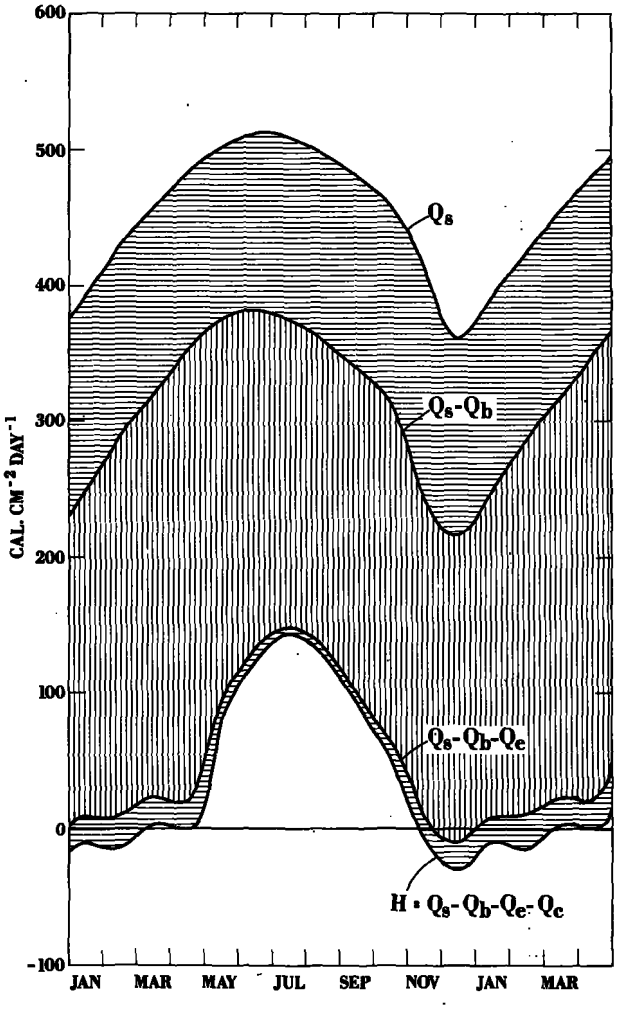

FIGURE 15.—Relative magnitude of the components entering into the net heat exchange across the sea surface at 20° N., 160° W. (Q_s—heat absorbed by the water, Q_b—back radiation, Q_e—heat used for evaporation, Q_c—conduction of sensible heat, H—net heat exchange across the sea surface.)

In December (fig. 16B), the total daily heat loss across the sea surface varies only by about 30 cal. cm.$^{-2}$ day^{-1} between 10° and 30° N.

It is now of interest to know how the net heat exchange affects the surface temperature of the water. According to the basic assumptions of the previous section, the absorbed heat remaining in the water after back radiation, evaporation, and conduction, would be uniformly distributed throughout the mixed layer. Therefore, according to equation 6, one obtains the change of surface temperature per month by dividing the net heat exchange, H, by the depth of mixed

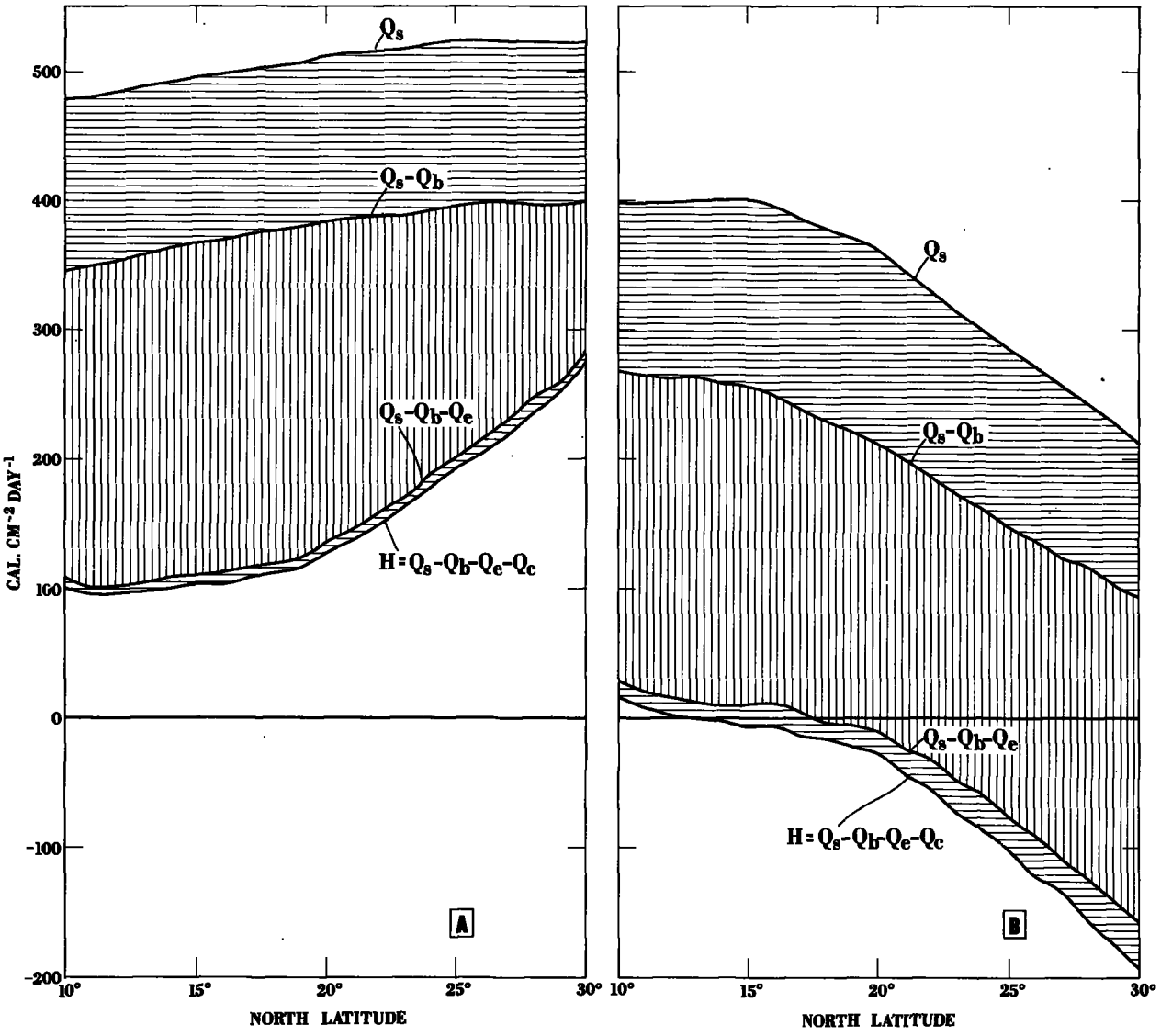

FIGURE 16.—Meridional profiles showing the relative magnitude of the components entering into the net heat exchange across the sea surface at 160° W. Panel A—June, panel B—December. (Q_s—heat absorbed by the water, Q_b—back radiation, Q_e—heat used for evaporation, Q_c—conduction of sensible heat, H—net heat exchange across the sea surface.)

layer, z, the specific heat, c_p, and the density of sea water, ρ.

This is illustrated in figure 17 by the meridional profile of the net heat exchange and the equivalent change of temperature at 160° W. in June and December. For convenience the net heat exchange is presented in units of kilocalories per square centimeter per month (kcal. cm.$^{-2}$ mos.$^{-1}$). At 12° N., for example, the net heat exchange varies from approximately +0.3 kcal. cm.$^{-2}$ mos.$^{-1}$ in December to +3.0 kcal. cm.$^{-2}$ mos.$^{-1}$ in June; a tenfold increase. The effect on the change of surface temperature, on the other hand, varies from about 0.1 °C. mos.$^{-1}$ to 0.3 °C. mos.$^{-1}$, only a threefold increase, reflecting the effect of the seasonal change in the depth of mixed layer at 12° N. (fig. 2).

At 30° N. the net heat exchange varies from about +7.9 in June to −5.9 kcal. cm.$^{-2}$ mos.$^{-1}$ in December. The equivalent change of surface

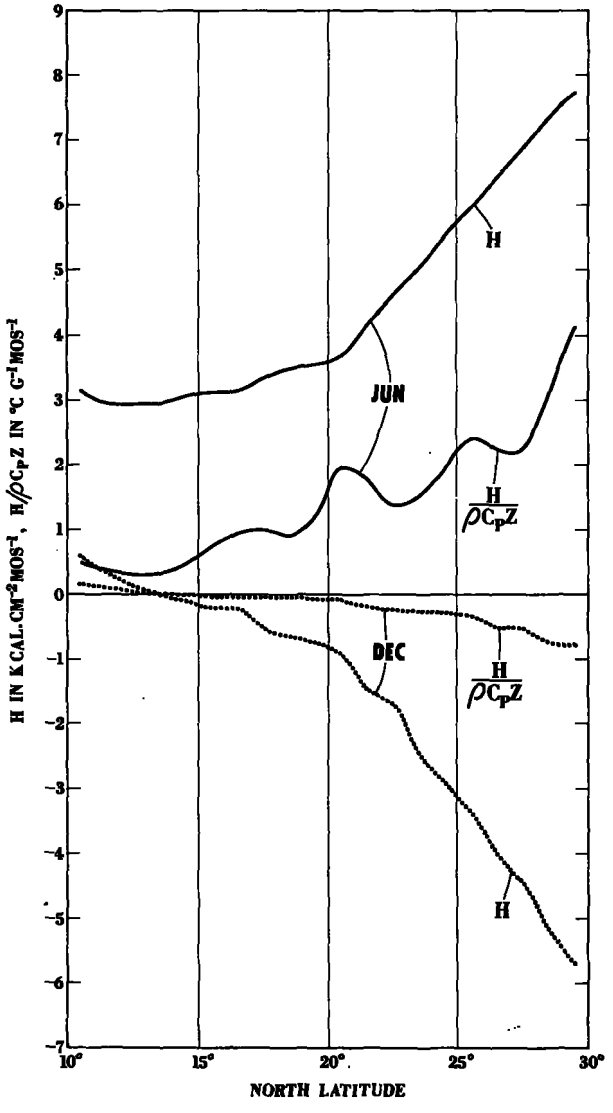

FIGURE 17.—Meridional profile at 160° W. of the net heat exchange and its equivalent rate of change of surface temperature during June and December.

temperature during those months would vary from about +4.5 °C. mos.$^{-1}$ to −1.0 °C. mos.$^{-1}$, respectively, again reflecting the effect of the seasonal change in the depth of mixed layer.

In the surface temperature discussion reference was made to the northward increase in the seasonal temperature range (figs. 5 and 7). For example, at 12° N. it is only 1.7 °C., whereas at 26° N. it is 5.3° C. Figure 17 shows that the seasonal range in the rate of change of temperature attributable to the net heat exchange to be only 0.2° C. mos.$^{-1}$ at 12° N., but 2.7° C. at 26° N. On the basis of the seasonal range of the net heat exchange, one would therefore expect a northward increasing, seasonal temperature range.

In the discussion of figure 7 reference was also made to the break in the meridional temperature gradient at 22° N. during November to May. This was attributed to a boundary of climatic significance. Such a boundary would be one south of which the net heat exchange is positive throughout the year and north of which it is positive during the summer and negative during the winter. Figure 17 shows this to occur at about 13° N. rather than at 22° N. as anticipated from figure 7. Further examination of figure 17, however, shows that the effect of the depth of the mixed layer is such that the monthly temperature change due to net heat exchange, although negative, remains negligibly small (0.1°C. mos.$^{-1}$) to 20° N. Therefore, again on the basis of net heat exchange as expressed in temperature change per month, one would expect the meridional temperature gradient to increase north of 20° N.

To show the mean meridional profile, between 150° W. and 180°, of the net heat exchange and its effect on the change of surface temperature, figure 18 has been included. It is similar to figure 17, except that it shows the net heat exchange to be positive throughout the year south of 18° N. Thus, certain features in the distribution of surface temperature appear to be associated with the net heat exchange across the sea surface.

Finally, the climatic boundary referred to above (where the negative change of temperature due to heat exchange becomes greater than 0.1° C. per month) may be of dynamic and biological significance. In those latitudes where the net heat exchange is always positive, it has a stabilizing influence on the water column throughout the year. To the north of the boundary, where the effect on the temperature decline is no longer negligible, the net heat exchange has a stabilizing effect tending to oppose the effect of wind stirring, during part of the year, and during the remainder of the year, when it is negative, tends to aid the effects of wind stirring by convection.

Biologically this boundary may be regarded as one which separates high and low latitude indices of production. For example, on the low latitude side nutrients in the water and plankton standing

619237 O—62——4

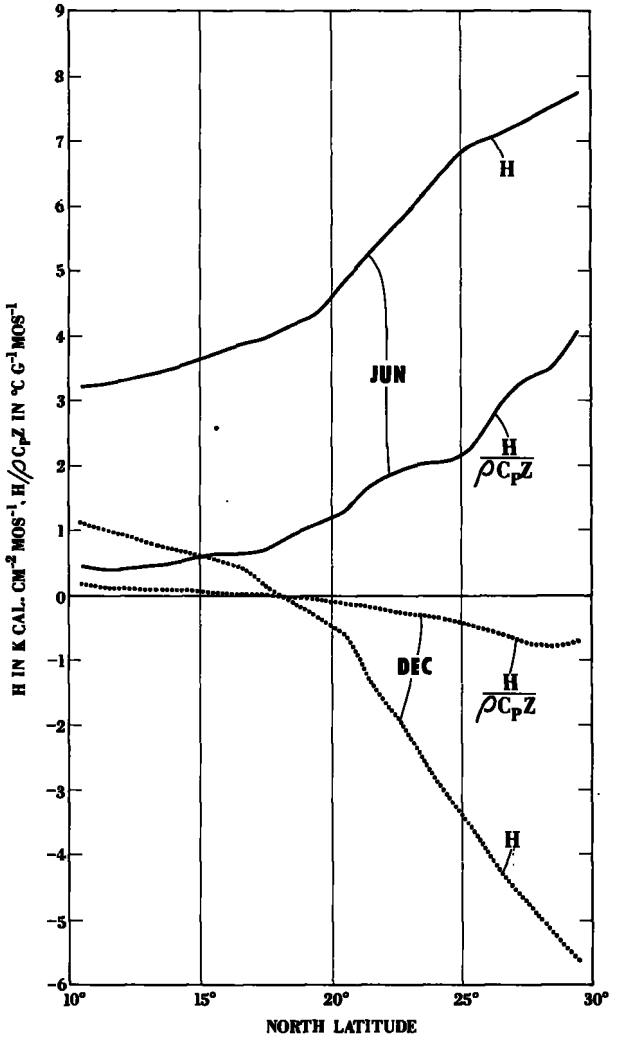

FIGURE 18.—Mean meridional profile (150° W.–180°) for the Hawaiian survey region of the net heat exchange and its equivalent change of surface temperature during June and December.

crops would show small seasonal variations, whereas on the other side these seasonal variations would increase toward higher latitudes.

B. Evaporation Minus Precipitation

The term in the salt budget (equation 7) which would be equivalent to the heat exchange in the heat budget (equation 6) is the freshwater exchange across the sea surface or the evaporation minus precipitation ($E-P$). Evaporation has the effect of increasing the surface salinity and precipitation of decreasing it. Although the salinity data in part I are inadequate for salt budget computations, they are sufficient to warrant a brief discussion of the evaporation minus precipitation.

Albrecht (1951), in connection with the water budget of the Indo-Pacific, computed the precipitation. His work was based on a revision of Schott's (1935) mean annual precipitation charts, McDonald's (1938) charts of frequency of precipitation, and precipitation data from island and coastal stations. Figure 19 shows the seasonal, meridional distribution of evaporation minus precipitation at 160° W., based on the revised charts of Albrecht (1951), received in a personal communication.

The northward progression of the maximum ($E-P$) with time is apparent. At 15° N. it occurs during December, at 20° N. in April and May, and at 28° N. during October. Maximum ($E-P$) is centered about 20° N. and the months about July, when it is higher than 10 cm. per month. Maximum and minimum ($E-P$) at 10° to 15° N. coincides with minimum and maximum

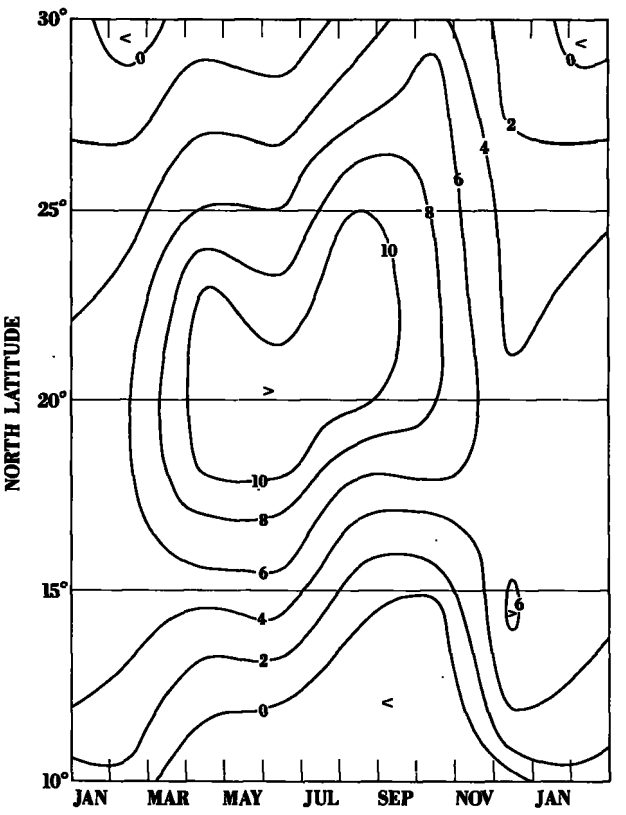

FIGURE 19.—Seasonal evaporation minus precipitation along 160° W. in cm. mos.$^{-1}$.

($E-P$) at 25°–30° N., respectively. An excess of precipitation over evaporation occurs south of 15° N. between March and December, reaching farthest north during September and October. Excess precipitation over evaporation also occurs north of 29° N. in February.

The seasonal variation of ($E-P$), together with the variation of evaporation as plotted in figure 20 for 20° N. 160° W., illustrates the manner in which precipitation modifies the evaporation. The precipitation is approximately 1.2 cm. mos.$^{-1}$ in July and 7.2 cm. mos.$^{-1}$ in December and January.

Meridional profiles of ($E-P$) and evaporation at 160° W., illustrating the modifying effect of precipitation, are shown in figure 21. In April, at the time of maximum evaporation at 20° N., the minimum precipitation of 4.8 cm. mos.$^{-1}$ occurs at 22° and 23° N. It increases northward to 10 cm. mos.$^{-1}$ at 30° N. and southward to 16 cm. mos.$^{-1}$ at 10° N. In August precipitation is essentially lacking between 21° and 24° N., but it increases northward and southward to 6 cm. mos.$^{-1}$ at 30° N. and 16.4 cm. mos.$^{-1}$ at 10° N. Finally, in December, the time of maximum ($E-P$) at 15° N., minimum precipitation of 7 cm. mos.$^{-1}$ has shifted southward along the meridian to 16° N., with 12.4 cm. mos.$^{-1}$ and 10.6 cm. mos.$^{-1}$ at 30° and 10° N., respectively.

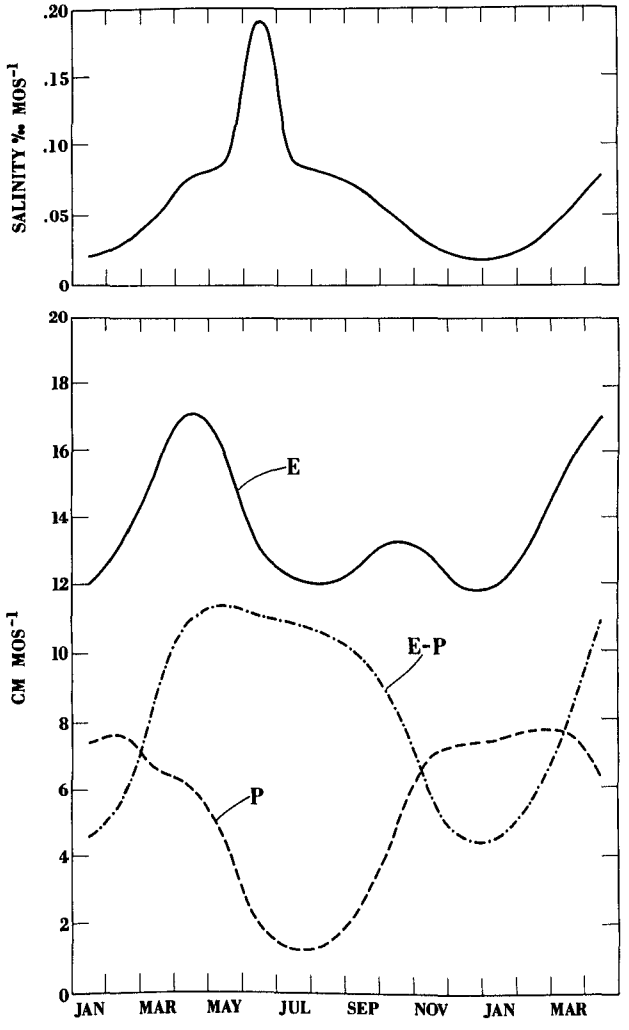

FIGURE 20.—Seasonal variation at 20° N., 160° W., in the rate of evaporation, precipitation, evaporation minus precipitation and equivalent salinity change per month (upper panel).

In order to illustrate the effect of evaporation minus precipitation upon the salinity in terms of change of salinity per month, equation 7 states that ($E-P$) must be divided by the depth of the mixed layer and multiplied by the salinity. The upper panel in figures 20 and 21 shows the change of salinity due to ($E-P$) in terms of parts per thousand of salt per month. Thus, at 20° N. 160° W., figure 20, the evaporation minus precipitation would increase the salinity by 0.02‰ mos.$^{-1}$ in December and January, 0.09‰ mos.$^{-1}$ in May and July, and in June by 0.19‰ mos.$^{-1}$ because of the shallow depth of mixed layer.

In figure 21 the April maximum change of salinity of 0.09‰ mos.$^{-1}$ occurs at 23° N. (maximum ($E-P$) occurs at 20° N.). During August the maximum change of 0.1‰ mos.$^{-1}$ occurs at 22° N., and in December the maximum of 0.04‰ mos.$^{-1}$ occurs at 13° N. During December the change of salinity due to evaporation minus precipitation is positive along the entire section shown, whereas during April and August it is negative south of 13° and 15° N., respectively.

The seasonal changes of salinity at 13°, 16°, 21°, and 26° N. (fig. 9) can now be examined in the light of the evaporation minus precipitation. At each of these latitudes except 13° N., ($E-P$) is positive throughout the year, so that declining salinities cannot be explained by excess precipitation, but must be associated with movement of the surface water.

At 21° N. the salinity is declining and reaches a minimum when the monthly change of salinity due to ($E-P$) is rising and reaches a maximum. This phenomenon can be explained by the northward movement of the high salinity gradient or boundary described on page 382 (fig. 10).

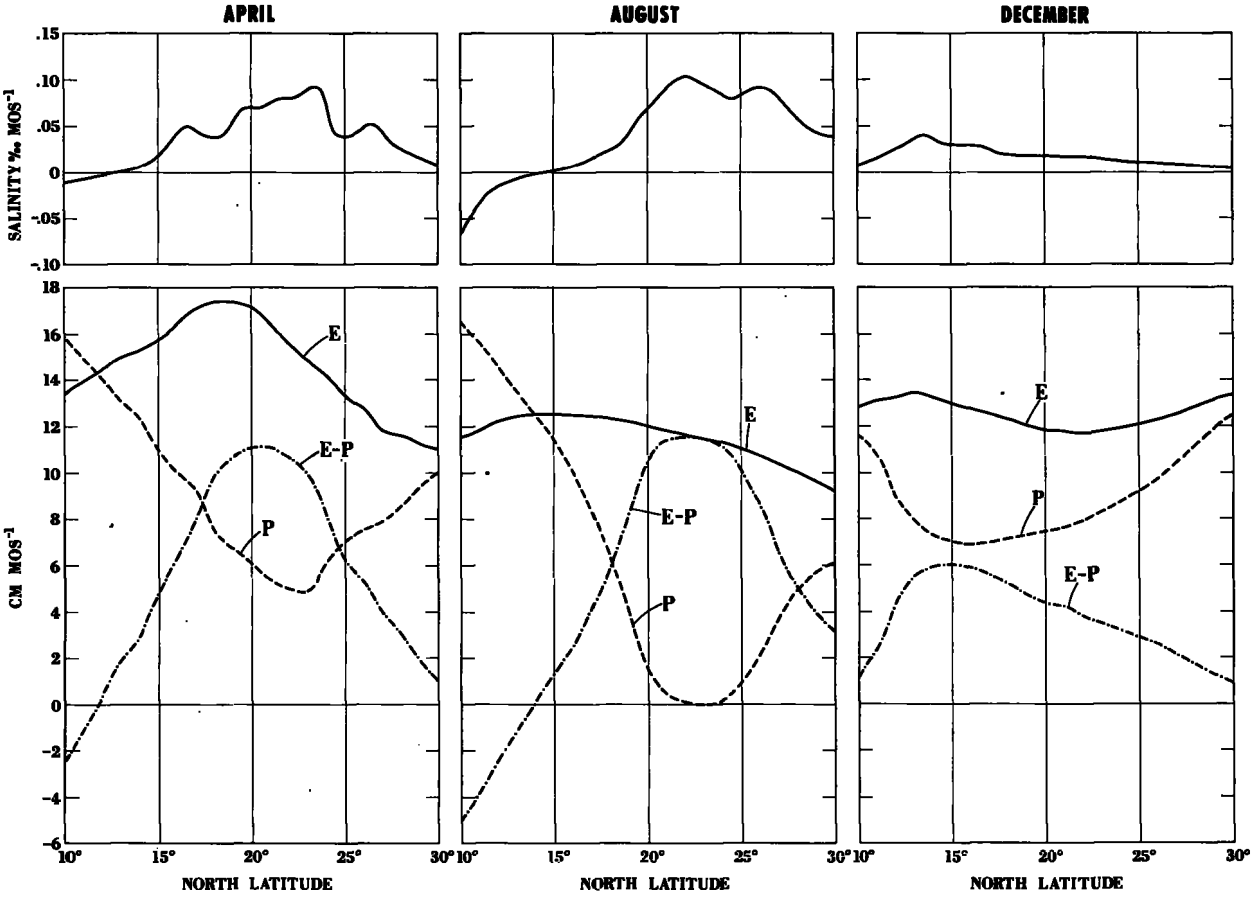

FIGURE 21.—Meridional profiles at 160° W. of evaporation, precipitation, evaporation minus precipitation, and equivalent salinity changes per month (upper panel) during April, August, and December.

It is also difficult to explain the sudden drop of salinity at 13° N. during October and November (fig. 9) in terms of evaporation minus precipitation. Here the decline of salinity occurs at the very time when there is a change from excess precipitation to excess evaporation. As at 21° N., this indicates the movement of a boundary, possibly due to the same forces which are involved in the rapid change of $(E-P)$.

3. ADVECTION

A. Characteristic Advection Diagram

The simplified heat (temperature) budget equation (equation 6) contains only three terms. Therefore, by using the temperature data from part I and the net heat exchange across the sea surface from the previous section, one can obtain a measure of the advection. This is best accomplished by drawing $\frac{H}{\rho c_p z}$ and $\frac{\Delta\theta}{\Delta t}$ versus time for any one location. Then, as the approximate temperature budget $\frac{H}{\rho c_p z}-\frac{\Delta\theta}{\Delta t}=\overline{V}\cdot\nabla\theta$ shows, the difference between the two curves indicates the magnitude of advection.

Figure 22 shows the $\frac{H}{\rho c_p z}$ and $\frac{\Delta\theta}{\Delta t}$ curves for the three-degree squares 14° to 17° N., 156° to 159° W., 20° to 23° N., 156° to 159° W., and 26° to 29° N., 156° to 159° W. One notes that the shape of the curves changes with location. For example, to the south of the islands the heat exchange across the sea surface, as it affects the surface temperature, reaches its maximum during September and October and its minimum during January. In the vicinity of the islands, the maximum occurs during July and the minimum during December. Finally, to the north of the islands the maximum heat exchange occurs in June and the minimum occurs

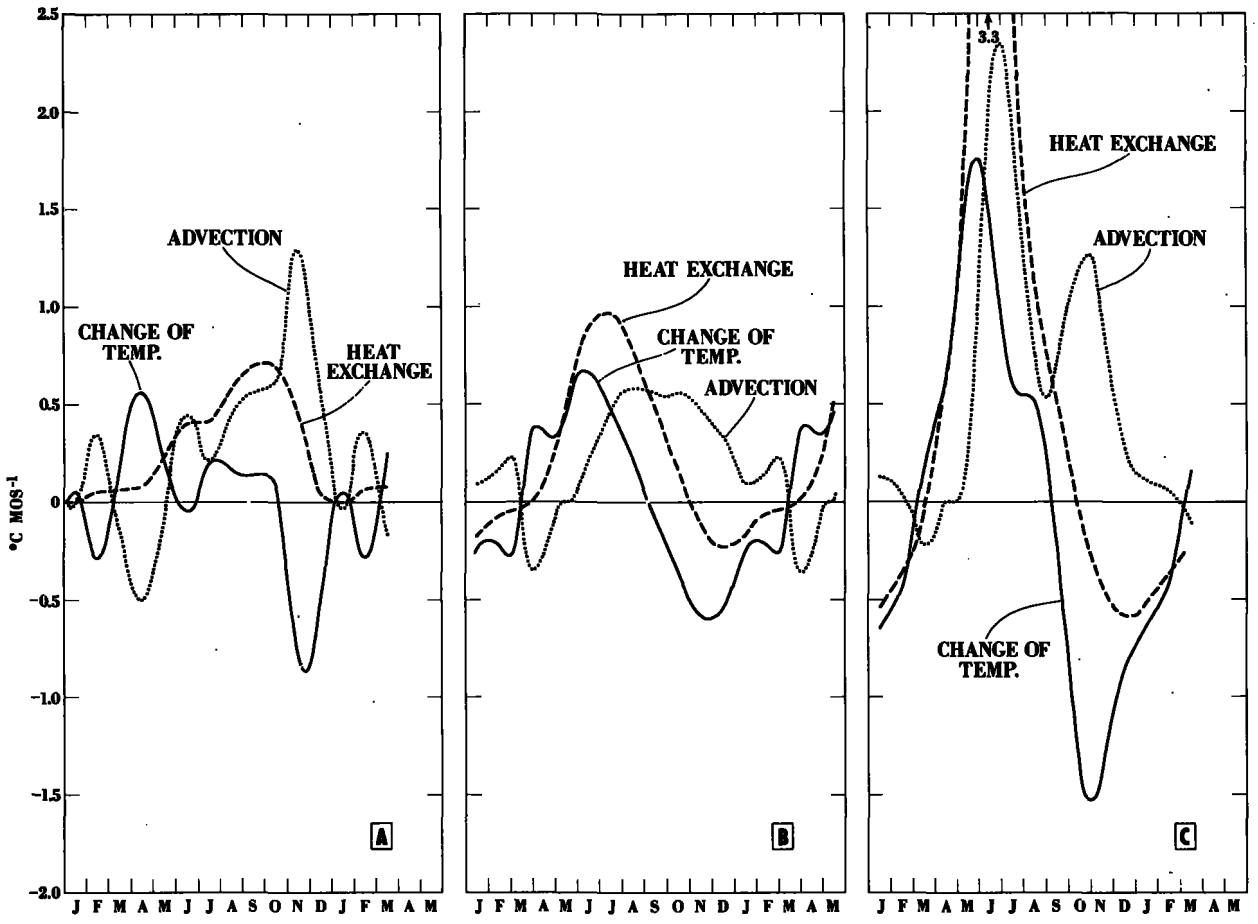

FIGURE 22.—Characteristic advection diagrams for the three-degree squares: A—14° to 17° N., 156° to 159° W.; B—20° to 23° N., 156° to 159° W.; and C—26° to 29° N., 156° to 159° W.

in December and January. It is also apparent that, during the summer, the change of temperature due to the heat exchange increases northward and, in winter, decreases northward (fig. 17).

South of the islands the maximum rate of temperature increase occurs in April and the maximum rate of decrease occurs in November and December. In the vicinity of the islands the time of maximum rate of increase has shifted to June, with the maximum rate of decrease occurring in November and December. To the north of the islands these maxima occur during May to June and October to November, respectively. Again, there are also changes in the magnitude of these extremes, which is particularly apparent to the north of the islands.

Together the $\frac{\Delta\theta}{\Delta t}$ and $\frac{H}{\rho c_p z}$ curves indicate advection and form combinations typical for their location. For example, during May in figure 22B and April in figure 22C, the two curves are superimposed or in phase for a brief period of time. This means that

$$\frac{H}{\rho c_p z}=\frac{\Delta\theta}{\Delta t}$$

and that there is no advection.

At other times, the heat exchange curve can be either above or below the temperature-change or heating curve, indicating either positive or negative advection, respectively. Positive advection means that colder water, and negative advection that warmer water, is moving into the area. In figure 22A and B, negative or warm advection occurs from March to May and positive, or cold advection, during the remainder of the year. This

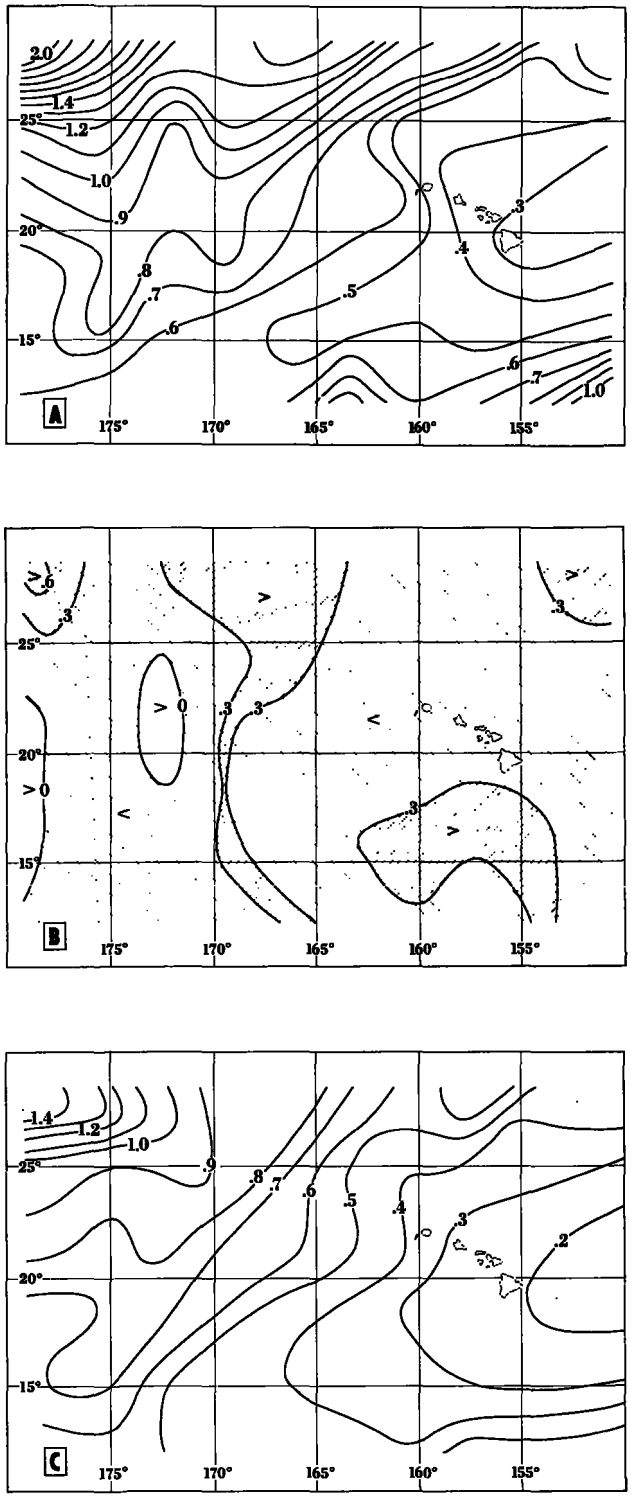

FIGURE 23.—Distribution of advection in the Hawaiian survey region (°C. mos.$^{-1}$). A—Mean positive (cold) advection; B—Mean negative (warm) advection; C—Mean annual advection.

is also true in figure 22C, except that negative advection is less pronounced and occurs earlier.

Phase differences between extremes of $\frac{H}{\rho c_p z}$ and $\frac{\Delta\theta}{\Delta t}$, and changing distances between these curves indicate a varying advention resulting in advection peaks. This is best illustrated by plotting the difference between $\frac{H}{\rho c_p z}$ and $\frac{\Delta\theta}{\Delta t}$ separately. North of the islands, for example, advection peaks occur in June to July and in October to November. To the south of the islands, advection peaks occur in February, June, and November. Within the island area, these peaks occur during February to March, August, and October.

Since both the $\frac{H}{\rho c_p z}$ and $\frac{\Delta\theta}{\Delta t}$ curves have shapes and times of maxima and minima typical for their location, one might call the $\frac{\Delta\theta}{\Delta t}$ curve, as may be obtained from an island monitoring station, a "characteristic heating curve." Similarly, the combinations of these curves form advection patterns typical for their location, so that curves, such as in figure 22, may be called "characteristic advection diagrams."

In order to explore the physical meaning of advection and discover its significance in the vicinity of the Hawaiian Islands, the region was divided into 60 three-degree squares for which characteristic advection diagrams were drawn. First, by measuring the area between $\frac{H}{\rho c_p z}$ and $\frac{\Delta\theta}{\Delta t}$ of each diagram, the mean positive, the mean negative, and the mean annual advection was obtained and their distribution plotted in figure 23.

Positive or cold advection occurs approximately from May to the following February and is distributed as shown in figure 23A. The feature of significance here is the trough of low advection extending southwestward from 21° N., 150° W., crossing the southern boundary of the region in the vicinity of 170° W. On both sides of the trough the mean advection increases to approximately 2° C. mos.$^{-1}$ in the northwest portion of the region and 1° C. mos.$^{-1}$ in the southeast.

Negative or warm advection occurs predominantly during March and April. Figure 23B shows that a distinct positive advection pattern

is absent and that the magnitude ranges from 0 to 0.6° C. mos.$^{-1}$.

The short duration and low values of negative advection indicate that this is not important when the mean annual advection is considered. Figure 23C shows that the latter is positive throughout the region and reveals a distribution similar to that of the distribution of the mean positive advection. Although the trough of low positive advection has other implications, it is sufficient to note at this point that it may indicate a transition zone between two climatic regions, one in the southeast portion and the other in the northwest portion of the Hawaiian region.

The next step in the analysis involved grouping of the characteristic advection diagrams by similarity in shape and phase. Upon examination of the 60 diagrams, 2 primary, climatic regions became apparent. One is located in the northwest portion of the Hawaiian region (area A, fig. 24), with dominant positive advection during June and July and a secondary positive advection peak during December and January. The other climatic region is located in the southeast portion of the region (area B, fig. 24), with a dominant advection peak in October and November. The intermediate area is under the influence of both climates. The characteristic advection diagrams were then combined on the basis of climatic similarities and their number thus reduced to the nine presented in appendix B, chart V.

The diagram characteristic of area A shows a pronounced advection peak of 3.5° C. mos.$^{-1}$ in June, which then decreases rapidly until the end

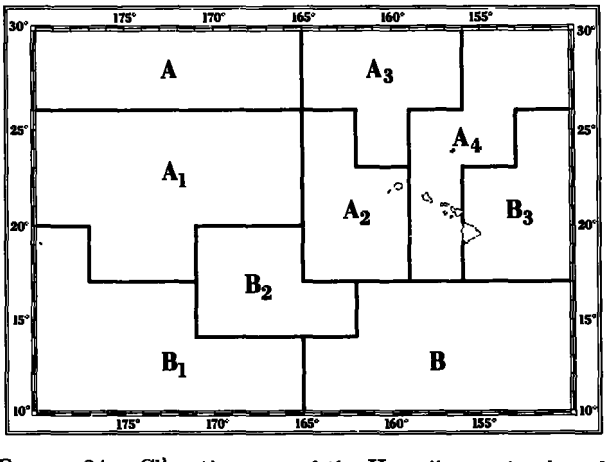

FIGURE 24.—Climatic areas of the Hawaiian region based on characteristic advection diagrams.

of November, except for a period of little change during October. A secondary advection peak of 1.1° C. mos.$^{-1}$ occurs during December and January and, finally, advection reaches a minimum of −0.5° C. mos.$^{-1}$ during March.

In area A_1, just south of area A, the June–July advection peak of 2° C. mos.$^{-1}$ and the secondary peak of 1.1° C. mos.$^{-1}$ in December–January are as pronounced as in area A, and, in addition, there is a secondary peak of 1.2° C. mos.$^{-1}$ in October. Area A_2, just to the west of the main islands, again exhibits these features: a primary peak of 1.2° C. mos.$^{-1}$ in June–July, a peak of 1° C. mos.$^{-1}$ in October–November and the third peak of 0.5° C. mos.$^{-1}$ in December–January. In area A_1, advection reaches a minimum of −0.2° C. mos.$^{-1}$ in March and in area A_2 −0.3° C. mos.$^{-1}$ in March–April.

In area A_3, east of area A, advection peaks of 2.1° C. mos.$^{-1}$ in June–July, of 1.1° C. mos.$^{-1}$ in September–October and of 0.7° C. mos.$^{-1}$ in November–December are present. A small advection peak also occurs in February–March, so that this, and the shift in the occurrence of the two secondary peaks, constitutes a departure from the periods of A, A_1, and A_2. One also notes that $\frac{H}{\rho c_p z}$ and $\frac{\Delta\theta}{\Delta t}$ are superimposed or in phase during May, as is also the case in area A_2, indicating a period of no advection during that month.

In area A_4, which extends from the northeast corner of the region through the main island group, the three pronounced advection peaks are again apparent. The main peak of 1° C. mos.$^{-1}$ has shifted to July–August. There is no phase shift in the October–November peak of 0.8° C. mos.$^{-1}$, and the February–March peak of area A_3 is now more pronounced at 0.5° C. per month. In addition, there appears a small peak during April–May. Minimum advection of −0.7° C. mos.$^{-1}$ occurs in March–April.

If one regards the advection pattern of area A_1 as typical, then that of area A_2 shows only a slight change in shape, but no change in the time of advection peaks. In areas A_3 and A_4, one notes both a change in shape and phase shift of the advection peaks, which may be due to the barrier effects of the island chain within a varying current field.

The characteristic advection diagram of area B shows an advection peak of 1° C. mos.$^{-1}$ during

October–November and another, slightly lower, during August–September. Minimum advection of $-0.1°$ C. mos.$^{-1}$ occurs during April. The primary distinction between area B and the other areas of the region is the absence of both the June–July and the December–January advection peaks. The August–September advection period occurs in only two of the nine advection diagrams of this climatic area, leaving October–November as the important advection period of area B.

In area B_1, the southwestern portion of the region, the advection pattern appears more complex. Maximum advection of 1.1° C. mos.$^{-1}$ occurs in December–January, with a noticeable peak of 0.9° C. mos.$^{-1}$ in October–November and another distinct peak of 0.8° C. mos.$^{-1}$ in June–July. Minimum advection of $-0.2°$ C. mos.$^{-1}$ occurs during February.

Area B_2, north of areas B and B_1, has two pronounced advection peaks; one of 0.9° C. mos.$^{-1}$ in June–July and another of 1.1° C. mos.$^{-1}$ in December–January. Minimum advection of $-0.3°$ C. mos.$^{-1}$ occurs in March.

Finally, in area B_3, east of Hawaii, the advection pattern again appears more complex. Maximum advection of $>0.5°$ C. mos.$^{-1}$ occurs in October–November and, in addition, there are peaks of 0.5° C. mos.$^{-1}$ in July–August and December–January. Minimum advection of $-0.4°$ C. mos.$^{-1}$ occurs in March–April. In addition, there is an advection peak of 0.2° C. mos.$^{-1}$ in May–June, which is also apparent one month earlier in areas B_1, B_2, and A_4.

To summarize, the Hawaiian region was divided into areas on the basis of time of occurrence of positive advection peaks. In the northwest portion, a primary peak occurs during June–July and a secondary peak during December–January. In the southeast portion, the dominant peak occurs during October–November. The areas between exhibit varying magnitudes of these advection periods. Differences from the basic patterns in areas A_3, A_4, and B_3 may be due to varying effects of the island barrier in a changing current field. Negative advection, generally of small magnitude, peaked during March and April.

Since heat (temperature) advection is the scalar product of the current velocity and horizontal temperature gradient, it is difficult to visualize it as a water displacement perpendicular to an isotherm. In order to do so and to explore the physical significance of advection further, the intrinsic temperature and advection charts will be developed in the next section.

B. Intrinsic Temperature and the Heat Advection Chart

A measure of advection as obtained in the previous section can provide, if the horizontal temperature gradient is known, information only about the component of the current in the direction perpendicular to an isotherm. For example, if the advection is 1° C. mos.$^{-1}$ and the horizontal temperature gradient 1° C. per 60 miles, then this advection is equivalent to water shifting 60 miles perpendicular to the isotherm. If the gradient is 0.5° C. per 60 miles then the shift would be 120 miles.

Now assume that the surface temperature is conservative or an "intrinsic" property of a parcel of water. Then, as before, there would be no advection for currents parallel to an isotherm. However, a component of flow perpendicular to an isotherm, the temperature now being an intrinsic property of the water, would result in a shift of the isotherm. In other words, advection can be interpreted as a shift of "intrinsic" isotherms with the displacement distance depending upon the temperature gradient. An "intrinsic" isotherm, therefore, exhibits properties of a movable streamline or boundary in that there is no flow across the isotherm. Thus, no information can be gained about the flow parallel to an isotherm, but a component of flow perpendicular to the isotherm, using "intrinsic" temperatures, must result in a shift of the boundary or the "intrinsic" isotherm.

Although any intrinsic isotherm or salinity isopleth in the ocean is a movable boundary, the resulting advection due to their displacement is magnified in transition zones marked by higher temperature and (or) salinity gradients. Thus, the areas of high advection in the northwest and southeast portions of the Hawaiian region (fig. 23) can be interpreted as transition zones, with moving boundaries, between climatic regions. These climatic regions were recognized by the characteristic advection diagrams of areas A and B in the previous section. Areas of high salt advection due to boundary movement are also to be expected during summer at 21° to 23° N., 155° to 160° W., and during fall at 13° N., 155° to 160° W., on the

basis of high salinity gradients shown in figures 10 and 9, respectively.

The foregoing discussion can be further illustrated by computing intrinsic temperatures with the help of the simplified heat budget, equation 6.

Since only two processes, the heat exchange across the sea surface and advection, are assumed to contribute to the change of temperature, one can compute what the change of temperature should be if there were no heat exchange. The heat budget equation

$$\frac{\Delta\theta}{\Delta t}=\frac{H}{\rho c_p z}-\overline{V}\cdot\nabla\theta$$

then becomes

$$\left.\frac{\Delta\theta}{\Delta t}\right]_a=-\overline{V}\cdot\nabla\theta,$$

the change of temperature due to advection only.

Considering the unit of time to be one month, one can compute the intrinsic temperature, θ_I, at the end of a month for any location, if that month's advection is known, from

$$\theta_I-\theta_1=-\overline{V}\cdot\nabla\theta \text{ or}$$

$$\theta_I=\theta_1-\overline{V}\cdot\nabla\theta$$

where θ_1 is the temperature at the beginning of the month. One can also obtain the intrinsic temperature by subtracting the net heat exchange during a month from the temperature at the end of the month:

$$\theta_I=\theta_2-\frac{H}{\rho c_p z}.$$

A chart of the temperature distribution at the beginning of the month and one for the intrinsic temperature at the end of the month can now be drawn and combined. This new chart then illustrates advection in terms of the displacement of intrinsic isotherms or boundaries.

For the Hawaiian region, four "advection charts" were prepared (chart VI, appendix B), one each for the three advection periods, June–July, October–November, and December–January, and one for the minimum or negative (warm) advection period of March–April.

In the first chart the solid and dashed isotherms show the mean temperature distribution for the beginning of March and April and the mean intrinsic temperature distribution for the end of March and April, respectively. The chart shows that the displacement of the intrinsic isotherm is small throughout most of the region and probably not significant. The 24° and 25° C. isotherms are displaced northward, however, by as much as 180 miles in the eastern portion of the region, indicating warm advection.

The March–April advection chart therefore indicates either no current flow, or currents parallel to the isotherms, with some warm advection in the eastern portion. This is compatible with the gross winter geopotential topography (chart IV), which indicates little flow in the northern half of the region and flow parallel to the isotherms in the southern half.

The June–July advection diagram shows the average isotherms for the beginning of these months slope from northwest to southeast, whereas the average intrinsic isotherms for the end of these months, except for the southwest portion, show an east-west direction. Thus, this advection chart for the principal advection period shows very little displacement of the 25° and 26° C. isotherms in the eastern portion of the region, whereas in the western portion displacement may be as high as 550 miles per month, indicating a southward component of flow of 0.7 to 0.8 knot. Although there are insufficient current data to compute the advection independently, a westerly setting current of 1 knot could accomplish this displacement. High advection is also indicated in the northern portion of the region, where the displacement increases westward from 150 miles per month to more than 500 miles per month.

This advection chart conveys a picture compatible with salinity changes if one postulates water entering the survey region from the east and pushing the intrinsic isotherms southward as if they were movable boundaries. The water entering the survey region from the east also decreases the salinity in the vicinity of the Hawaiian Islands during the spring, reaching a minimum in July (fig. 9), despite the fact that this is a period of maximum evaporation minus precipitation (fig. 20).

High heat advection in the vicinity of Midway Island during June and July is also compatible with the sharp salinity decline during those months (fig. 9).

The characteristic advection diagrams of the previous section (chart V) show that the advection

declines after the primary peak in June–July, but then rises again in August or September to reach a secondary peak in October–November. The advection chart for the October–November period shows no material difference between the mean isotherm pattern for the beginning of these months and the mean intrinsic isotherm pattern for the end of these months. High advection continued in the western half of the region, with the principal change from the previous chart occurring in the southeast portion. There advection was low during the June–July period and then increased to 1° C. mos.$^{-1}$ in October, as shown in the characteristic advection diagram of area B (chart V).

The displacement speeds of the 26° and 27° C. isotherm in the southern portion of the region are as high as 0.9 knot, in the northwest portion they are about 0.5 knot and, in the northeast portion the 25° isotherm was displaced at a speed of about 0.2 knot.

To explain this advection picture one can postulate that the westerly flow of the June–July period slackened and shifted to the southeast portion of the region. This is coincident with the intrusion of lower salinity water into that area, as indicated in figure 9 showing the seasonal salinity variation at 13° N. One can further postulate that with the relaxation and southward shift of the flow from the east, higher salinity water from the northwest reoccupies the region from which it had been displaced during the primary advection period. This, again, is in agreement with the salinity data as shown in figure 8.

The final advection period, as indicated by the characteristic advection diagrams, occurs during December and January in all the areas except in area A_4 where it is delayed until February and area B where it is absent. The mean temperature for December and January at the beginning of these months, and the mean intrinsic temperature for the end of these months are beginning to assume the distribution of the March–April period. The chart shows displacements of the 25° and 26° C. isotherms in the central portion of the region of up to 360 miles or at a rate of about 0.5 knot. To the north, the 24° C. isotherm is displaced by up to 120 miles or at a rate of less than 0.2 knot.

The primary advection during June and July can be associated with an intensification of the tradewind system and the secondary period during October and November with its relaxation. However, there appears no wind pattern which could be associated with the December–January advection peak. In the vicinity of the main Hawaiian Islands the salinity reaches a peak during the December to February period and northeast of the Marshall Islands the horizontal temperature distribution at 400 ft. (Robinson, 1954) suggests intensified circulation. This points to an inertial surge in the high salinity circulation system as the explanation for the advection peak.

Although the water movement as suggested by the advection periods has not been observed directly, present knowledge of the general Pacific circulation, and the sketchy salinity data, are compatible with the advection model. In the next section, therefore, it will be shown that the surface temperature can be used to monitor physical processes.

C. Characteristic Heating Curve

The simplified heat budget, equation 6, shows the rate of change of temperature to be a function of the two independent variables; the heat exchange across the sea surface and the heat advection. Since the seasonal variation of the heat exchange across the sea surface and the seasonal variation of the advection are characteristic of the oceanographic climate at any location, the dependent, seasonal variation in the rate of change of temperature should also be characteristic of the location. A graph of the seasonal rate of change of temperature can therefore be called the characteristic rate of change temperature curve, or, simply, the "characteristic heating curve."

The characteristic advection diagrams of chart V show, with the exception of areas B and B_1, that the heat exchange curves have a regular seasonal shape, with a maximum in June and a minimum in December or January. Changes in advection should therefore be reflected in irregularities of the characteristic heating curves. For example, in April the change of slope in the characteristic heating curve of most areas in the survey region (chart V) indicates a change from negative (warm) advection to positive (cold) advection. In the northeastern portion of the survey region (areas A_4 and B_3), the pronounced dip in the characteristic heating curve during April and May signifies an initial surge of cold advection, which then slackens during May and June, as indicated by the rapid rise of the rate of change of temperature.

Again, in most areas of the survey region, the rapid decline in the characteristic curve, after reaching a peak in May–June, is associated with the June–July advection peak. The slackening of the primary advection is reflected in a change of slope in the characteristic heating curve or a secondary peak as in areas A_2, A_3, A_4.

In areas A, A_1, A_2, A_4, and B_3, both the October–November and the December–January (February for A_4) dips in the characteristic heating curves can be interpreted as advection peaks at those times. In areas B_1 and B_2, these advection periods overlap in such a way as to produce only a single minimum in the characteristic heating curve.

Generally, the characteristic heating curve is expected to be sensitive to cold advection during a period of rising heat exchange and most sensitive to warm advection during declining heat exchange. During the winter months in areas where heat exchange is small, the characteristic heating (cooling) curves would be very sensitive to changes in advection. This is illustrated in the characteristic advection diagram of area A_1, where the secondary advection peaks produce large changes in the characteristic heating curves during October–November and December–January.

The characteristic advection diagrams of chart V are useful in discovering gross climatic features and in delineating climatic regions. More useful, however, are the characteristic heating curves drawn from data regularly collected at fixed monitoring stations, particularly if features of the curve can be related to other continuously monitored events or processes. Gross climatic processes, as discovered in the characteristic advection curves, should again be reflected in the shape of the heating curves.

Figure 25 represents the characteristic heating curve as drawn from mean data collected in the vicinity of Koko Head, Oahu, from 1951 to 1958. It differs from that of figure 22B primarily during the winter months, when it forms only one minimum in December, whereas the latter forms a minimum in November–December and another dip in the characteristic temperature curve during January–February. The March–April and the June peaks are in phase on both diagrams. These differences are to be expected, since the curve of figure 22B represents data collected in a three-degree square covering both sides of the island chain. The Koko Head curve, on the other hand,

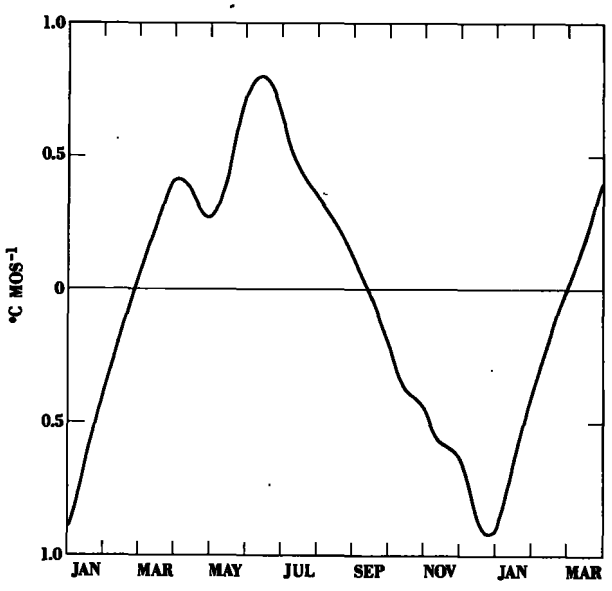

FIGURE 25.—Mean (1951–58) characteristic heating curve for the vicinity of Koko Head, Oahu.

represents data collected only at a point on the "island barrier" within a large circulation system.

The mean characteristic heating curve at Oahu, then, shows that the rate of change of temperature becomes positive at the end of February, indicating warm advection. The commencement time is similar to that in area A_2, just to the west of Oahu. The rapid rise in the rate of change of temperature during May can be interpreted as a period of low advection, as in figure 22B where the rate of change of temperature is the same as the net heat exchange across the sea surface. Since, during this time of the year, the isotherms are approximately parallel to the islands (see May temperature chart II), this means that the flow is also parallel to the island chain. Then, again as in figure 22B, the rate of change of temperature reaches its maximum in June, slightly later than in area A_2 and earlier than in area B_3. This is also apparent in area A_4, where a combination of maximum rates of change of temperatures occurring either during May–June or June–July produce the wide peak in the characteristic heating curve.

Since the flow during the June–July advection period is from east to west, at a low angle of incidence within the island chain, one can postulate that its deflecting effect is at a maximum. However, as the incident flow acquires a southerly component and the angle between it and the island

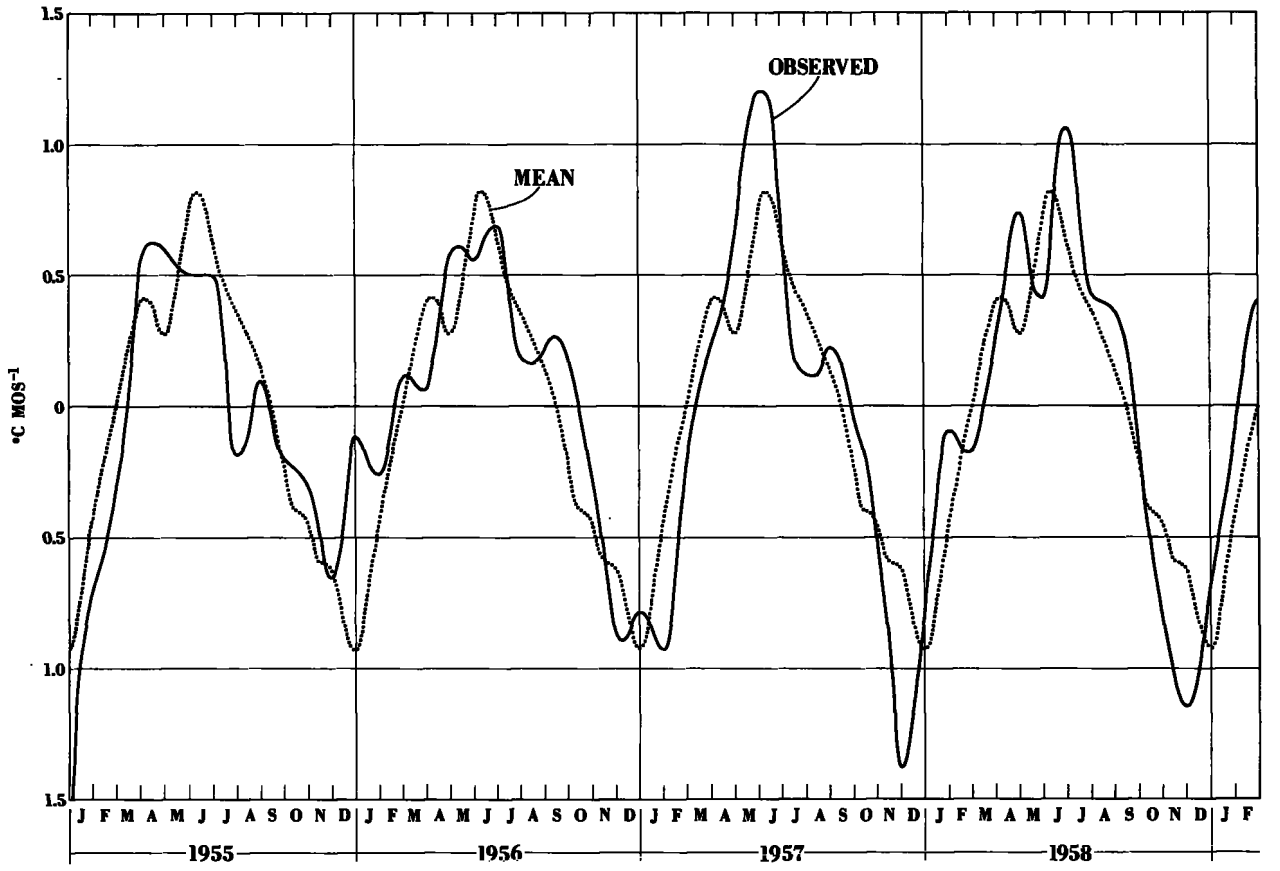

FIGURE 26.—Characteristic heating curve at Koko Head, Oahu, 1955 through 1958.

chain becomes larger, water will pass through the channels and cold advection becomes apparent. This has the effect of delaying and damping the June–July advection so as to merge it with the October–November period, as is indicated in the advection curve of figure 22B. The advection diagram of area A_4 does not exhibit this feature, since it is a combination of diagrams primarily of the northeast portion of the region, where the June–July advection peak is delayed but not damped out.

Finally, the characteristic heating curve for Oahu reaches a minimum during December, indicating that the December–January advection peak is affecting this area, rather than the delayed February peak to the northeast of the islands.

Figure 26, showing the rate of change of temperature of the Koko Head (Oahu) monitoring station from 1955 through 1958, further illustrates the utility of characteristic heating curves. Here the dashed line represents the mean characteristic curve discussed above and the solid line, the observed data. Pronounced deviations from the mean characteristic curve are apparent during 1955 and 1957. In 1955, the maximum rate of change of temperature occurred during April and then decreased irregularly to reach its minimum during November–December. The early peak and the generally decreasing trend in the rate of change of temperature are comparable to curves found south of the islands, such as in figure 22A for the three-degree square 14° to 17° N., 156° to 159° W.

Similarly, the shape of the characteristic heating curve in 1957, with a peak 0.4° C. mos.$^{-1}$ higher than the mean peak, resembles curves found north of the islands, such as in figure 22C for the three-degree square 26° to 29° N., 156° to 159° W. In

short, since the shape of the characteristic heating curves reflects the oceanographic climate, one can say that, during 1955, Oahu was located within an oceanographic climate normally to be found to the south, and, during 1957, Oahu was located within an oceanographic climate normally to be found to the north.

During 1956, the dip in the heating curve which signals the end of the warm advection period occurred during March–April, approximately one month earlier than in the mean curve. The significance of two peaks during the May to July period rather than one as in the mean Koko Head curve is not apparent. The dip in the heating curve during August of 1956 to below and, subsequently, to above the mean curve can be interpreted as more pronounced cold advection.

From March to October 1958, the shape of the heating curve resembled the mean curve except that the March–April peak, the April–May dip, and the June peak, occurred approximately one month later.

During the autumn and winter months from October 1955 to March 1958, the dual dips in the heating curve are as apparent as in figure 22C. They reflect the cold advection peaks of November–December and January–February, and in each case deviate from the mean Koko Head curve.

Thus, certain changes in the surface temperature can be interpreted in terms of physical processes. Figure 26 also shows that deviations from the mean characteristic heating curve can be large, exhibiting features which can be found in the characteristic curves of adjacent areas.

Before closing the discussion on heat advection, the validity of the results will be examined. Although shapes of curves and times of advection peaks and dips in the rate of change of temperature were stressed, it is useful to review the magnitude of advection encountered. In the previous section displacement velocities of up to one knot were calculated, which seem high for the mean conditions discussed here. However, on the basis of the assumption used in the derivation of the simplified heat budget, high advection values are to be expected. First, it is probable that the actual depth through which heat is distributed, or the "effective" mixed layer, is greater than the measured mixed layer so that the computed heat exchange in terms of temperature change, $\frac{H}{\rho c_p z}$, would therefore be too high and result in excessive heat advection. Neglecting the effects of diffusion in the simplified heat budget equation would also tend to increase the computed advection.

The assumptions, then, would affect the magnitude of advection, but not necessarily the advection periods. This view is supported by the consistency of the advection periods throughout the survey region, despite data of less than desirable quality.

In the discussion of the characteristic heating curves obtained from the Oahu monitoring station (fig. 26), deviations of the rate change of temperature from the mean were explained in terms of advection. This implies that year-to-year changes in the heat exchange and diffusion are insufficient to account for these deviations.

In the vicinity of the Hawaiian Islands, examination of the vertical temperature gradient below the mixed surface layer suggests that the stability remains relatively constant throughout the year. Significant changes in the vertical diffusion are therefore unlikely, even though diffusion may not be negligible in heat budget considerations. The calculated heat losses from the sea surface (evaporation, back radiation, and conduction of sensible heat) seasonally vary by about 5 percent. On a year-to-year basis, then, the variation of these heat losses would probably be less than 5 percent.

Remaining is the incident radiation at the sea surface which, due to cloud cover, can vary considerably. Maximum deviations in the characteristic heating curve due to this cause would occur during May, June, and July, when insolation is at a maximum and the depth of mixed layer is at a minimum. To estimate reasonable deviations, assume that the year-to-year variation in the mean monthly cloud cover is less than the seasonal range of one tenth. On this basis, deviations of less than 0.2° C. mos.$^{-1}$ in June and less than 0.1° C. mos.$^{-1}$ in December can be expected.

Deviations from the mean characteristic heating curves in figure 26, which were interpreted in terms of advective changes, were as follows:

April 1955	+0.25° C. mos.$^{-1}$
June 1955	−0.3° C. mos.$^{-1}$
December 1955–January 1956	+0.8° C. mos.$^{-1}$
March–April 1956	−0.3° C. mos.$^{-1}$
September 1956	+0.2° C. mos.$^{-1}$

October 1956	+0.35° C. mos.$^{-1}$
November–December 1956	−0.2° C. mos.$^{-1}$
January–February 1957	−0.5° C. mos.$^{-1}$
June 1957	+0.4° C. mos.$^{-1}$
November–December 1957	−0.7° C. mos.$^{-1}$
April–May 1958	+0.4° C. mos.$^{-1}$
June–July 1958	+0.3° C. mos.$^{-1}$
November–December 1958	−0.45° C. mos.$^{-1}$

These are all in excess of changes to be expected from the assumed year-to-year variations in the net heat exchange.

PART III. OCEANOGRAPHIC CLIMATE OF THE HAWAIIAN ISLANDS REGION

In the first section of this atlas, the distribution of surface variables and their gross seasonal changes in an area bounded by 10° N., 30° N., 150° W., and 180°, were described. These consisted of surface temperatures, salinities, depths of the mixed layer, and dynamic heights. In the second section, the changes of surface variables were studied in terms of physical processes, such as the net heat exchange across the sea surface and advection.

In this final section, an attempt will be made to use the results of the first two sections to construct a climatic model of the Hawaiian region. This, of necessity, will only be a first approximation, since none of the data used here were collected for purposes of a climatic study. This first approximation, however, may be of use in designing experiments to correct and improve the climatic model.

The currents and water masses of the North Pacific were described by Sverdrup et al. (1942, ch. XV). They defined the Subarctic Pacific water mass, the Eastern and the Western North Pacific Central water mass, and the Pacific Equatorial water mass on the basis of temperature-salinity relations below the surface layer. Approximately associated with these subsurface water masses one also finds surface water types. These are the Subarctic Pacific Water type, the North Pacific Central Water type, and the North Pacific Equatorial Water type as illustrated in figure 27. On the basis of Schott's (1935) temperature and salinity charts, the Subarctic Pacific type would be cold and have a salinity of 33°/$_{oo}$ or less, the North Pacific Central type would be warm and have 35°/$_{oo}$ or more, and the North Pacific Equatorial type would be warm and have about 34°/$_{oo}$ or less. The chief distinction between water types and masses is that the former are under the direct influence of the physical processes taking place at the sea surface, whereas the latter are not. One would therefore expect relatively large seasonal

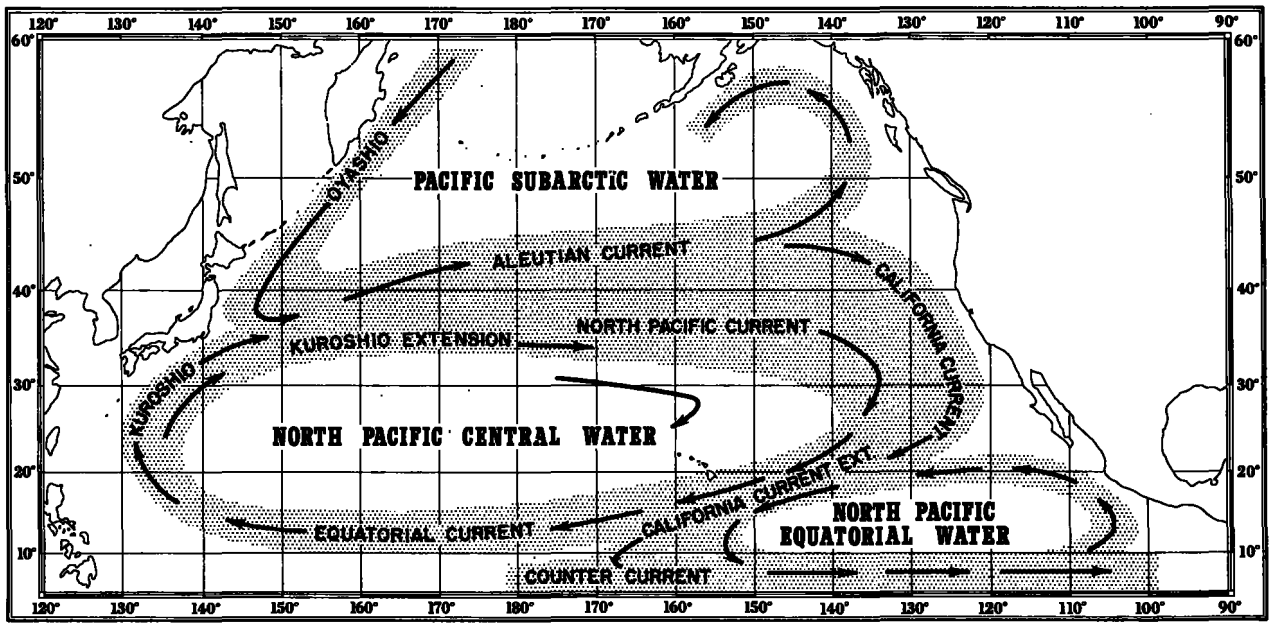

FIGURE 27.—A schematic chart showing the major North Pacific water types and currents.

temperature and salinity changes in the surface water types. The position of their boundaries would also be subject to changing wind stresses, so that they would not always coincide with the corresponding water-mass boundaries.

The water types mentioned also form centers of the large circulation systems of the North Pacific, since one finds the major ocean currents on their periphery. Thus, the currents are located in the transition zones between the principal water types and one would expect this to be reflected in the changing composition of the water as it flows across the Pacific. For example, a parcel of water starting in the Kuroshio would be mixed with water from the Oyashio and then in its passage across the Pacific acquire new chemical characteristics during possibly two or three seasons of winter overturn. Then, this parcel of water would be further modified, first in the California Current by American coastal water and later, in the California Current Extension, by North Pacific Equatorial water. Finally, southeast of the Hawaiian Islands, one would expect its chemical composition to differ from both its original composition in the Kuroshio and from that of the North Pacific Central Water.

This, of course, is supposition, since no supporting measurements of chemical tracers are available. However, the relatively high salinity gradient at 35°/oo in the vicinity of the Hawaiian Islands (fig. 10) can be interpreted as the boundary between the Western North Pacific Water and the transition water called here the California Current Extension.

The oceanographic environment of the Hawaiian Islands, therefore, corresponds with that described by Sverdrup et al. (1942), except that they based their analysis on a study of water masses, in contrast to the water types considered here. Thus, on the basis of Schott's (1935) temperature charts, the North Pacific Equatorial water type is distinct from the South Pacific Equatorial type.

Sverdrup et al. also distinguish between the Eastern North Pacific and the Western North Pacific Central water mass. Surface salinity data for the November to February period (chart III) show only a single high salinity cell to extend eastward across the northern portion of the region and, on the basis of winter data collected on *Hugh M. Smith* cruise 25 (McGary, 1956), there is no evidence of an Eastern North Pacific cell. The April to August surface salinities (chart III) show two high salinity cells in the northern portion of the area. This can be explained as a separation of the single, winter cell caused by the deflecting effect of the island chain on a westward setting current. The surface water in the two high salinity cells is therefore believed to be of the North Pacific Central type.

New information to be added to this general picture is concerned with the three types of boundaries described in part I. First, there was the boundary separating areas in which the times of maximum and minimum depths of mixed layer differed (fig. 3). This is also coincided with the node at 15° N. (fig. 2) and the associated, seasonal displacement of the depth of mixed layer trough (chart I). Then there was a boundary at about 18° N. south of which the seasonal temperature range remained relatively constant and north of which it increased rapidly northward (fig. 5). The relatively high salinity gradient of figure 10, moving seasonally through the Hawaiian Islands, was identified as the third type of boundary separating two types of water.

In order to interpret these features, a simplified heat budget was formulated in part II. This related the rate of change of surface temperature with the processes of net heat exchange across the sea surface and advection. The meridional profiles of figures 17 and 18 revealed a boundary south of which the net heat exchange across the sea surface was positive throughout the year and north of which it was positive during the summer and negative during the winter. The boundary, located at about 18° N., coincided approximately with the temperature boundary. The meridional distribution of the net heat exchange across the sea surface therefore appears to be associated with the seasonal changes in the meridional temperature distribution described in part I.

On the basis of the net heat exchange (fig. 15), one would also expect maximum and minimum sea surface temperatures to be reached in November and April, respectively. Figure 7 shows that the maximum temperature at 20° N. is reached in September and the minimum in March, illustrating that these times are primarily determined by the net heat exchange across the sea surface. However, particularly in autumn, there is an important phase difference attributable to advection.

Since no direct measurements of this term were available, it was estimated by subtracting the rate of change of surface temperature from the rate of change of temperature caused by the net heat exchange across the sea surface. The advection can also be obtained graphically by measuring the difference between the seasonal rate of change of the temperature curve and the seasonal heat exchange curve, as in the advection diagrams of figure 22. This method was applied to three-degree square areas in the Hawaii region and revealed four distinct advection periods. The first period during March and April was one of low or warm advection and the others were periods of cold advection during June–July, October–November, and December–January.

The advection diagrams also suggested different climatic zones. In the northwest portion of the region, area A of chart V, the primary advection peak occurs during June–July and a secondary peak during December–January. In the southeast portion of the survey region, area B of chart V, the primary advection peak occurs during October–November and the June–July and December–January periods are absent. In the intermediate areas the diagrams of chart V exhibit varying magnitudes of these advection peaks, which suggest a transition from one to the other climatic zones. Area B also corresponds approximately with the area south of the depth of mixed layer boundary in which the times of maximum and minimum depths differed from those to the north. Thus, the depth of mixed layer boundary and the advection peaks appear to be closely associated with seasonal changes in water motion.

In order to illustrate the physical meaning of heat advection, the change of temperature caused by advection can be added to the temperature at the beginning of the month in order to obtain the "intrinsic" temperature at the end of the month. If the two temperature distributions are then plotted on the same chart, the displacements of isotherms are then equivalent to boundary movements, as shown in chart VI, for the four advection periods in the Hawaii region. Of particular importance are the June–July and October–November charts, since the independently observed salinity changes mentioned above both support and supplement the information obtained from heat budget considerations. First, within the island area, the June–July advection period coincides with the northward motion of the salinity boundary and the declining salinity which reaches a minimum in July. Later, the October–November heat advection period coincides with the southward retreating salinity boundary and increasing salinity within the islands. In addition, the October–November advection peak in the southeast portion of the survey region coincides with the rapid salinity decline at 13° N. The salinity decline at 21° N. and at 13° N. can only be explained by salt advection, since, at 21° N., evaporation minus precipitation is positive throughout the year and increasingly positive at 13° N. during November (fig. 19).

The displacement of the 26° C. "intrinsic" isotherm and the spring and autumn movement of the salinity boundaries as indicated by the 35 °/oo and 34 °/oo isopleths are illustrated in figure 28. The June–July displacements (fig. 28A) are best explained by an intensified westward component of flow between 15° and 25° N. The October–November displacements (fig. 28B) are best explained by an intensified southward component of flow in the northern half of the region, and an intensified westward component of flow in the southeastern portion.

It is now apparent that the trough of low advection during the cold advection period in figure 23A is associated with the transition zone between two climatic regions. In addition, one can postulate that the trough coincides with the core of the California Current Extension and that the areas of high advection on both sides of the trough are the areas of the seasonally moving current boundaries. The latter can also be expressed as the areas through which the boundaries of the seasonally dilating and contracting North Pacific Central and North Pacific Equatorial systems move.

The surface temperature distribution and its seasonal changes primarily reflect the seasonal changes in the heat exchange across the sea surface. Features in the temperature distribution which may be due to the surface circulation are therefore obscured, except for the tongue-shaped area of lower temperature protruding westward south of the islands during the summer months (chart II), reflecting the increased westward flow.

The surface salinity distribution, on the other hand, appears to be more closely related to the

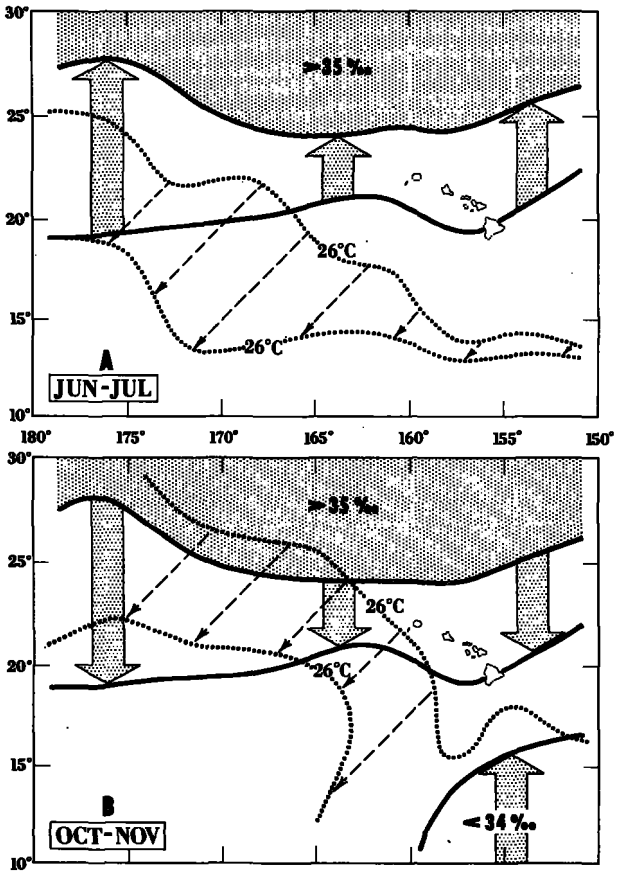

FIGURE 28.—Advection charts: A. Displacement of the June–July 26° C. "intrinsic" isotherm and schematic spring displacement of the 35°/oo isopleth. B. Displacement of the October–November 26° C. "intrinsic" isotherm and schematic autumn displacement of the 35°/oo and 34°/oo isopleths.

circulation systems. This can be explained by the fact that since the Hawaii region is neither one of extreme evaporation nor precipitation, the surface salinity is affected less by evaporation minus precipitation than the temperature is by the heat exchange. In other words, in the Hawaii region the surface salinity is less "non-conservative" than the temperature. The salinity boundary passing seasonally through the islands is therefore not obscured by the events at the sea surface, which is the case with an "intrinsic" temperature boundary that would exist between the Western North Pacific water and the California Current Extension. Of course, faint traces of a temperature boundary similar to the salinity boundary were noted in the zonal temperature distribution (fig. 6).

The seasonal variations in the heat advection appear to be closely related to climatic features in the distribution of the surface depth of mixed layer which probably reflect changes in the wind stresses at the sea surface. Advective peaks also coincide with changes in salinity which must be attributed to salt advection. The temperature and salinity gradients, however, differ both in magnitude and direction, so that one would not expect isopleths of salinity to move in the same direction as the isotherms (fig. 28).

It is now possible to add seasonal, climatic changes to the circulation model which was schematically illustrated in figure 27. During spring and early summer, the California Current system intensifies and as a result the California Current Extension spreads and displaces the North Pacific Central water within the Hawaiian Islands. The peak displacement of this water, as illustrated by the 35°/oo isopleth in figure 8, is reached during July and coincides with the June–July heat advection peak. In late summer and early autumn, as the California Current system weakens, the transition type of water of the California Current Extension retreats and is again replaced by the higher salinity North Pacific Central type of water. This movement of the boundary between the two types of water is associated with the October–November head advection peak. Concurrently with the weakening of the California Current system, North Pacific Equatorial water spreads into the southeast portion of the survey region, as reflected both in the sharp salinity decline and the major October–November heat advection peak for that area.

During this period the surface temperature charts also show a counterclockwise rotation of the tongue-shaped lower temperature water south of the islands from the July position to the November position (chart II). In addition, there is an appearent southward displacement of the depth of the mixed layer boundary in the western portion of the region. These features can be interpreted to mean that, as the California Current Extension weakens, its recirculation into the Countercurrent shifts from west of 175° W. to between 160° and 170° W.

In the Hawaii region the February to April period appears to be one of relaxation. In the northern half, the parallel structure of isotherms probably reflects negligible net current motion, as

is also indicated in the winter geostrophic current chart (chart IV). In the southern half, the flow is probably parallel to the isotherms.

The picture, therefore, is one of dilation and contraction of the North Pacific Central and the North Pacific Equatorial systems associated with the seasonal variation in the intensity and position of the surface currents.

This model can be monitored by means of a "characteristic heating curve," which is produced simply by plotting the rate of change of surface temperature at any given location. The curve for Koko Head, Oahu (fig. 20) showed, for example, that in 1955 the North Pacific Central system near Hawaii was displaced northward, and in 1957 southward. Varied magnitudes and displacements in the characteristic fluctuations of the curve reflected changes both in the intensity and time of the advection periods.

Returning to the original motivation for this climatic study, one finds that the Hawaii skipjack season coincides with the period from April or May to September or October, when the boundary of the North Pacific Central types of water passes Oahu in its northward and southward motion, respectively. This may mean that the availability of skipjack is associated with either the transition water of the California Current Extension and (or) a dynamic effect which is produced when this current enters the island area.

In conclusion, Gosline and Brock (1960:21) state that none of the Hawaii inshore fishes have come from the North American coast. This provides independent support for the climatic model according to which the Hawaii archipelago is predominantly bathed by North Pacific Central water.

LITERATURE CITED

ALBRECHT, F.
1951. A. Monatskarten des Niederschlages im Indischen und Stillen Ozean.
B. Monatskarten der Verdunstung und des Wasserhaushaltes des Indischen und Stillen Ozeans. Berichte des Deutschen Wetterdienstes in der U.S.-Zone No. 29. 39 p.

AUSTIN, T. S.
1954. Mid-Pacific oceanography Part V, Transequatorial waters, May-June 1952, August 1952. U.S. Fish and Wildlife Service, Special Scientific Report—Fisheries No. 136. 86 p.
1957. Summary, oceanographic and fishery data, Marquesas Islands area, August-September 1956 (EQUAPAC). U.S. Fish and Wildlife Service, Special Scientific Report—Fisheries No. 217. 186 p.

BRUNEAU, L., N. G. JERLOV, and F. F. KÓCZY.
1953. Physical and chemical methods. Appendix: Table 1. Physical and chemical data. Reports of the Swedish deep-sea expedition 1947–48, vol. III, fasc. II.

CROMWELL, T.
1951. Mid-Pacific oceanography, January through March 1950. U.S. Fish and Wildlife Service, Special Scientific Report—Fisheries No. 54. 9 p.

CROMWELL, T. and T. S. AUSTIN.
1954. Mid-Pacific oceanography II, by T. Cromwell, and Mid-Pacific oceanography III, by T. S. Austin. U.S. Fish and Wildlife Service, Special Scientific Report—Fisheries No. 131. (Part II, 13 p.; Part III, 17 p.)

FLEMING, J. A., C. C. ENNIS, H. V. SVERDRUP, S. L. SEATON, and W. C. HENDRIX.
1945. Scientific results of cruise VII of the Carnegie during 1928–1929 under command of Captain J. P. Ault. Oceanography-I-B, Observations and results in Physical Oceanography. Carnegie Institution of Washington, publication 545. 315 p.

GOSLINE, W. A. and V. E. BROCK.
1960. Handbook of Hawaiian Fishes. University of Hawaii Press, Honolulu. 372 p.

HOLTSMARK, B. F.
1949. Final report: the SOFAR project: Hawaiian oceanographic survey, USS *Fieberling*, February to July 1947. Report 139, U.S. Navy Electronic Laboratory, San Diego. 58 p.

JACOBS, W. C.
1951. The energy exchange between sea and atmosphere and some of its consequences. Bulletin of the Scripps Institution of Oceanography, vol. 6, No. 2, p. 27–122.

KING, J. E. and T. S. HIDA.
1954. Variations in zooplankton abundance in Hawaiian waters, 1950–52. U.S. Fish and Wildlife Service, Special Scientific Report—Fisheries No. 118. 66 p.
1957. Zooplankton abundance in Hawaiian waters, 1953–54. U.S. Fish and Wildlife Service, Special Scientific Report—Fisheries No. 221. 23 p.

LEIPPER, D. F. and E. R. ANDERSON.
1950. Sea temperatures, Hawaiian Island area. Pacific Science, vol. IV, No. 3, p. 228–248.

LIST, R. J.
1951. Smithsonian Meteorological Tables, 6th revised edition. Smithsonian Miscellaneous Collections, vol. 114. Smithsonian Institution Washington. 527 p.

LUMBY, J. R.
1956. The depth of the wind-produced homogeneous layer in the oceans. Great Britain, Minister of Agriculture, Fisheries and Food, Fish. Investigations Ser. 2, vol. 20, No. 2, p. 1–12.

MCDONALD, W. F.
1938. Atlas of climatic charts of the oceans. U.S. Weather Bureau, Washington.

MCGARY, J. W.
1955. Mid-Pacific oceanography, Part VI, Hawaiian offshore waters, December 1949–November 1951. U.S. Fish and Wildlife Service, Special Scientific Report—Fisheries No. 152. 138 p.

MCGARY, J. W. and E. D. STROUP.
1956. Mid-Pacific oceanography, Part VIII, middle latitude waters, January–March 1954. U.S. Fish and Wildlife Service, Special Scientific Report—Fisheries No. 180. 173 p.

MUNK, W. H. and E. R. ANDERSON.
1948. Notes on a theory of the thermocline. Journal of Marine Research, vol. VII, No. 3, p. 276–303.

NATIONAL DEFENSE RESEARCH COMMITTEE, OFFICE OF SCIENTIFIC RESEARCH AND DEVELOPMENT.
1946. Application of oceanography to subsurface warfare. Reprinted 1951. National Research Council and Office of Naval Research. Washington. 106 p.

OCEANOGRAPHIC OBSERVATIONS OF THE PACIFIC: 1955
1960. THE NORPAC Data Volume. University of California Press, Berkeley. 582 p.

RIEHL, H., T. C. YEH, J. S. MALKUS, AND N. E. LA SEUR
1951. The northeast trade of the Pacific Ocean. Quarterly Journal of the Royal Meteorological Society, vol. 77, No. 334, p. 598–626.

ROBINSON, MARGARET K.
1954. Sea temperature in the Marshall Islands area. Bikini and nearby atolls. Part 2, Oceanography (physical). Geological Survey Professional Paper 260-B,C,D.

SCHOTT, G.
1935. Geographie des Indischen und Stillen Ozeans. C. Boysen, Hamburg. 413 p.

SECKEL, G. R.
1955. Mid-Pacific oceanography, Part VII, Hawaiian offshore waters, September 1952–August 1953. U.S. Fish and Wildlife Service, Special Scientific Report—Fisheries No. 164. 250 p.

STROUP, E. D.
1954. Mid-Pacific oceanography. Part IV. Transequatorial waters, January–March 1952. U.S. Fish and Wildlife Service, Special Scientific Report—Fisheries No. 135. 52 p.

SVERDRUP, H. V.
1936. Das maritime Verdunstungs problem. Annalen der Hydrographic und maritimen Meteorologie, vol. 64, p. 41–47.

SVERDRUP, H. V., M. W. JOHNSON AND R. H. FLEMING.
1942. The oceans; their physics, chemistry and general biology. Prentice-Hall, New York. 1087 p.

U.S. NAVY, CHIEF OF NAVAL OPERATIONS.
1956. U.S. Navy marine climatic atlas of the world. Vol. II. North Pacific Ocean. 275 p.

WALDRON, K., E. L. NAKAMURA, AND H. H. SHIPPEN.
Changes in the catch of skipjack and in their environment, Hawaiian waters, 1955–56. U.S. Bureau of Commercial Fisheries Biological Laboratory, Honolulu. (Manuscript.)

YAMASHITA, D. T.
1958. Analysis of catch statistics of the Hawaiian skipjack fishery. U.S. Fish and Wildlife Service, Fishery Bulletin, No. 134, vol. 58, p. 253–278.

APPENDIX A

SOURCE OF DATA

The data used in the Atlas were primarily collected during the years from World War II to 1957 in the area bounded by 10° N., 30° N., 150° W. and 180°.

The surface temperatures and depths of mixed layer were obtained from the bathythermograph deck at the Scripps Institution of Oceanography through the kind cooperation of Mrs. Margaret Robinson. The deck contained between 10,000 and 11,000 cards from bathythermograph observations made through 1955 by the staff of the Biological Laboratory, U.S. Bureau of Commercial Fisheries (Honolulu), the Scripps Institution of Oceanography, the U.S. Coast Guard, and the U.S. Navy. These data were supplemented by additional observations of the Honolulu Biological Laboratory through 1957.

Surface salinities were obtained from published oceanographic cruise reports, supplemented by unpublished data from the files of the Honolulu Biological Laboratory.

The dynamic topography, chart IV, was drawn from published data by Austin (1954, 1957), Bruneau et al. (1953), Cromwell (1951), Cromwell and Austin (1954), Fleming et al. (1945), Holtsmark (1949), McGary (1955), McGary and Stroup (1956), Oceanographic Observations of the Pacific: 1955 (1960), Seckel (1955), and Stroup (1954). In addition, there were some unpublished

data from the files of the Scripps Institution of Oceanography which are scheduled for publication in Oceanic Observations of the Pacific.

TREATMENT OF DATA

Charts I and II, the distribution of the depth of the mixed layer and the surface temperature were all based on bathythermograph observations which were read and tabulated by 1° squares. These data were then averaged for each month of each year. Since in the Hawaiian region meridional gradients are generally greater than zonal gradients, the averaged data were plotted for each month in the ten meridional strips: 150° to 152° W., 153° to 155° W., 156° to 158° W., 159° to 161° W., 162° to 164° W., 165° to 167° W., 168° to 170° W., 171° to 173° W., 174° to 176° W., and 177° to 179° W. Needless to say, data for various months in different areas were missing or biased toward a single year. These difficulties were in part overcome by interpolation from seasonal curves and from comparisons with adjacent meridional distribution. The meridional surface temperature and depth of mixed layer profiles were then used to draw the monthly charts, where smoothing was done only after re-examination of the data.

Scarcity of salinity and dynamic height data prevented construction of monthly or quarterly charts. In grouping the data for the construction of two charts, a compromise between months of maximum observations and months of oceanographic significance had to be made. By "grouping data" is meant plotting all the observations for a period of months onto a single chart and then drawing contours through the mean values.

The number of salinity observations were relatively high during June to September and during January to March and predominated in the eastern portion of the region. On the basis of the seasonal salinity variation, the April to August data and the November to February data were grouped to draw chart III, representing the low and high salinity period near Hawaii, respectively. This grouping of months does not quite correspond with the maximum occurrence of data, nor, as is apparent from the salinity discussion in Part I, is it in phase with the high or low salinity north of 15° N. generally, or the extremes in the southeast portion of the region.

Significant grouping of the dynamic height data, which were collected predominantly during June to August and January to March, was more difficult. In the estimation of geostrophic currents, gradients rather than the absolute magnitudes of geopotentials are of importance. This makes grouping of several months' data, collected during a number of years, questionable. In addition, the dynamically significant periods as reflected in the geopotential topography are not known and may not correspond with any or all of the advective periods discussed in the atlas. Despite these shortcomings, the data from December to April and June to October were grouped to draw chart IV. These, therefore, roughly bracket the period of low advection during the winter and high advection during the summer months.

APPENDIX B

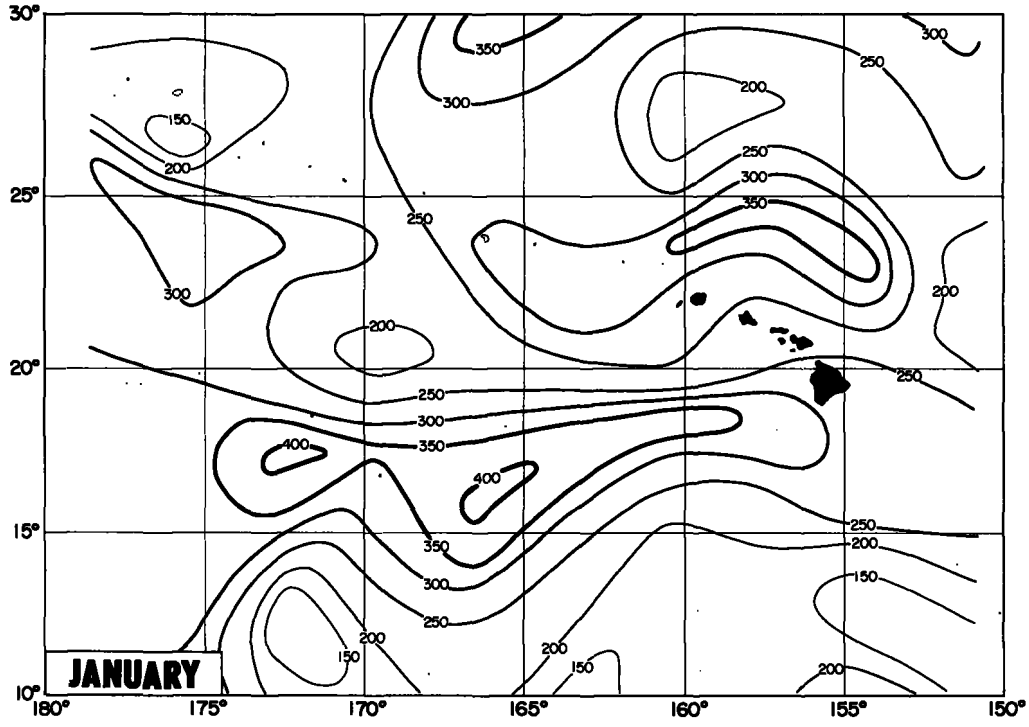

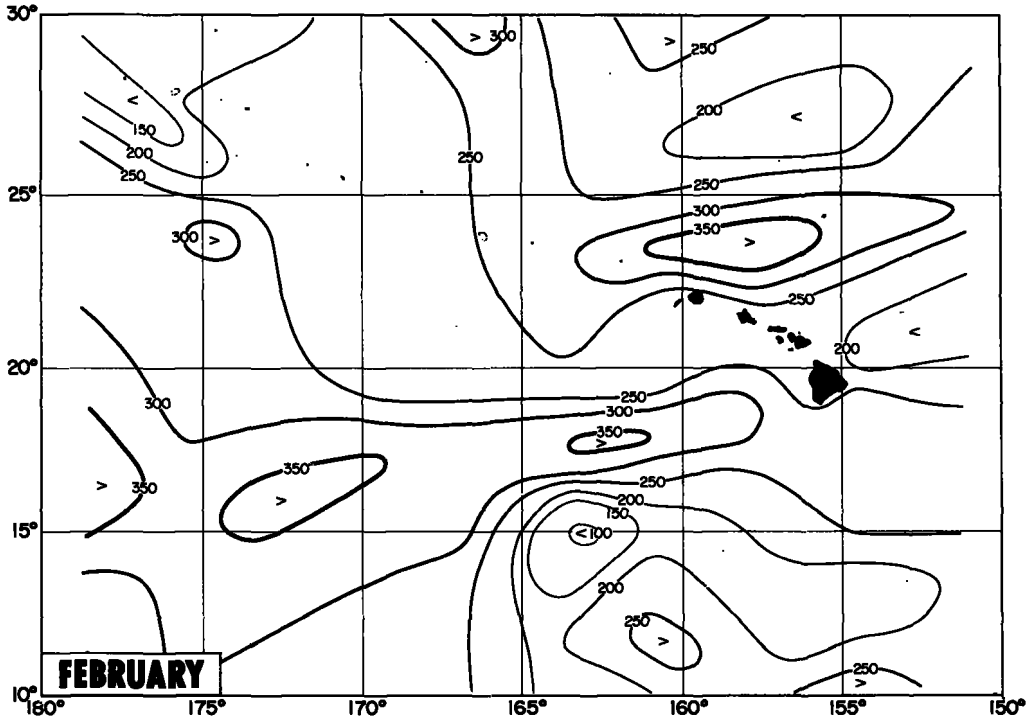

CHART I.—Distribution of the depth of mixed layer feet.

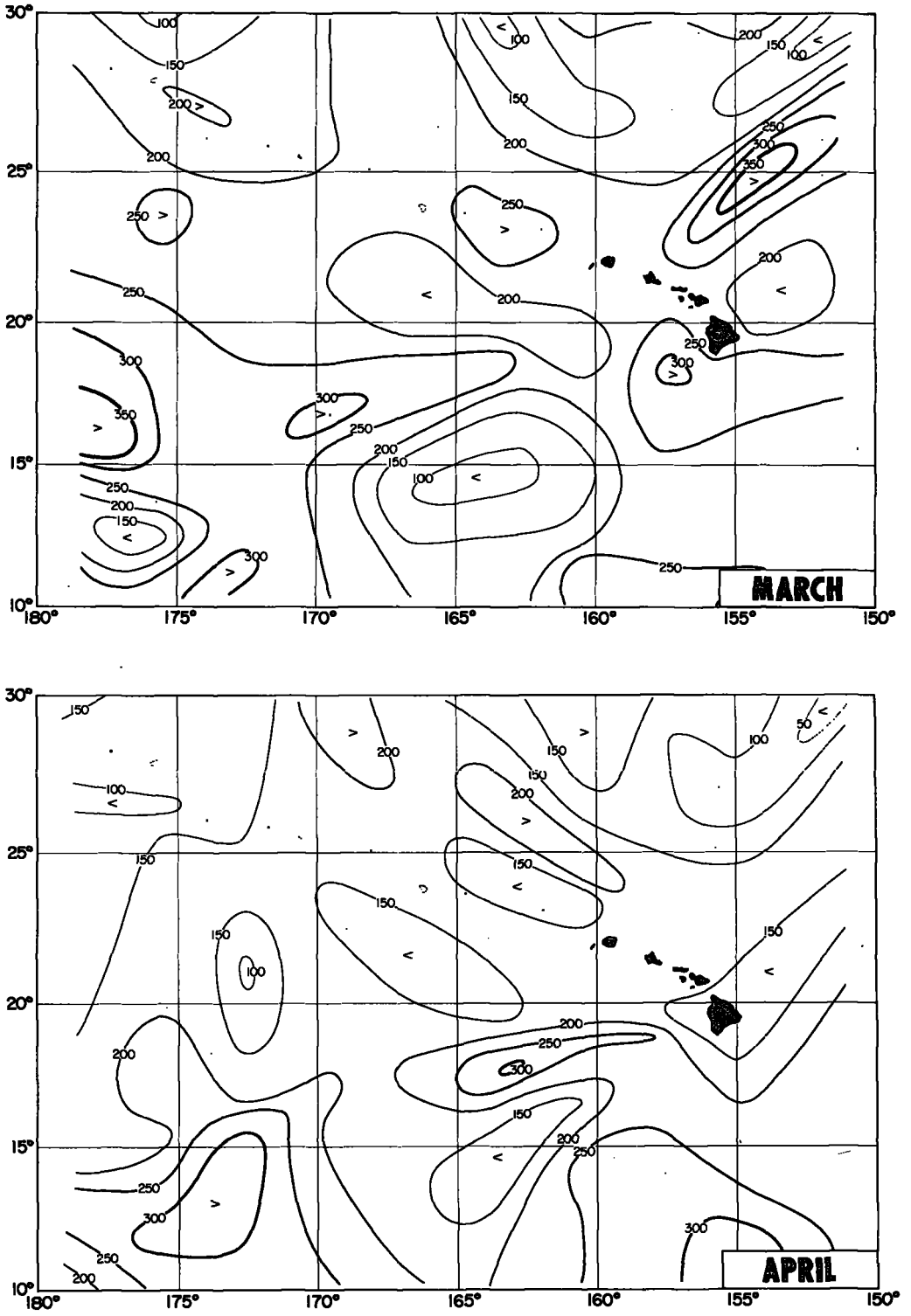

CHART I.—Distribution of depth of mixed layer (feet)—Continued.

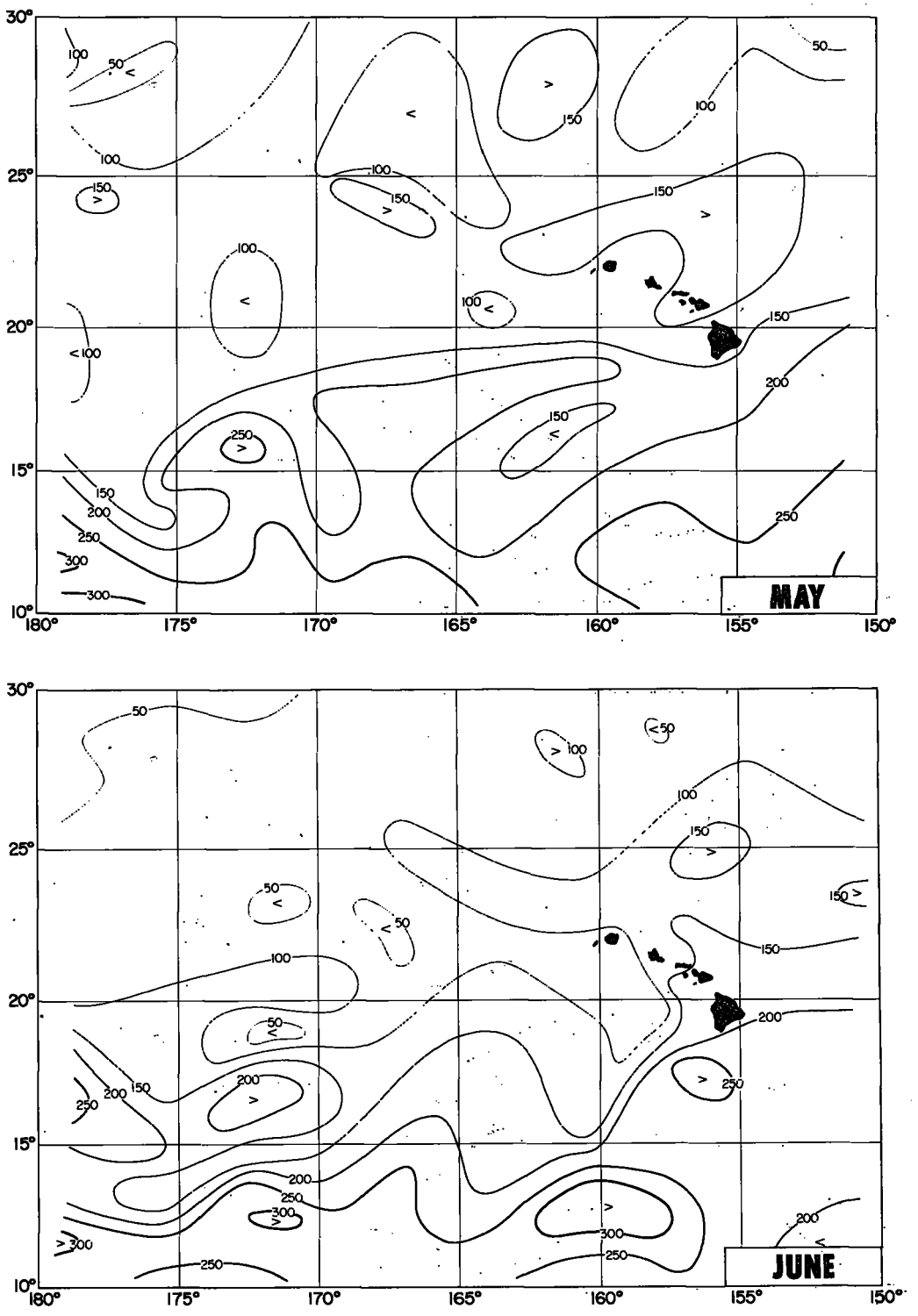

CHART I.—Distribution of depth of mixed layer (feet)—Continued.

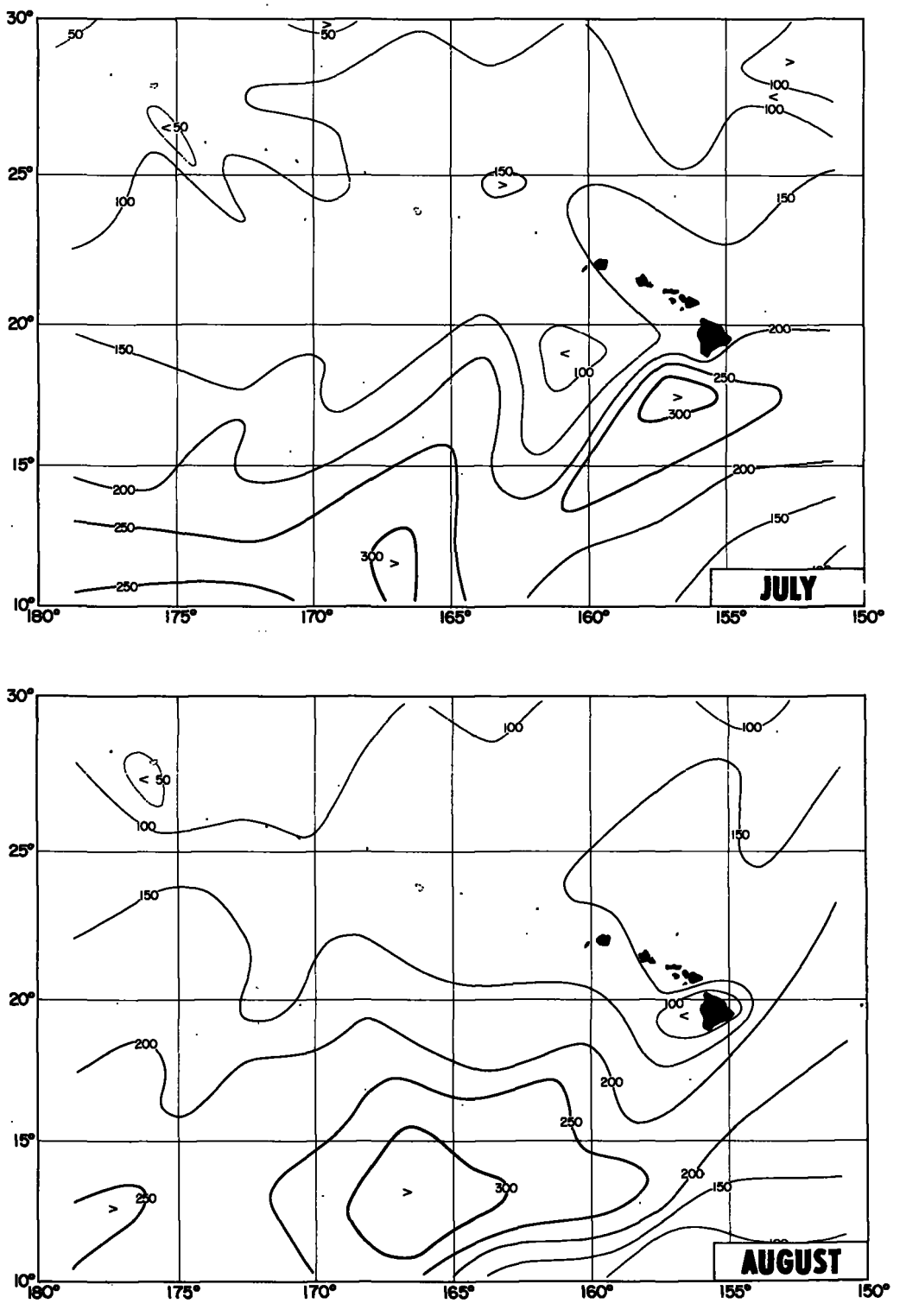

CHART I.—Distribution of depth of mixed layer (feet)—Continued.

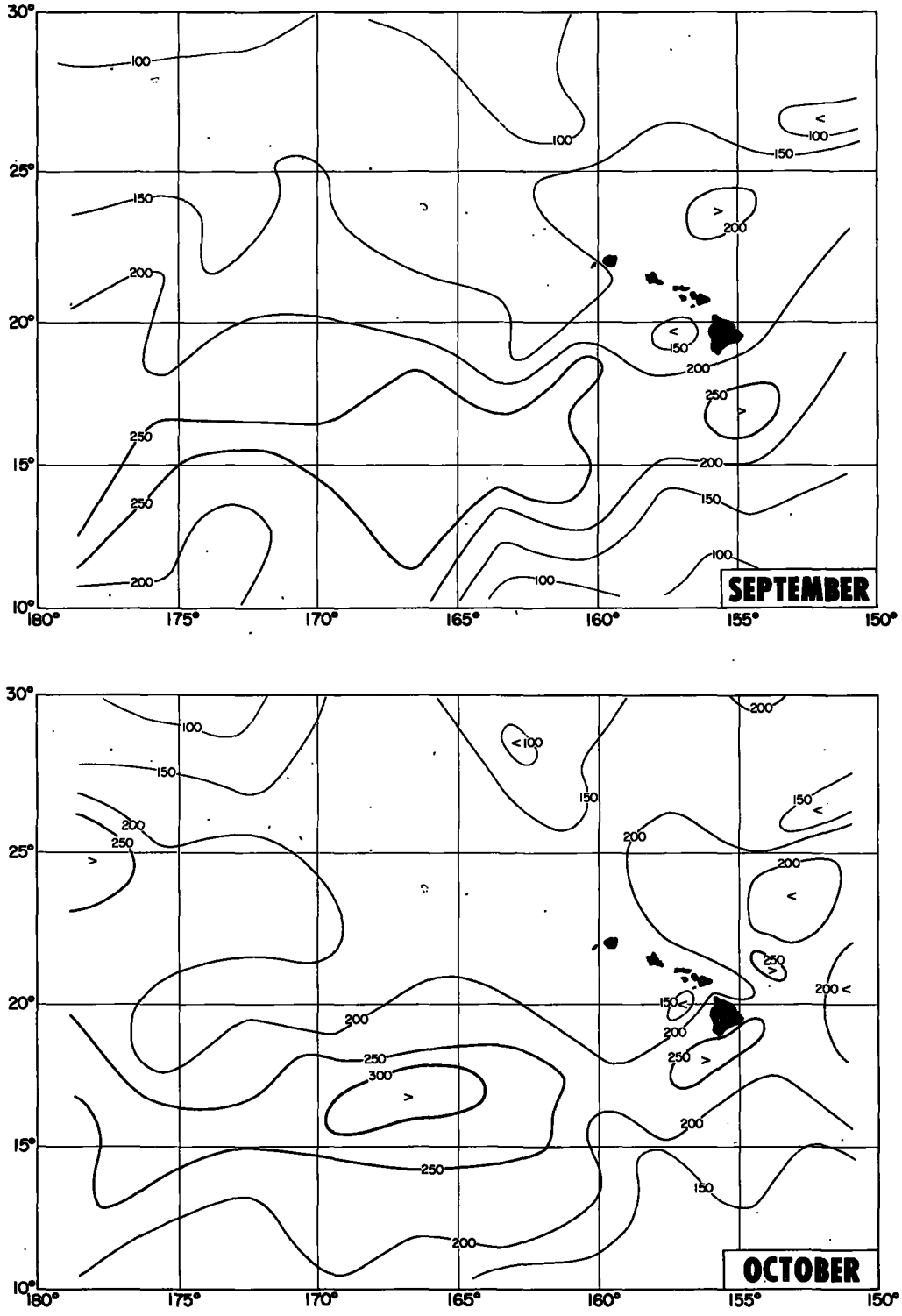

CHART I.—Distribution of depth of mixed layer (feet)—Continued.

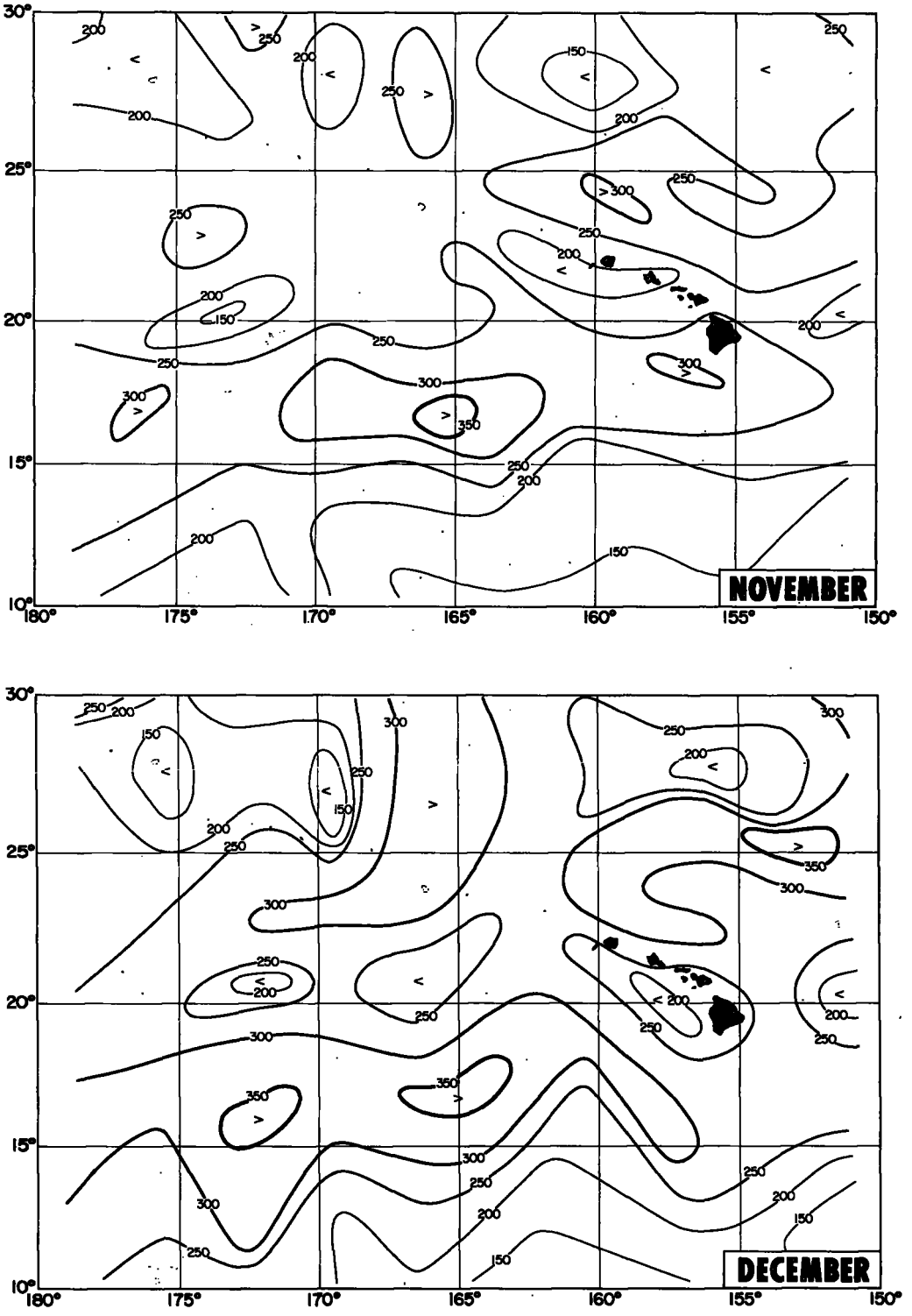

CHART I.—Distribution of depth of mixed layer (feet)—Continued.

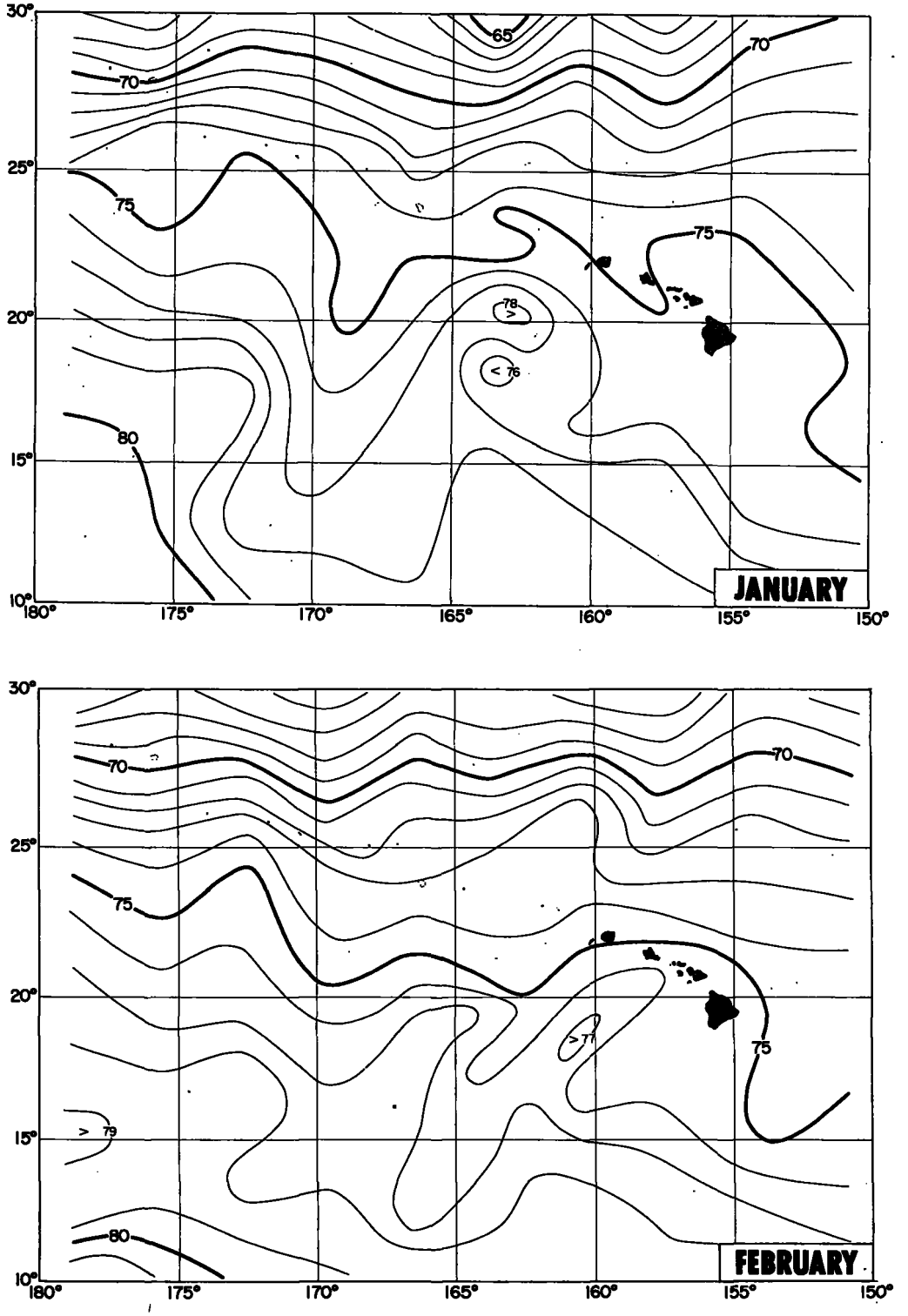

CHART II.—Distribution of surface temperature (° F.)

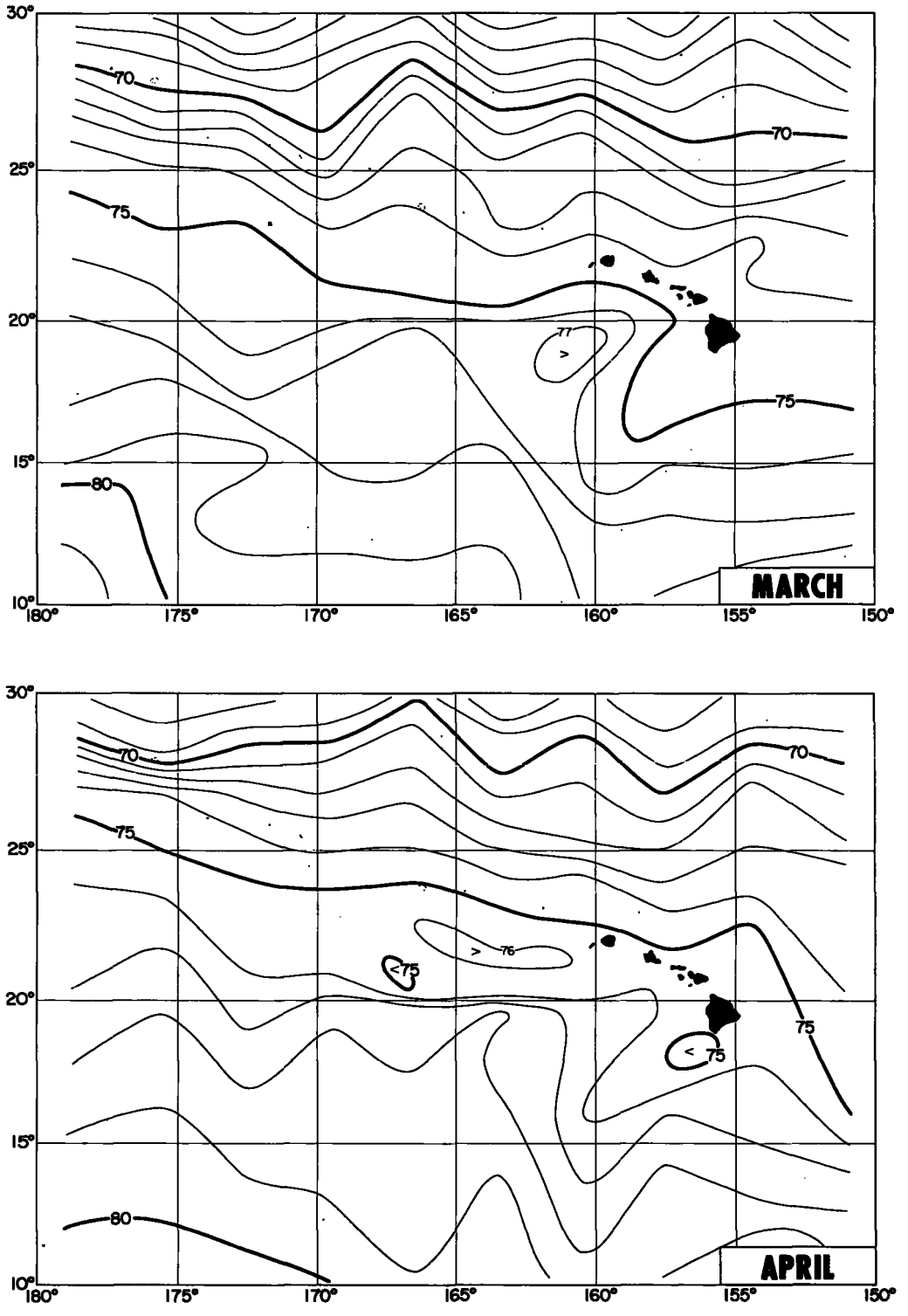

CHART II.—Distribution of surface temperature (° F.)—Continued.

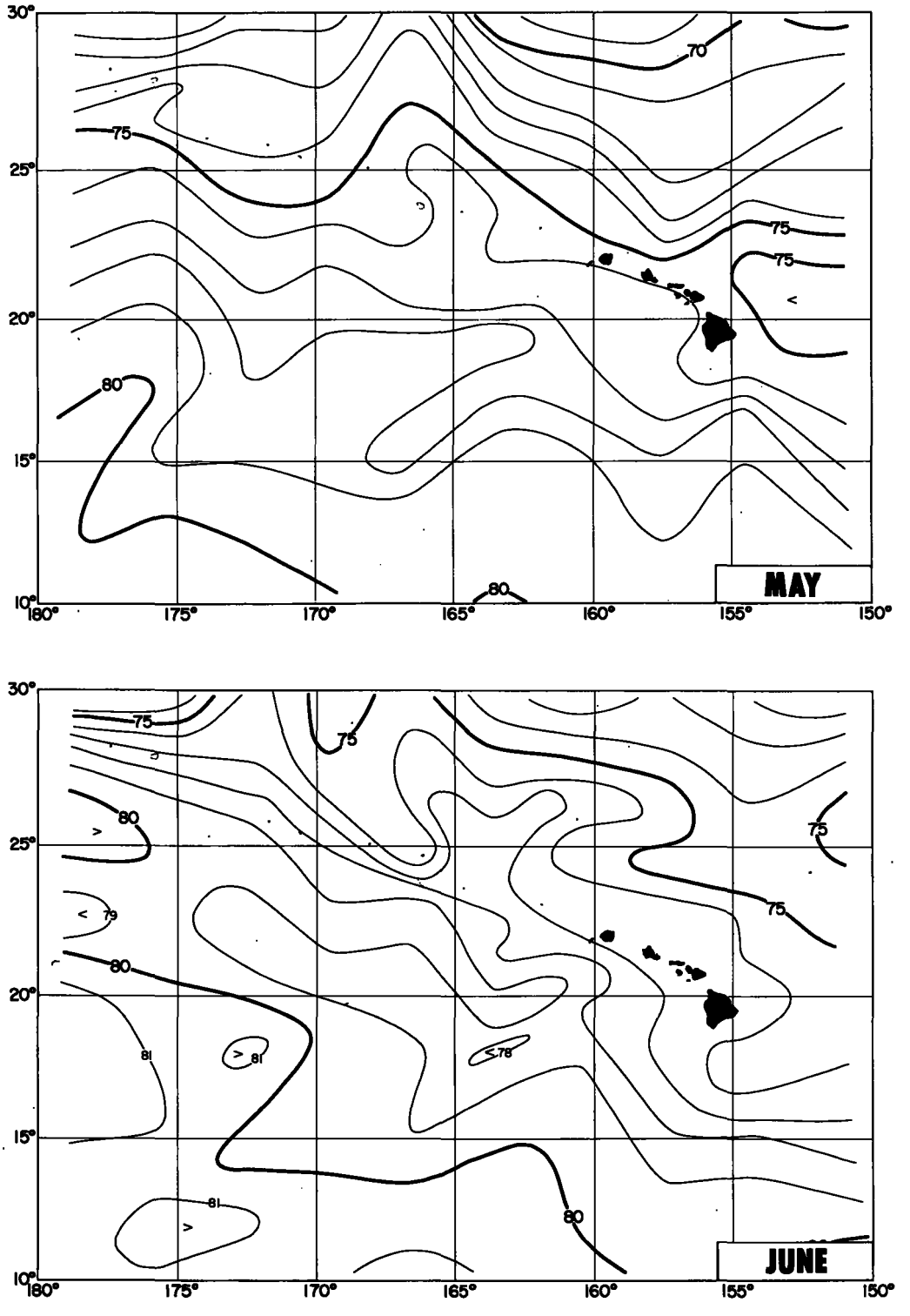

CHART II.—Distribution of surface temperature (° F.)—Continued.

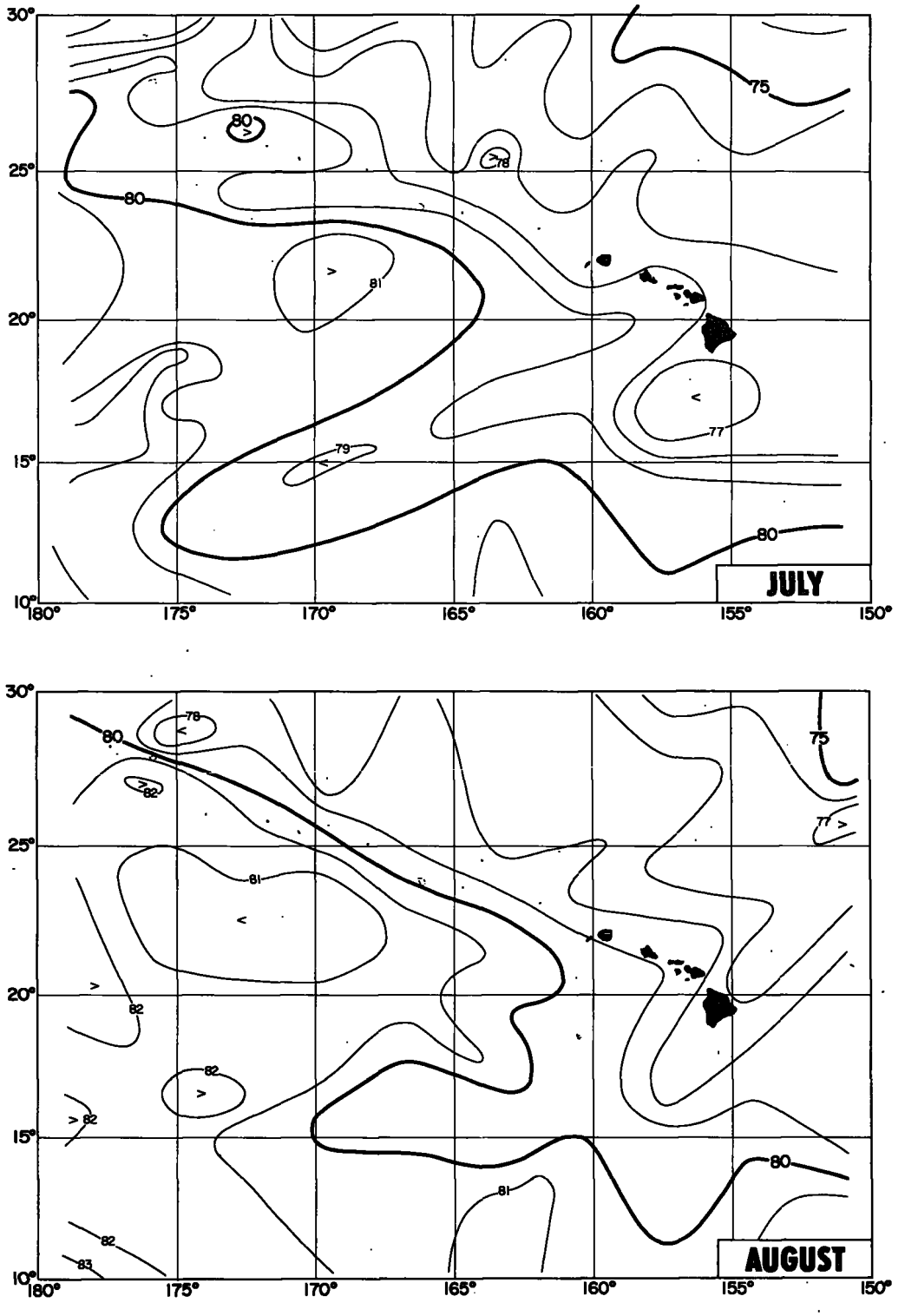

CHART II.—Distribution of surface temperature (° F.)—Continued.

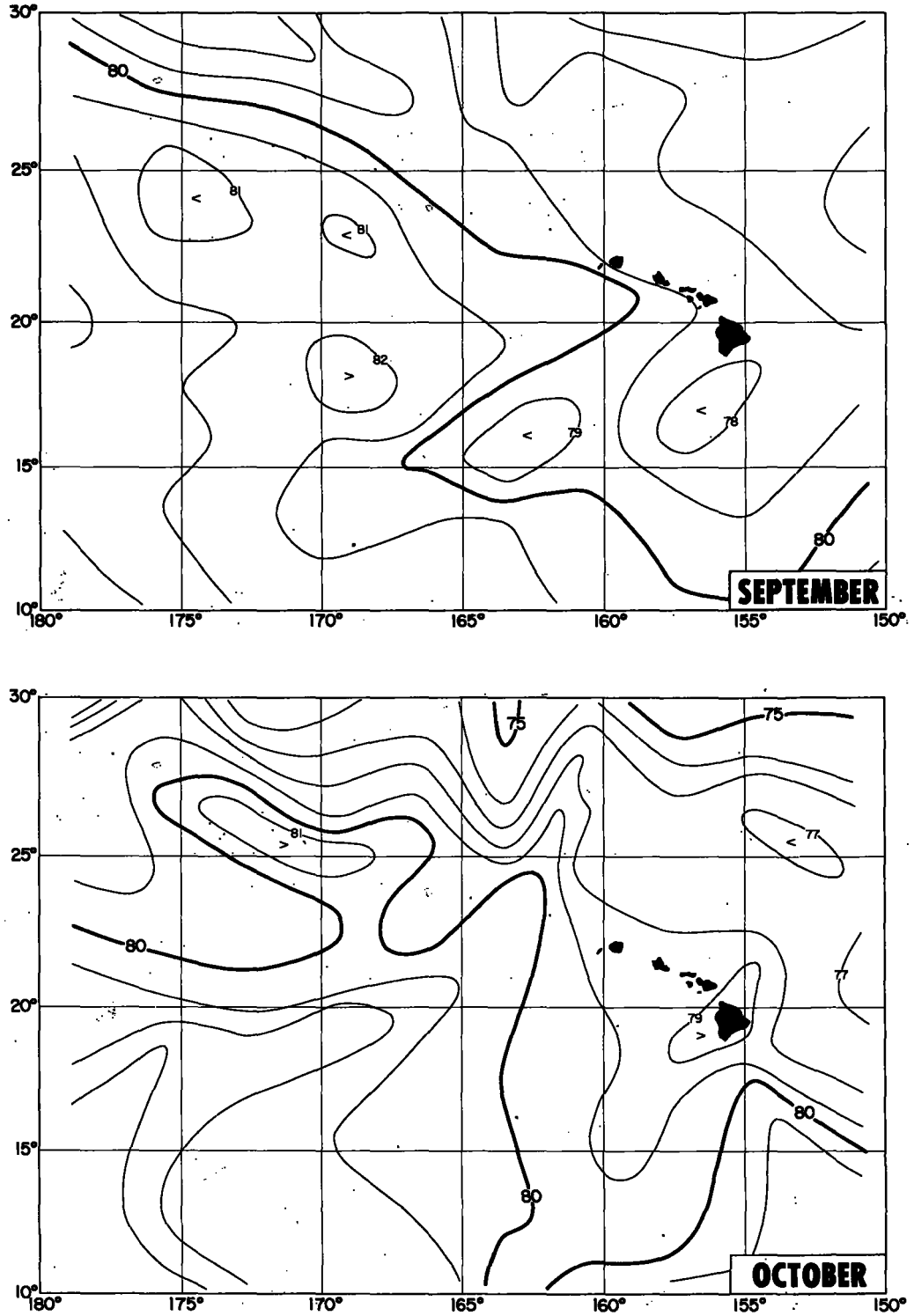

CHART II.—Distribution of surface temperature (° F.)—Continued.

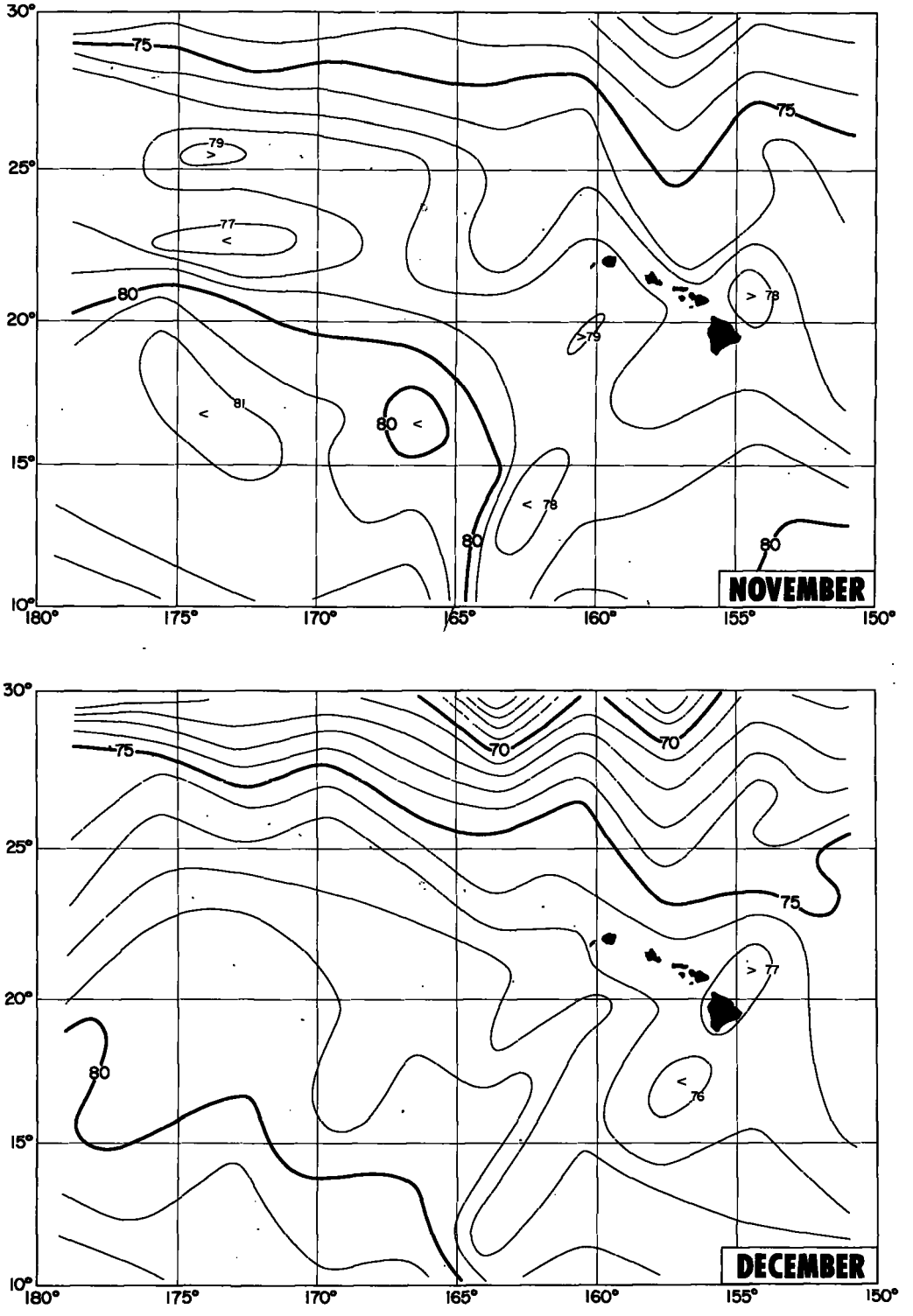

CHART II.—Distribution of surface temperature (° F.)—Continued.

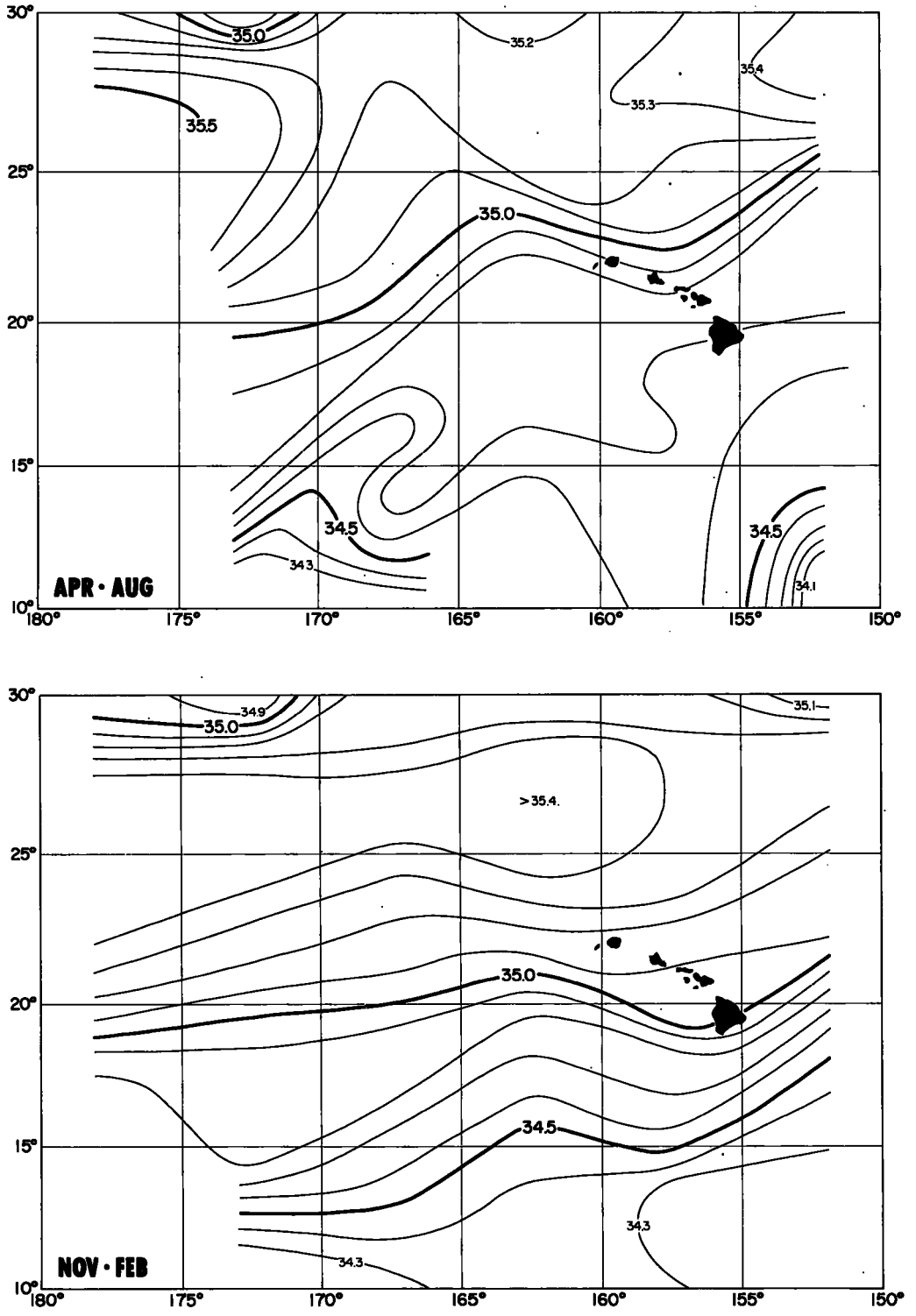

CHART III.—Distribution of surface salinity (parts per thousand).

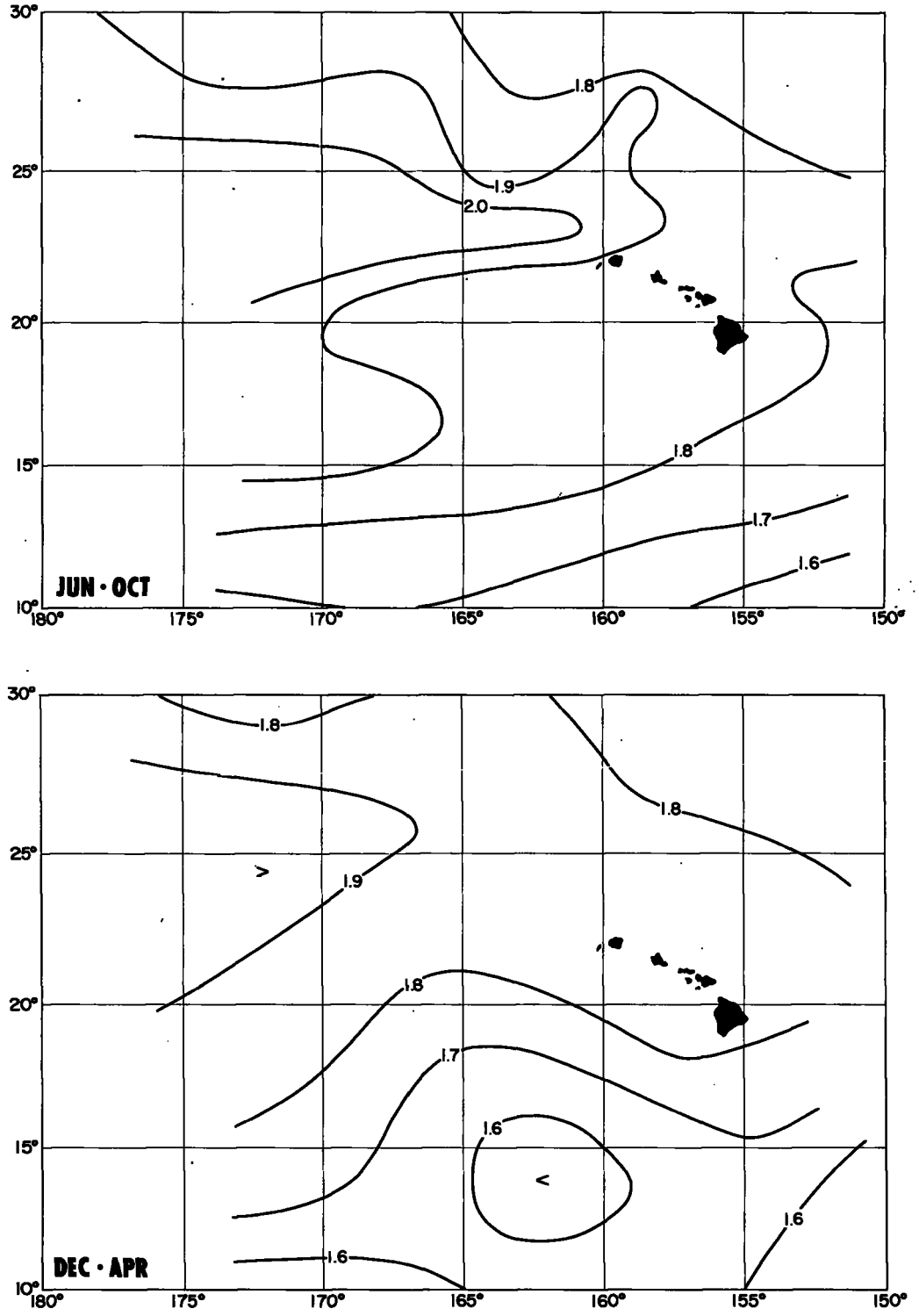

CHART IV.—The surface dynamic topography (in dynamic meters relative to 1,000 M.).

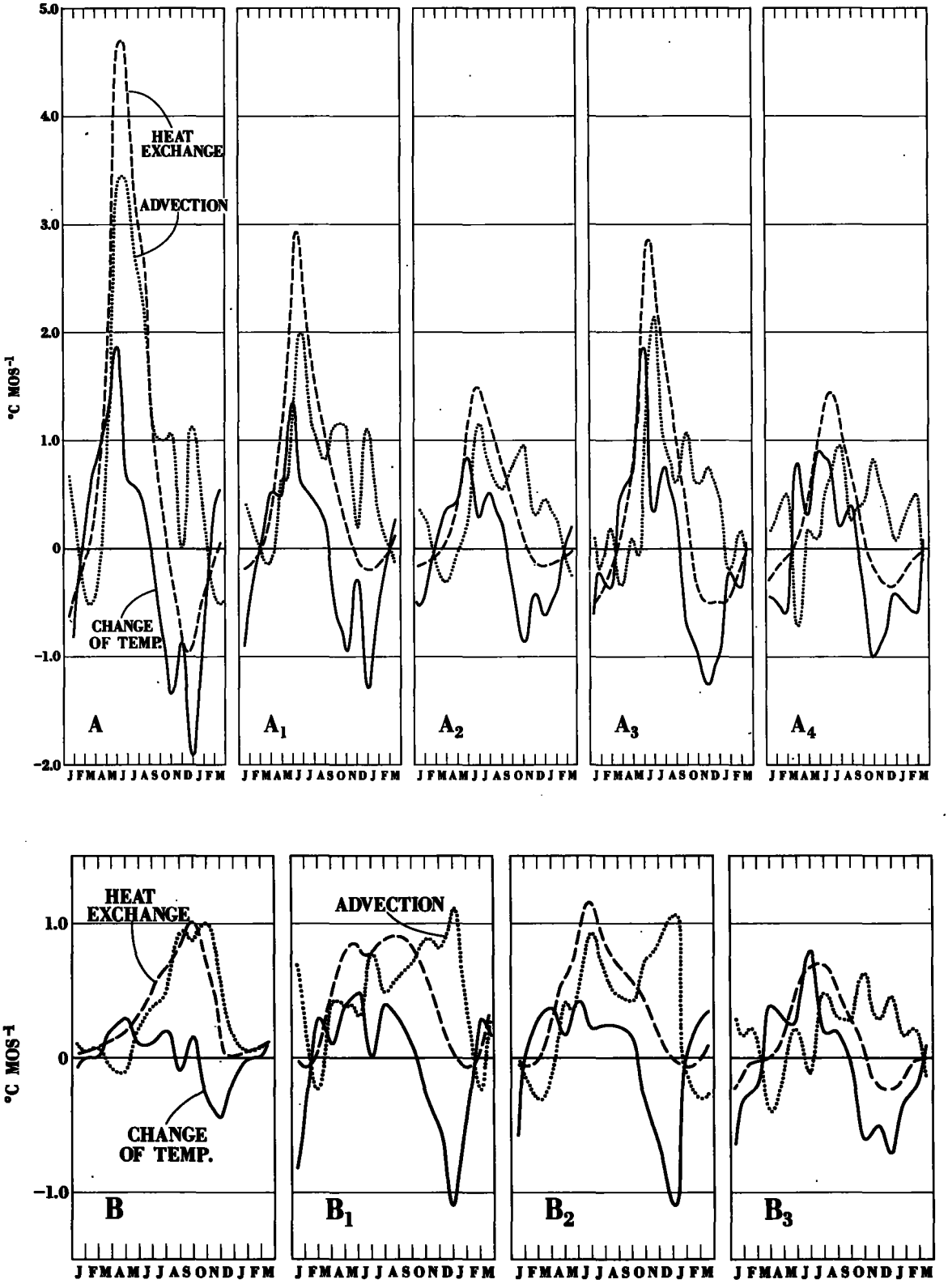

CHART V.—Characteristic asvection diagrams. For the areas designated by A, A_1, and so forth, see figure 24, page 397.

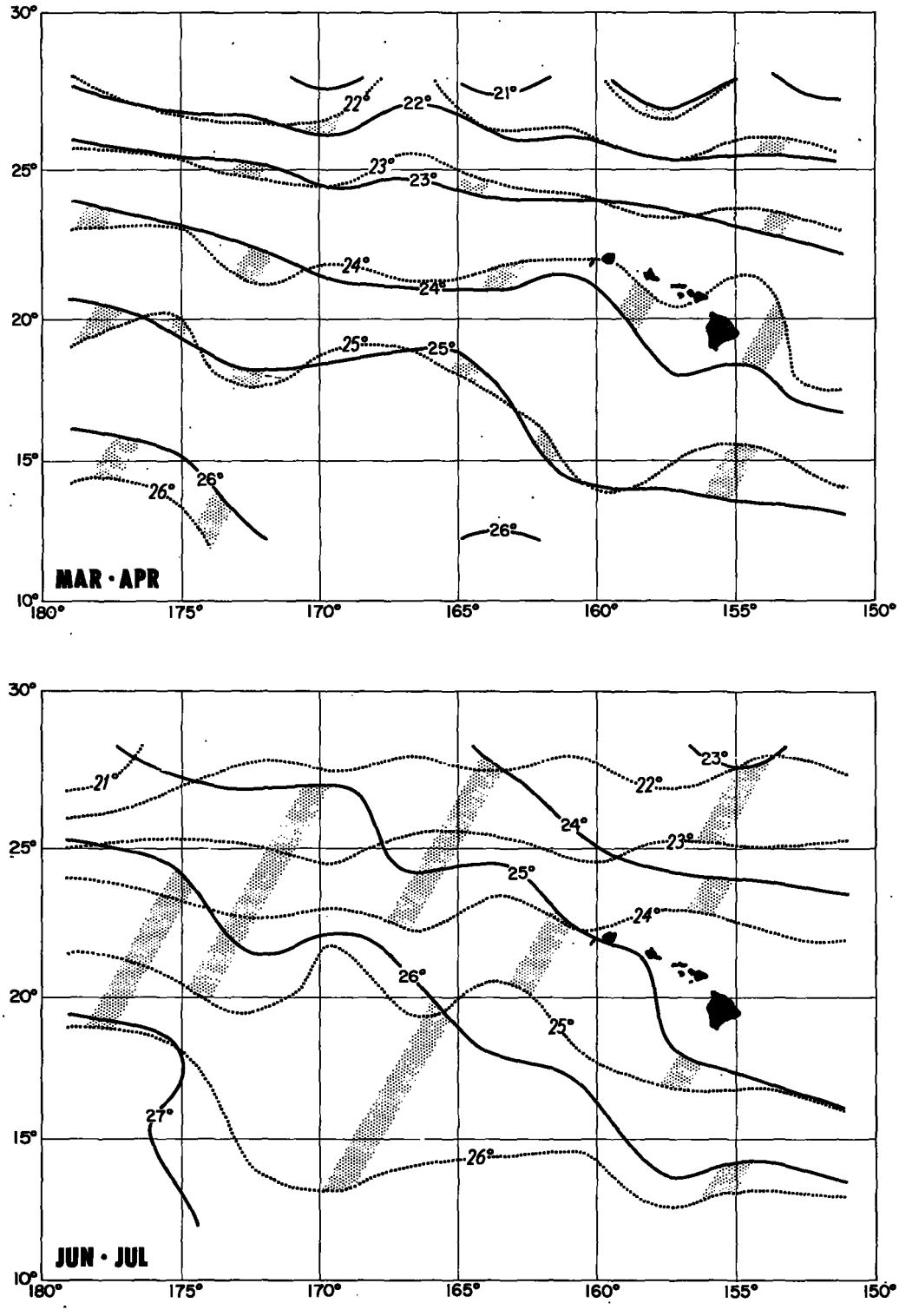

CHART VI.—Heat advection chart (° C.)

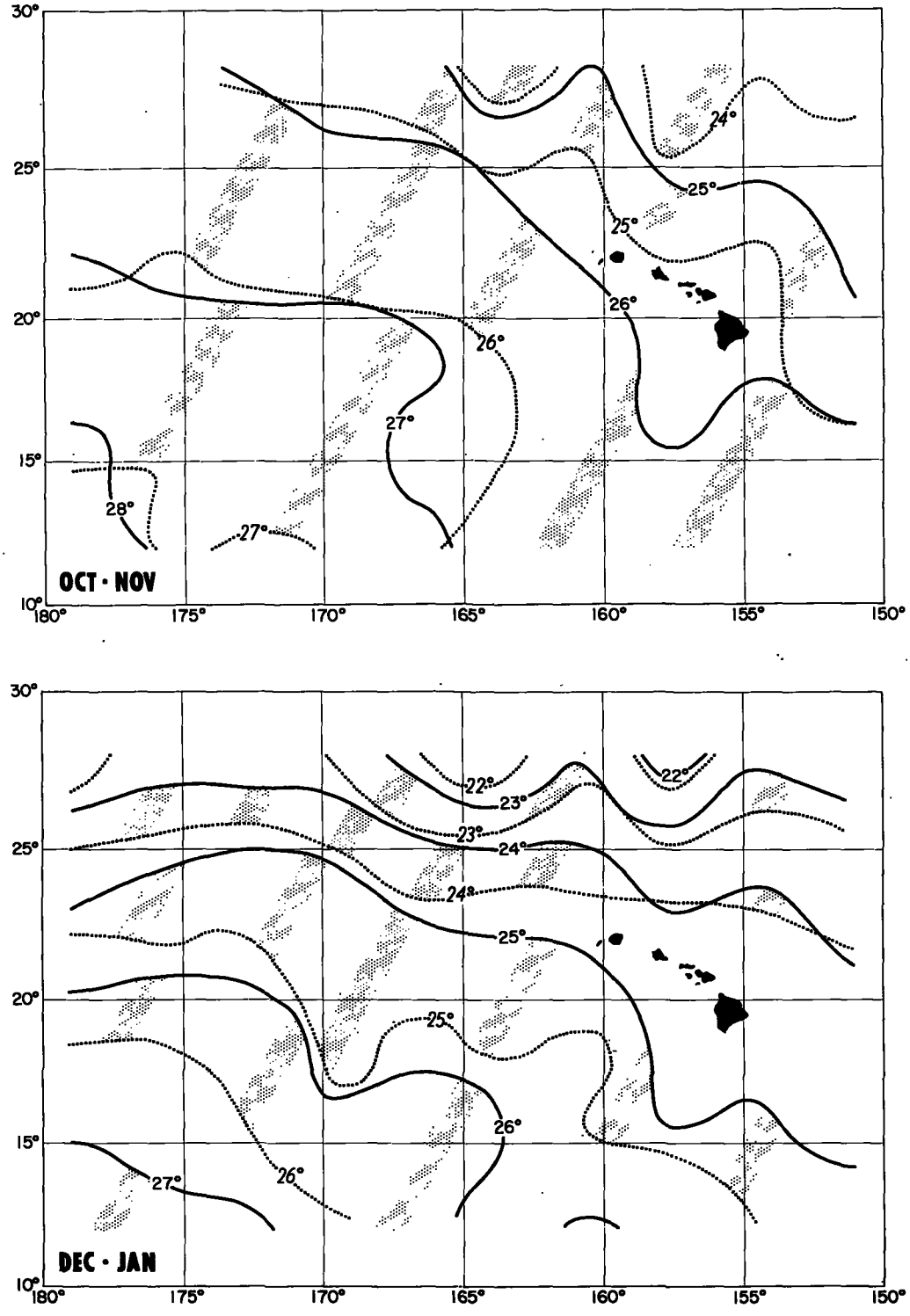

CHART VI.—Heat advection charts (° C.)—Continued.